UNIVERSITY OF CALIFORNIA,
IRVINE

Spatial Stream Segregation in the Awake Cat Auditory Cortex

DISSERTATION

submitted in partial satisfaction of the requirements
for the degree of

DOCTOR OF PHILOSOPHY

in Cognitive Sciences

by

Akshat Arneja

Dissertation Committee:
Professor John Middlebrooks, Chair
Professor Virginia Richards
Professor Gregory Hickok

2022

DEDICATION

To

My partner, my family, my friends, and my teachers
For their love, support, and guidance

ॐ भूर्भुवः स्वः
तत्सवितुर्वरेण्यम
भर्गो देवस्य धीमहि।
धियो यो नः प्रचोदयात

TABLE OF CONTENTS

LIST OF FIGURES

ACKNOWLEDGEMENTS

This dissertation work has been the result of years of work and would not have been possible without the constant support and guidance from my mentors, colleagues, friends, and family.

I would like to first express my deepest gratitude and appreciation for my mentor, Dr. John Middlebrooks. John, thank you for constantly encouraging to work harder, learn more, and push past the setbacks throughout this work. Without your guidance, support, ceaseless patience and immense knowledge, this dissertation would not be possible. It has been a joy to learn from you and to have had the opportunity to work alongside you as you developed new methodologies and conducted research. I have grown and learned so much in your laboratory. Thank you for being persistent in your help, for lifting me up when I stumbled, and for your constant belief in me. I could not have asked for a better advisor and mentor.

I would also like to thank my committee members, Dr. Virginia Richards and Dr. Gregory Hickok. Ginny, I have learned so much from being around you, speaking with you, and in your classes. Additionally, I would like to thank you for your continued kindness. From the beginning, you have always made me feel welcome and worthy in the program. I cannot express how much that meant to me throughout my experience. Greg, I have truly enjoyed speaking with you, being in your classes, and TAing for you. I have learned so much from your approach to asking questions about the world, and your approach to science. Additionally, I would like to thank you for the kindness you have showed me throughout my experience. I feel incredibly lucky to have known and worked with such extraordinary thinkers and scientists.

I would like to thank everyone in the Middlebrooks Laboratory. Work like this takes a village to achieve and would not be possible without the support and work of the members in the

lab. Beth, thank you for all the work you did to make this dissertation possible. Thank you for always being a wonderful friend, for always caring about my mental health, and for taking such wonderful care of the cats. I could not have done this work without your help. I cannot thank Matt Richardson enough for all the kindness, friendship, and support he gave me. Matt, I could not have done these experiments without your help. Thank you for always encouraging me and believing in me. You are a brilliant scientist and an even better friend. Emily Angelopolous, thank you for being my "lab sibling", for your encouragement and belief in me, and for being a wonderful friend. I would like to thank Zekiye Onsan for being a warm and caring presence for the first few years in the program. I would also like to thank Lauren Tolentino, Justin Yao, and Alessandro Presacco for their help and support. In addition to the Lab, I would like to thank the ULAR and UCI veterinary staff for their expertise and cat care. I would especially like to thank Dr. Roger Geertsema and Dr. Stacey Kang for help in the surgeries and cat care, and Rommel Medina for caring for the cats every day and for the great conversations.

Thank you to my friends, who supported me, listened to my complaints, and cheered me on throughout this experience. I would especially like to thank Alex Bower. Alex, I could not have done this without your help and encouragement throughout this work. I feel incredibly lucky to have met such a wonderful person in this journey and time in my life. I would also like to thank Andrew Burton, who has always supported me and helped me. Andrew, thank you for all the conversations, long walks, and fun adventures.

Cassie, I could not have done any of this without you by my side. I can never fully express my gratitude for everything you have done. Thank you for always being by my side, for being on my side, for pushing me to work hard and try my best. Thank you for serving as a shining example of what it means to be a good scientist, and a good graduate student. Thank you

for inspiring me every single day. I cannot wait for the next adventure. Let's keep climbing mountains.

Abhinav, this work would not be finished without your guidance, your support, and your love. Thank you for the daily encouragement. Thank you for inspiring me to think more broadly and keep working through the hardships. You will always be the person I look up to and will always be the most brilliant scientist and thinker that I know. Thank you to my parents, for all of the sacrifices and the constant love and support.

I would also like to thank my high school biology teacher, Jeffrey Ponto. Mr. Ponto, thank you for believing in me so long ago, and for going out of your way to hold me to a high standard and imbuing a love of biology in me at a young age.

Lastly, none of this work is possible without the cats that contributed to this research. Throughout my time, the cats were not only my research subjects but also my friends. Thank you all for teaching me persistence, patience, and how to find joy in the darkest times. I would specifically like to thank Ozzie for being a constant source of love and kindness, and Yoshi, Peach, and Daisy for helping me in the last stretch. I will always remember my "furry coworkers" and cherish the time I was able to spend with each one.

VITA

Akshat Arneja

2012	B.S. in Neuroscience, B.S. in Psychology,
	University of Minnesota, Twin Cities
2012-15	Junior Scientist, Multi-Sensory Perception Laboratory,
	University of Minnesota, Twin Cities
2015-20	Teaching Assistant, Department of Cognitive Science,
	University of California, Irvine
2015 - 22	Graduate Student Researcher, University of California, Irvine
2021 - 22	Center for Hearing Research Training Grant Recipient,
	Center for Hearing Research
	University of California, Irvine
2022	Ph.D. in Cognitive Sciences,
	University of California, Irvine

FIELD OF STUDY

Auditory scene analysis in awake animal physiology

PUBLICATIONS

Tonotopic selectivity in cats and humans: electrophysiology and psychophysics. Authors: Francois Guérit, John C. Middlebrooks, Matthew L. Richardson, **Akshat Arneja**, Andrew J. Harland, Robin Gransier, Jan Wouters, Robert P. Carlyon (*In Review)*

Spectral and temporal coding properties of the awake cat cortex. Authors: John C. Middlebrooks, **Akshat Arneja**, Lauren Tolentino(*In preparation)*

ABSTRACT OF THE DISSERTATION

Spatial Stream Segregation in the Awake Cat Auditory Cortex

by

Akshat Arneja

Doctor of Philosophy in Cognitive Sciences

University of California, Irvine, 2022

Professor John Middlebrooks, Chair

Listeners have a remarkable ability to perceptually segregate interleaved sequences of sounds in complex auditory environments, a process referred to as *stream segregation*. Previous studies of psychophysical measures of this process in humans and the cat animal model have shown that physical separation of sound sources aids in the process of segregating competing noises. This finding has also been observed in the physiological response of the anesthetized cat primary auditory cortex, wherein neurons tend to synchronize to one of two competing sound sequences differing in their source location. The goal of this dissertation is to evaluate the coding properties of the awake cat auditory cortex and explore the neural mechanisms underlying stream segregation using spatial cues. The cat animal model has been used extensively in auditory research due to their well-developed auditory cortex, and their sound localization abilities to support nocturnal hunting behavior. Here, we trained cats on a psychophysical spatial stream segregation task (Chapter 1). Then, we implanted cats with chronic neural electrodes to record single- and multi-unit activity in the primary auditory cortex. We studied spectral and temporal coding properties of primary auditory cortical neurons in awake cats (Chapter 2), and spatial stream segregation in the response of cortical neurons in off-task conditions (Chapter 3). Our

findings show that 1) cats can segregate competing interleaved noise bursts with spatial acuity matching prior measurements in feline and human listeners. 2) Neurons in the primary auditory cortex of awake cats display sharp frequency tuning, temporally dynamic responses, and synchronous and non-synchronized coding of stimuli with high repetition rates—properties that have only previously been observed in the awake marmoset cortex. 3) Neurons in the auditory cortex of cats not overtly engaged in a stream segregation task show weaker segregation than is observed in anesthetized preparations. It may be that presenting stimuli with faster rates, or other mechanisms such as selective attention, are necessary to observe stream segregation in the awake cortex. Further, it may be possible that spatial stream segregation is processed in cortical areas beyond A1. Overall, these findings provide insight into the coding properties of the auditory cortex in awake cats and the neural mechanisms underlying stream segregation using spatial cues.

INTRODUCTION

Everyday listening environments expose the auditory system to multiple competing sounds. The process of isolating sounds of interest among competing sequences of noise has been referred to as auditory scene analysis (Bregman, 1990). A key component of auditory scene analysis is stream segregation, or the ability to isolate and perceptually group a sequence of sounds from competing temporally interleaved sequences. The auditory system uses various features to segregate one stream from another; differences in frequency, timbre, amplitude and temporal envelope, among others, provide key information to aid in the stream segregation process. Spatial differences between sound sources also provide robust cues for segregating competing streams; this process is specifically referred to as spatial stream segregation. Psychophysical measures of stream segregation have evaluated the conditions needed for interleaved stimuli to elicit the perception of segregated streams. Early evidence comes from the work of van Noorden (1975). In his experiments, van Noorden characterized the time scale in which stream segregation is most likely to occur when listeners are presented with stimuli interleaved in time. Specifically, van Noorden found that interleaved tone pips presented within the time scale of 2-10 Hz were most likely to elicit a percept of segregated streams. Stimuli below 2 Hz were more likely to be heard as one single stream, and streaming itself was less likely to occur at very slow presentation rates. Stimuli presented at much faster rates (>10Hz) were more likely to be heard as one single, fused stream. Recent work has also explored the spatial threshold of human listeners (Middlebrooks and Onsan, 2012). Researchers in this study found a median threshold of ~8° degrees; sound sources were difficult to disentangle for listeners when presented closer than this threshold in space. Similar thresholds have also been observed for the spatial acuity of animal models (Javier et al., 2015).

Spatial stream segregation has also been demonstrated in the physiology of cortical neurons in the anesthetized cat (Middlebrooks and Bremen, 2013). In this study, researchers observed that cortical neurons had the robust ability to synchronize to one of two competing interleaved sound sequences. The goal of this dissertation is to explore the neurobiological basis of spatial stream segregation in the response of cortical neurons in the cat animal model in the absence of anesthesia. The cat animal model was chosen due to its extensive use in auditory research and natural sound localization ability due to its nocturnal hunting behavior.

In chapter 1, we evaluated the ability of cats in performing a stream segregation task using spatial cues. This task was based on sequential stream segregation, in which the competing stimuli were interleaved with no temporal overlap, had shared spectral and temporal properties and only differed in their sound source location. Here, we observed that cats were able to successfully learn and perform an established hold-release paradigm. Further, we observed that cats had similar spatial thresholds to past studies of feline listeners performing the same task (Javier et al., 2016), and close to thresholds by human listeners in a similar task (Middlebrooks and Onsan, 2012).

In chapter 2, we investigated frequency and temporal coding properties in the physiology of cortical neurons in the absence of anesthesia. We implanted chronic recording arrays in the primary auditory cortex of cats and presented stimuli varying in rate as well as stimuli varying in frequency and level. Previous studies have demonstrated that cortical neurons in the anesthetized cat cortex typically display broad tuning curves, including the presence of V-shape frequency response areas (FRAs) (Schreiner & Sutter, 1992), and limited synchrony to periodic stimuli (Eggermont, 1991). A wider array of coding properties has been observed in the awake cortex of the marmoset animal model (Lu and Wang, 2000; Sadagopan and Wang, 2008), but these

properties have not been previously seen in other animal models. In this chapter, we observed a wide array of response properties in the response of cortical neurons in the primary auditory cortex of cats in an awake preparation. These properties include sharp spectral coding, including the presence of I- and O-shape FRAs. We further observed that neurons in the awake auditory cortex displayed sustained firing to preferred stimuli and displayed temporally dynamic responses. We additionally observed sharpening in the frequency tuning bandwidth of broadly tuned V-shape FRAs in the latter half of the duration of the stimulus. Study of the temporal coding properties of the awake cat cortical neurons demonstrated synchronous firing to click rates as high as 226 clicks per second, as well as non-synchronous coding in response to slow and fast rates. These properties have not previously been observed in the primary auditory cortex of the cat animal model in anesthetized preparations.

After characterizing mechanism in the awake cortex that could represent sounds on the basis of their detailed spectral and temporal properties, we then explored the response of cortical neurons to spatial stream segregation stimuli in idle conditions (Chapter 3). We first observed that cortical neurons had the ability to encode trains of noise bursts as high as 40 bursts per second, a finding that has not been observed previously in the awake cortex. We then presented cats with sequences of interleaved competing noise bursts in idle conditions. Study of the spatial stream segregation stimuli revealed that most neurons displayed synchrony to both competing streams regardless of spatial separation. These results contrasted with our results in Chapter 1, wherein we found that cats were able to perform stream segregation with spatial acuity close to human listeners (Chapter 1). These findings also contrast with prior work in the primary auditory cortex in anesthetized cortex, in which neurons in the primary auditory cortex show a robust ability to segregate between two interleaved competing sound sources. It may be that spatial

stream segregation could be observed in idle conditions with stimuli presented at higher rates. It may also be that an additional mechanism such as selective attention is required for the observation of stream segregation, or that spatial stream segregation is processed in cortical areas beyond the primary auditory cortex.

This dissertation provides insights into the spectral and temporal coding properties of awake cortical neurons, and into the auditory mechanisms underlying aspects of spatial stream segregation. These findings contribute to our understanding of the neurobiological basis of stream segregation and our understanding of the basic physiological properties of the primary auditory cortex.

Chapter 1
Spatial Stream Segregation in an Animal Model

Introduction

In complex auditory environments, normal hearing listeners can isolate a single source of sound among competing noises. This process has been referred to as the cocktail party problem (Cherry, 1953), or auditory scene analysis (Bregman, 1990). A key feature of auditory scene analysis is the ability to perceptually sort temporally interleaved sequences of sounds into distinct perceptual stream in the presence of competing sounds, a process referred to as stream segregation. Multiple sound cues can contribute to stream segregation, including differences in fundamental frequency, phase, and spectral and temporal envelopes (for review, see Moore & Gockel, 2002). The present report focuses on the study of stream segregation based on spatial differences in sound source locations.

Previous psychophysical studies in our laboratory have focused on spatial stream segregation in humans (Middlebrooks & Onsan, 2012), and cats (Javier et al., 2016; Middlebrooks & Bremen, 2013). Middlebrooks and Onsan (2012) asked listeners to discriminate between two rhythms of a target sequence of sound bursts, in the presence of a masker sequence interleaved in time. The stimuli were constructed such that, when co-located, the target and masker sequences were perfectly interleaved, leading to the percept of an undifferentiated sequence of noise bursts which made discrimination of the rhythms impossible. Listeners performed at chance in this task when the sounds were co-located but improved when there was an adequate spatial separation between the target and masker sources. Additionally, when target and masker sources were sufficiently separated, listeners reported hearing segregated streams,

and could identify the rhythm. Those authors observed a median threshold separation of 8.1° in the horizontal dimension across their subjects.

The present study is modeled after the work in Javier et al., 2016. In that study, researchers trained cats to perform a spatial stream segregation task, in which cats pressed a pedal to initiate a target sound sequence presented in a particular rhythm. After a variable hold time, the target rhythm changed, and the cat could release the pedal to receive a food reward. The target sound sequence was presented in the presence of a temporally interleaved masker sequence that differed from the target sequence only in its spatial location in the horizontal plane. The authors observed that cats had a median rhythmic masking release threshold of 9.4° for broadband conditions. This suggested that cats' rhythmic masking release thresholds were only slight broader than humans for similar sound stimuli. Javier et al., (2016) analyzed different passband conditions to demonstrate that cats perform better in highpass conditions, in which the noise bursts were filtered to the 4-25 kHz frequency range, compared to the lowpass conditions in which the noise bursts were filtered to the 0.4-1.6 kHz range. This suggested that cats perform better segregation with interaural level difference (ILD) cues compared to interaural timing difference (ITD) cues.

In the present study, we trained cats with the same spatial stream segregation task that was used by Javier et al., (2016). Following training and data collection, the cats in our study were implanted with a 32-channel recording array, placed in the right primary auditory cortex. The purpose of this implant was to record the response of cortical neurons in the primary auditory cortex as cats were exposed to the stream-segregation stimuli. We successfully recorded cortical responses to the stream-segregation stimuli (Chapter 3) and to other frequency and temporal probes (Chapter 2) during conditions in which the cats were not engaged in task

performance. As shown in Chapter 2, most of the recording sites exhibited neuronal characteristic frequencies within a 2-octave band centered on 8 kHz. That corresponded to the frequency range of stimuli that yielded highest spatial acuity in the study by Javier and colleagues (2016). A number of unresolved technical difficulties precluded cortical recording during task performance. Nevertheless, the cats were capable of behavioral spatial stream segregation with performance comparable to published results. That task performance is the topic of this chapter.

Methods

Animals

All procedures were in accordance with the NIH Animal Welfare Guidelines and with a protocol approved by the Institutional Animal Care and Use Committee at the University of California at Irvine. Three domestic shorthair cats (*Felis catus*), 1 male and 2 female, were obtained from a breeding facility at the University of California Davis. No hearing deficits were evident, and animals were 6 months old at the beginning of training. All cats were neutered to reduce aggressive behavior, and to allow new animals to be introduced to the colony for co-habilitation. Food was restricted on days animals were performing the behavioral task (5 days a week). On those days, cats received moist food as behavioral reinforcement during a training or testing session and were allowed free dry food for up to an hour following each session. On weekends, cats were given free access to dry food for 3 hours each day in the housing area. Water was freely available at all times in the housing area.

Experimental apparatus

Experiments were conducted in a double-walled sound-attenuating anechoic chamber (Industrial Acoustics; inside dimension 2.6 x 2.6 x 2.5 m) lined with SONEXone absorbent foam to suppress sound reflections. A circular hoop, 1.2 m in radius, supported 8.4-cm-diameter two-way loudspeakers in the horizontal plane at 0° and at ±10°, 20°, 40°, 60°, and 80° relative to the front of the apparatus. The cat was supported on a raised platform which was adjusted in height to center the cat's head in the array of loudspeakers. The animal was restrained to the platform with a harness but permitted free motion of the limbs and head. A feeder was mounted on a pneumatic cylinder located on the animal pedestal. The feeder was lowered during sound

presentation and raised to provide behavioral reinforcement. All behavioral sessions were conducted in the dark and were monitored with video using infrared illumination.

Stimulus generation and data acquisition used System III hardware from Tucker-Davis Technologies (TDT; Alachua, FL). Custom MATLAB software (Mathworks; Natick, MA), on a Windows-based computer, controlled stimulus presentation and data acquisition Sounds were generated at a sample rate of 97,656 s^{-1} with a 24-bit precision. Loudspeakers were calibrated in the absence of the cat using a precision ½" microphone (ACO Pacific) positioned at the center of the chamber at the normal location of the animal's head. Golay codes were used as broadband probe sounds (Zhou et al., 1992). The calibration procedure for broadband stimuli yielded a 1029-tap finite-impulse-response correction filter for each speaker. The filters flattened and equalized the responses of each loudspeaker such that, for each loudspeaker, the standard deviation of the magnitude spectrum across the .2-25 kHz calibrated passband was <1 dB. The responses rolled off by 10 dB from 25 to 40 kHz.

Stimuli consisted of sequences of noise bursts generated in real time by gating a continuous Gaussian noise source generated by the TDT RZ6 digital signal processor. Each noise burst was 20 ms in duration and gated with raised cosine functions with 1-ms rise and fall times. The noise presented from each speaker was filtered with the corresponding speaker correction filter. Each sequence was presented with a rate of 5 s^{-1}; the aggregate presentation rate for both sequences was 10 s^{-1}. All sounds were presented at 60 dB SPL during data collection. Target sound sequences were presented with two temporal patterns, referred to as rhythm 1 and 2. Each rhythm was 1200 ms in duration. Each trial began with one to five continuous sequences of rhythm 1; the number of continuous sequences of rhythm 1 were varied from trial to trial. The presentation of the rhythm 1 sequence was followed in each trial by a rhythm 2 sequence

repeated 1.5 times. Rhythm 1 transitioned into Rhythm 2 without interruption. Target sounds were interleaved in time with a masker sound sequence. The masker sound sequence was spectrally identical and exactly complementary to the target sound sequence, such that when both target and masker sound sequences were co-located at 0°, that pattern was undistinguishable from a continuous sequence of noise bursts with a rate of 10 s^{-1}. Two light-emitting diodes (LEDs), colored blue and green, were positioned at 0° azimuth below the loudspeaker and used to signal that the cat could initiate a trial (green) or to indicate time-out periods (blue).

Behavioral Task and training procedure

The behavioral task and training procedures used in this study were modeled after the procedure used by Javier et al. (2016). Each trial was initiated by a researcher who monitored the activity of the cat on through a video. Initiation of each trial by the researcher illuminated the green LED placed below the 0° speaker and signaled the cat to depress a pedal which initiated the sound stimuli. When the cat pressed the pedal, the green LED was deactivated and the Rhythm 1 began to play. The signal sequence was always presented by a source fixed at 0°. The complimentary masker sequence, interleaved in time with the signal sequence, varied in source location from trial to trial. After a variable hold time, the target sequence changed from rhythm 1 to rhythm 2, and the cat was required to release the pedal when this change occurred to receive a food reward. The duration of sequences of rhythm 1 varied from 1200 ms to 6000 ms in 1200 ms increments—these were labeled as Hold times of 2 through 5. Performance on each trial was scored based on the latency of pedal release time relative to the first sound burst that differed from rhythm 1. This sound burst occurred 600 ms after the change from rhythm 1 to rhythm 2. From stimulus onset to 1200 ms prior to onset of this sound burst, pedal releases were scored as "early releases". Pedal releases that occurred in the 1200 ms to 0 ms time window prior to the

first rhythm 2 sound burst were scored as “false alarms”. The early release time window varied depending on the hold time, whereas the duration of the false-alarm window was constant across hold times, thereby equalizing the probability of a chance pedal release during the false-alarm window. Starting from the first sound burst that was definitive of rhythm 2, the cats had a 1200 ms time window to release the pedal for the trial to be scored a “hit”. Release times after this 1200 ms time window were scored as “misses”. In a “hit” trial, immediately following the pedal release, the pneumatic feeder system raised and delivered a small amount of pureed cat food (Purina Friskies) as a reward. All other trials were followed by a flashing blue light lasting four seconds signifying a time out. During a time out, no sound stimulus was presented, and new trials could not be initiated. Trials with hold times of 3, 4, and 5 were considered catch trials for trials with hold times of 2, 3, and 4, respectively. That is, a hit or miss on a trial with a hold time of 4 was also considered a correct rejection (not a false alarm) of the hold time of 3. Hits at the longest hold time were rewarded but not considered for analysis. This allowed us to collect a roughly equal number of catch and non-catch trials, which in turn allowed us to potentially collect a hit or miss and false alarm data point in each trial (except for Hold 5 trials). Figure 1.1 displays an example of the hold 2 condition. The target pattern is represented by blue bars, and the masker pattern is represented by the yellow bars. In hold time 2, the rhythm change occurs at 2.4s post sound onset. The first burst that is different from Rhythm 1, and therefore definitive of Rhythm 2, occurs 600 ms after the onset of Rhythm 2. For a Hold 2 condition, this means the first burst occurs at 3s post sound onset. This definitive burst also marks the beginning of a 1200 ms hit window. Task training consisted of presentation of the target sound sequence without the competing masker sequence. Further, rhythm 2 was presented at a sound level 10 dB higher than rhythm 1. In this phase, cats were rewarded for detected the change from rhythm 1 to rhythm 2

based on sound level or the temporal pattern. As cats became proficient in this task, the sound

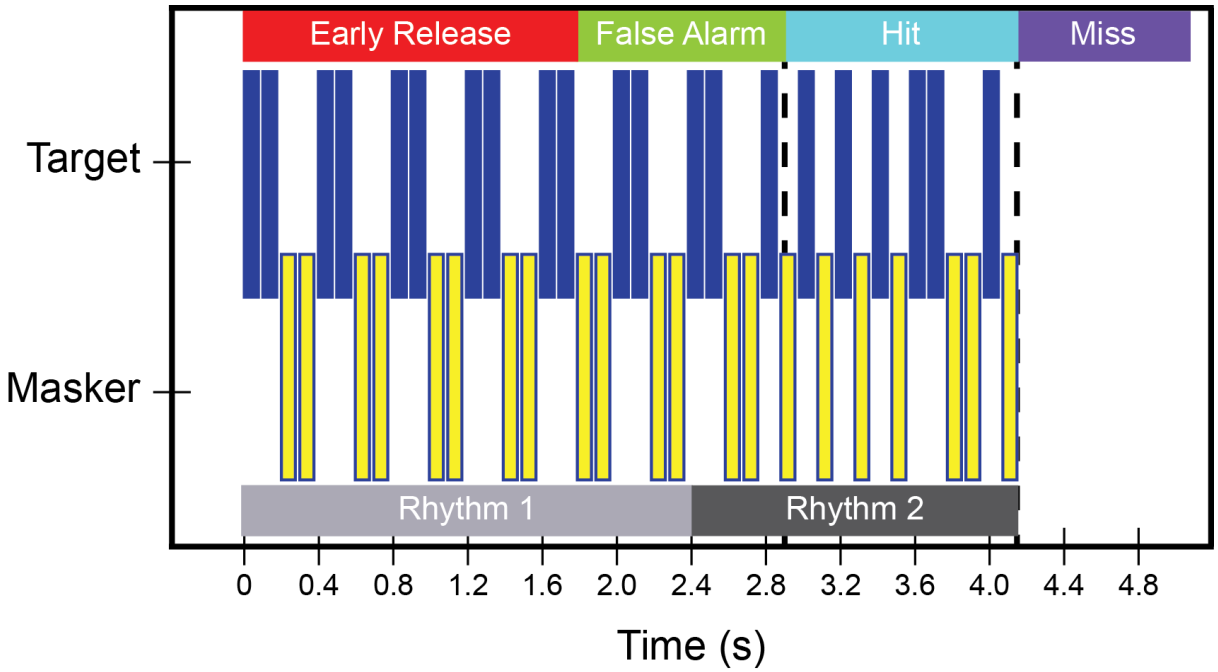

Figure 1.1. Stimulus for spatial stream segregation task. Figure 1.1 illustrates an example of a Hold 2 condition. The target and masker were interleaved in time, and the masker pattern remained complementary to the target pattern throughout the stimulus. Blue bars represent the target pattern, and yellow bars represent the masker pattern. The cat pressed a pedal to begin the presentation of Rhythm 1. Rhythm 1 was presented for 2.4 s, and the earliest detectable change occurred 600 ms after the onset of Rhythm 2. Pedal releases 1200 ms window prior to the first detectable change were scored as "False Alarms", and releases earlier than the false alarm window were scored as "Early Release". The hit window lasted for 1200 ms, and pedal releases in that time window were scored as "Hits" and produced a food reward for the cat. Pedal releases after the end of the hit window were scored as a "miss".

level difference was lowered until the sound levels of rhythms 1 and 2 were the same, and only the change in the temporal pattern was detectable. In the next phase, the masker sequence was introduced at the farthest sound separations (±80°), at a sound level 10 dB lower than the signal sequence. As task performance improved, the masker separation was gradually lowered to include all sound source locations, and the masker level was gradually increased until it was equal to the signal level. Hold times were varied randomly in all phases of training. After cats could reliably perform the task with these stimulus parameters, the task was presented with randomized masker locations.

Each training session lasted for at least 15 minutes, and up to as long as the cat was willing to work, typically 30 minutes each day. The training period varied for each cat, ranging

from 6 – 9 months among the three animals. Data collection lasted 8 months – 1 year depending on the cat.

Data Analysis

Performance on trials was measured by calculating the discrimination index, *d'* for each masker location (Green & Swets, 1966). For each masker location, *d'* was defined as:

$$d' = z(P_{hit}) - z(P_{false\ alarm})$$

The proportion of hits (P_{hit}) was given by the number of hits divided by the number of hits and misses across trials with hold times of 2, 3 and 4. The proportion of false alarms ($P_{false\ alarms}$) was given by the number of false alarms divided by the number of false alarms, hits, and misses across trials with hold times of 3, 4, and 5. Proportions of hits and false alarms were then transformed to *z*-scores, and the difference in *z*-scores yielded the discrimination index, *d'*. In conditions where P_{hit} was 1, or $P_{false\ alarm}$ was 0, the *z*-score was undefined and the proportion of hits or false alarms for N trials were expressed as $(N - ½)/N$ or $(½)/N$, respectively (Macmillan & Kaplan, 1985). Values of *d'* for each cat were calculated for each masker location. Rhythmic masking release (RMR) thresholds were calculated by plotting *d'* values as a function of masker locations. Then, the masker location at which the interpolated line of *d'* values crossed a threshold of *d'=1* was used as the rhythmic masking release threshold.

Results

After full training, animals performed the hold-release task enthusiastically in each session. All animals displayed high hit rates for the broader target/masker separations, and declining performance for the narrower target/masker separations. Performance for all cats declined to chance when the target and masker were co-located (i.e., 0° target/masker separation).

Figure 1.2 displays distributions of pedal release times relative to the onset of sound sequences. The different rows indicate the four hold times—the different durations of the presentation of Rhythm 1 prior to the change to Rhythm 2. Each distribution displays the counts of trials scored as early release (red), false alarm (green), hit (blue), and misses (purple). All misses are grouped together in a single bar—pedal release times were not measured following the end of the hit window, and all pedal releases after the 1200 ms presentation of Rhythm 2 were scored as misses. The four different hold times were presented randomly from trial to trial to confound efforts to score a hit and obtain reinforcement by releasing the pedal at a constant latency. The miss rates in the histograms are somewhat inflated because the plots include trials across all target/masker separations, including 0° separation trials in which stream segregation was not possible.

For each animal, the number of pedal releases were relatively low during the presentation of Rhythm 1 and rose sharply as the stimulus pattern changed to Rhythm 2, indicating a release in the correct time window. The number of false alarms typically increased with increasing hold times, which we attribute to a general impatience in anticipation of the food reward. Similarly, early releases also increased with longer hold times, and more early releases

can be observed in the latter half of the early release window across all animals. Most pedal releases in the hit window occurred in the first half of the duration, indicating that the

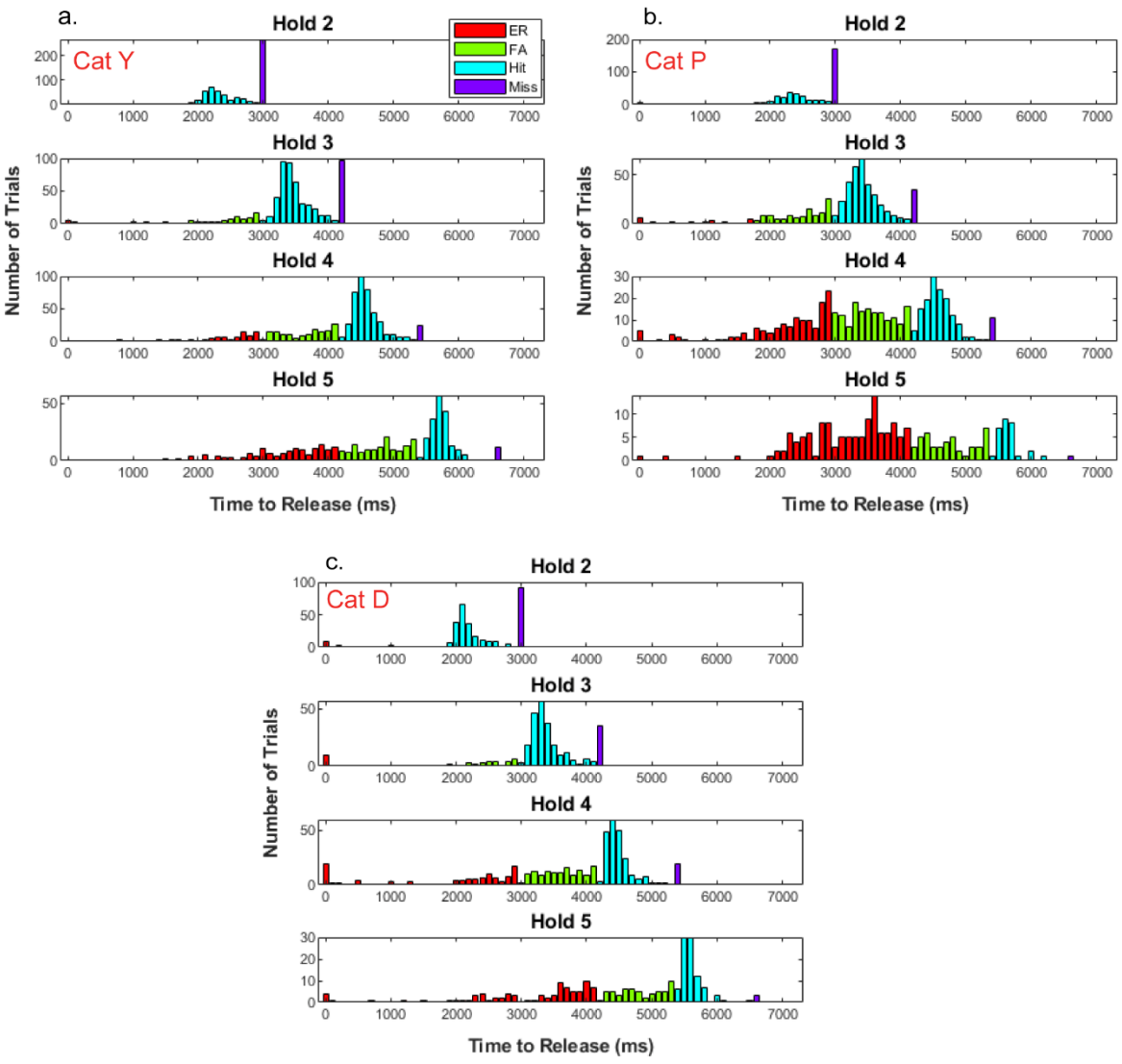

Figure 1.2. Latency to pedal release values for each hold time. Figure 1.2 displays the latencies for pedal release for each cat (Cat Y: Figure 1.2a; Cat P: Figure 1.2b; Cat D: Figure 1.2c). Each row of panels displays all scored trials for different hold conditions; each panel represents a particular hold time, as indicated. The histograms display scores across all trials; different colors of bars denote trials scored as "early release" (red), "false alarm" (green), "hit" (blue), and "miss" (purple).

animals were able to detect the increased duration between bursts that characterized Rhythm 2 and did not have hear the entire Rhythm duration before recognizing the change and releasing the pedal. The distributions of pedal release latencies also highlight different approaches taken

by each animal in completing this task. Specifically, Cat Y (Fig. 1.2a) and Cat D (Fig 1.2c) displayed a general willingness to wait for the Rhythm change, and most pedal releases by these

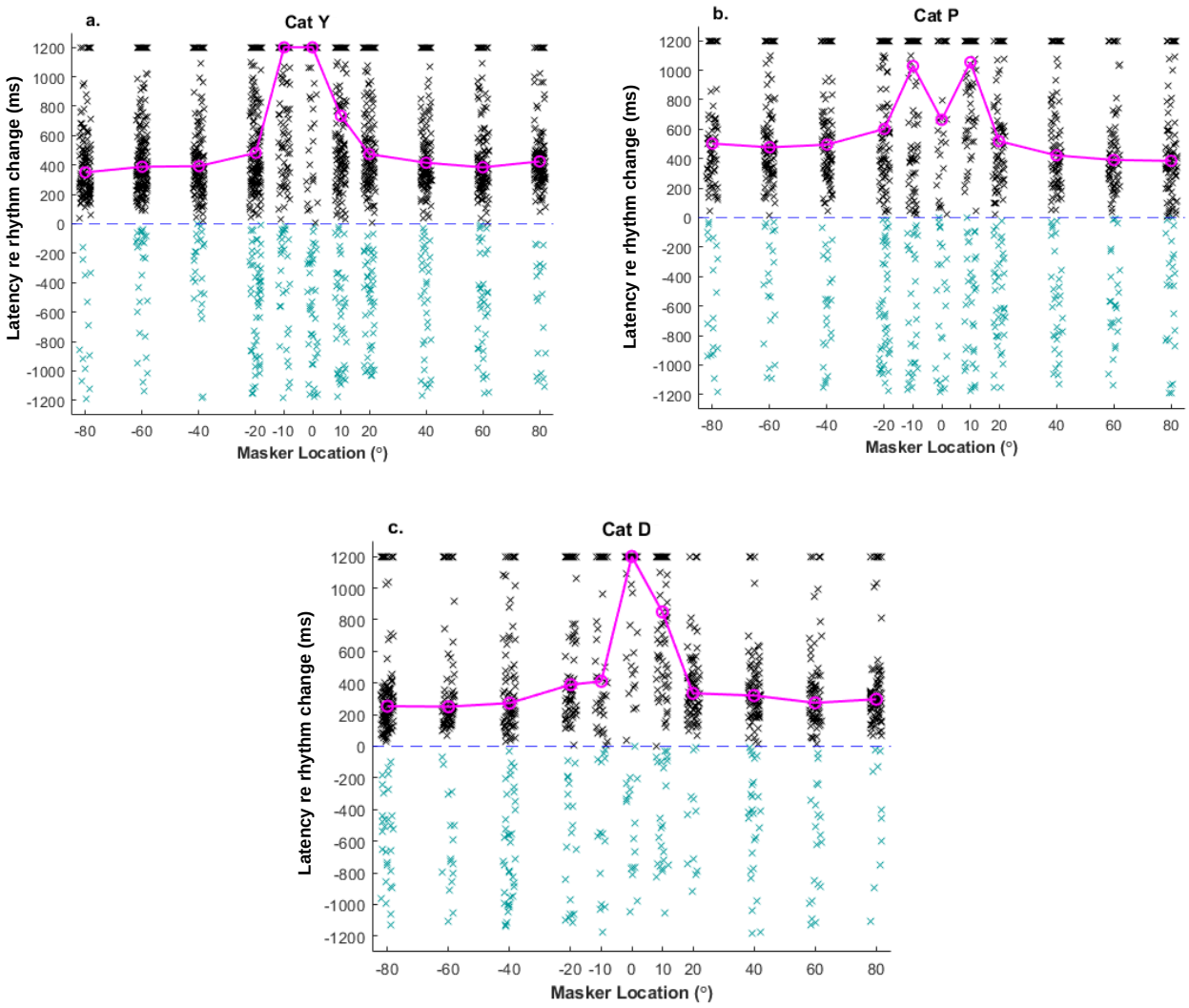

Figure 1.3. Latency re rhythm change values as a function of masker location. Figure 1.3a, 1.3b, and 1.3c display the latencies to pedal release for Cat Y, Cat P, and Cat D, respectively. Individual x symbols represent trials that were scored as "hits" (black) and "false alarms" (blue). The target was always located at 0° in azimuth; the x axis represents trials with different masker locations. The dashed blue horizontal line represents the presentation of the first discernable burst of Rhythm 2 and start of the "hit" time window—pedal releases that occurred up to 1200 ms after this point were scored as "hits" and releases up to 1200 ms before this point were scored as "false alarms". The magenta curve represents the median latencies of "hit" responses.

animals occurred after the change to Rhythm 2. In contrast, Cat P (Fig 1.2b) was displayed a general impatience at Hold times of 4 and 5, and more often released the pedal prior to the change to Rhythm 2.

Figure 1.3 displays the distributions of latency to pedal release as a function of target/masker separation; the data are aggregated across Hold times. In each figure, the dashed blue line indicates the onset of Rhythm 2—black marks above the blue line indicate pedal release in the hit window, and cyan marks below the blue line indicate pedal releases in the false alarm time window. Medians for pedal releases in the hit time window are plotted by the magenta line for each target/masker separation. For each cat, the largest latency for pedal release occurred at a separation of 0°, where stream segregation was not possible. Increased latencies are also seen in target/masker separations of 10°, which approaches the threshold separation for these cats to perform stream segregation in this task. Further, at narrower separations, the number of false alarms increased, and pedal release times for hits were scattered across the time window, with a majority of hits occurring in the latter half. Increased latency to pedal release at narrow masker separation are likely explained by the increased difficulty in the task for the animals. At the farther target/masker separations (±80°, ±60°), there are few false alarms and a high number of hits, with pedal releases largely occurring in the first half of the hit window.

Figure 1.4 displays the percentage of hits (left column, red curve), false alarm rate (middle column, blue curve), and the discrimination index values (right column, black curve) for each animal. Each row represents one animal. All display strong performance at the farthest target/masker separation, and performance near chance at the narrowest target/masker separations. False alarm rates also increase at the narrowest target/masker separation. This is

likely due to the cat's difficulty in segregating target and masker streams during the period of Rhythm 1 presentation, leading to more guessing by the animals.

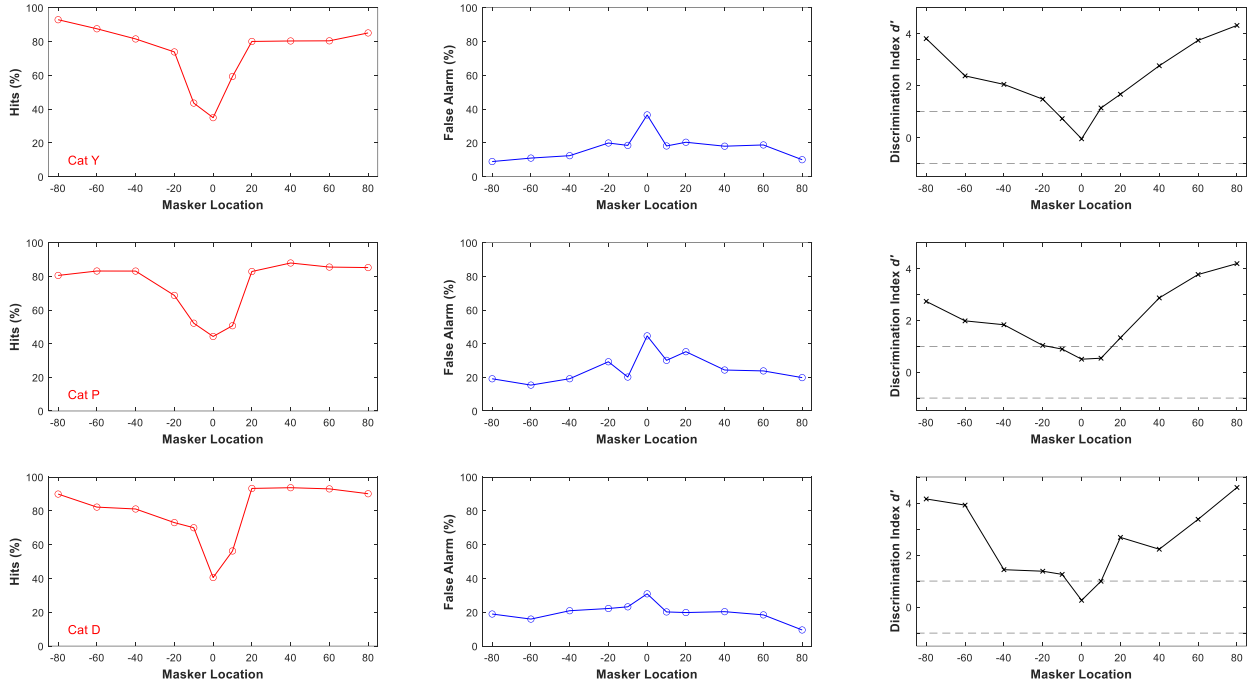

Figure 1.4. Task Performance based on masker location. Figure 1.4 displays task performance for each cat as a function of masker location. The target pattern was always presented from 0° in azimuth. The three columns represent the percentage of trials scored as "hits" (left column, red curve), "false alarms" (middle column, blue curve), and the discrimination index *d'* (right column, black curve). Each row represents the performance for one individual cat. The dashed black horizontal lines in the right column represent the threshold for significance for discrimination index values (*d'* = ±1).

For all cats, the discrimination index is near chance (*d'* = 0) for the target/masker separation of 0° and increased sharply with increasing separation between the two sound sources. Cat Y and Cat D displayed *d'* values at or greater than 4 at the farthest target/masker separations, indicating very strong performance. It is interesting to note that although Cat P was generally impatient at the longer hold times, performance for this animal was still strong at the farther masker separations and approached the performance of the more patient animals in the left hemifield. The median threshold of separation across all three animals for significant

discrimination index values (i.e. $d' > 1$) was 9.8°. This result is in accordance with past studies measurements of feline listeners in the same behavioral task (Javier et al., 2016).

Discussion

We evaluated the performance of three cats engaged in a spatial stream segregation task. Cats were able to reliably perform the task and displayed strong performance consistent with previous findings with similar stimulus conditions (Javier et al., 2016).

Spatial Stream Segregation in Psychophysics

Stream segregation using spatial cues has been demonstrated previously in our laboratory in cats (Javier et al., 2016). In their work, Javier and colleagues manipulated stimulus bandwidths in different conditions to limit spatial cues available to listeners performing the stream segregation task. The cats in our study matched the task performance of the animals reported in Javier et al., (2016) with the same broadband stimuli, suggesting that they successfully learned the hold/release task, and likely used similar ILD cues to drive their acuity in for spatial stream segregation. Spatial stream segregation has also been explored in our laboratory in human listeners (Middlebrooks and Onsan, 2012). Results from that study demonstrate that human listeners have greater acuity in a spatial stream segregation task when ITD fine structure cues were available. In contrast to feline listeners, performance in conditions in which ITD fine structure cues were available matched conditions with broadband noise, and performance where only ILD cues were available was diminished.

The cats in this chapter were trained with the eventual goal of understanding the physiological correlates of spatial stream segregation in the awake primary auditory cortex. Stream segregation based on spatial cues has been explored in the primary auditory cortex of cats in anesthetized conditions in our laboratory (Middlebrooks and Bremen, 2013). Neurons in the anesthetized cortex of cats synchronized to one of two interleaved competing broadband noise burst rhythms with as little as 10° degrees of spatial separation. The cats in this study were

similarly able to perform stream segregation with 10° degrees of spatial separation between the target and masker rhythm in a psychophysical task. The following chapters of this dissertation will focus on spectral and temporal properties of the awake cat auditory cortex (Chapter 2), and how the base properties influence streaming in physiological of cortical neurons in idle conditions (Chapter 3).

Chapter 2
Spectral and Temporal Response Properties of the Awake Cat Auditory Cortex

Introduction

The basic coding properties of the primary auditory cortex (area A1) have been studied primarily in anesthetized animals. The responses of a neuron to pure tones of varying frequency and sound level are given by its frequency response area (FRA). Neurons in the primary auditory cortex (A1) of anesthetized animals typically show V-shaped FRAs with sharpest frequency tuning around the characteristic frequency (CF) near threshold. At moderate sound levels, e.g. 40 dB above threshold, FRAs typically broaden, ranging from 0.5 octaves to >2 octaves (Cheung et al., 2001; Heil et al., 1992; Kajikawa et al., 2005; Moshitch et al., 2006; Philibert et al., 2005; Schreiner & Sutter, 1992). Cortical neurons in anesthetized conditions also are limited in their representation of temporal properties of sounds. Phase locking of response to amplitude-modulated sounds is limited to rates substantially lower than is seen at sub-cortical levels. In anesthetized cats, for example, phase-locking of cortical neurons to clicks is rarely observed at rates higher than ~25s^{-1}, and most are limited to rates of 20 s^{-1} or lower (Lu & Wang, 2000; Eggermont, 1998). Non-synchronous coding—tonic firing of neurons that increases with increasing sound presentation rate — is not seen in the auditory cortex in anesthetized conditions (for review, see (Wang, 2007).

A series of studies of the auditory cortex in awake marmosets has demonstrated distinctive spectral and temporal sensitivity that is not seen in cortical recordings in anesthetized cats. In addition to V-shape FRAs, the awake marmoset cortex exhibits I-shape and O-shape FRAs (Bartlett et al., 2011; Sadagopan & Wang, 2008), which were first described in the brainstem in decerebrate cats (Ramachandran et al., 1999; Young & Brownell, 1976). The I-

shape FRAs maintain a narrow, relatively constant frequency bandwidth across a wide range of sound levels. The O-shape FRAs exhibit even sharper spectral tuning as well as a response limited to a narrow range of sound levels. Cortical neurons in the awake marmoset also can show tonic responses to tones throughout the duration of a sound, in contrast to the typically onset-only response in anesthetized cats (Wang et al., 2005; Zurita et al., 1994). Marmoset neurons can phase lock to clicks at rates up to >40 s^{-1} (Lu et al., 2001b), in contrast to anesthetized cats in which phase locking beyond 25 s^{-1} has rarely been observed. Neurons in the marmoset also display non-synchronized rate coding—non-synchronized neurons can response with tonic firing rates that increase with stimulus modulation rates up to 330 s^{-1}.

The Wang lab has hypothesized that the distinctive properties for coding sound spectra and timing seen in the auditory cortex in awake marmosets might be unique specialization for representing that species' rich vocal repertoire (Sadagopan & Wang, 2008; Watkins & Barbour, 2011). Further, it has been suggested that sharp spectral tuning can be blurred by the use of multi-unit recordings in past investigations (Sadagopan & Wang, 2008).

Here, we tested the alternative hypothesis that many of the features observed in the marmoset are instead general properties of the auditory cortex that have been obscured in previous studies by the use of general anesthesia. We used chronically implanted recording arrays to record from cortical area A1 in alert cats. Pure-tone stimuli that were varied in frequency and level revealed V-, I-, O-shape FRAs like those seen in awake marmosets, with frequency bandwidths often narrower than 0.2 octaves. Similar FRA characteristics were recorded both in isolated single units and in undifferentiated clusters of 2 or more units. That observation suggests that nearby neurons share common FRA shapes. Click trains varying in rate were used to assess the temporal coding properties of the alert cat cortex. Single and multiple

units exhibited phase locking to click rates as high as 226 s^{-1}. We also observed non-synchronized rate coding in response to all presented click rates. These results suggest that the remarkable array of spectral and temporal coding observed in the marmoset auditory cortex may be a general property of the unanesthetized mammalian cortex.

Methods

Overview

Extracellular spike activity was recorded with multi-channel recording arrays chronically implanted in the primary auditory cortex (area A1) of 12 cats. Seven of the cats (2 female and 5 male) were trained in an auditory psychophysical task (spatial stream segregation; Javier et al., 2016 and Chapter 1). The results in the present report, however, were obtained entirely during non-task conditions. That is, the response pedal and automatic feeder were removed from the apparatus, and the cat was given small amounts of food intended to keep it alert and oriented toward the center of the coordinate system.

Animal Preparation

All procedures were conducted in accordance with the National Institute of Health guidelines and with the approval of the Institutional Animal Care and Use Committee for the University of California—Irvine. Twelve domestic shorthair cats (*Felis Catus*), 9 males and 3 females, were obtained from a breeding colony at the University of California at Davis. In each animal, a chronic multi-site recording array, described below, was implanted in the auditory cortex using aseptic procedures. During surgery, anesthesia was induced with ketamine (25 mg/kg), maintained during surgery with isoflurane in 100% oxygen delivered through an endotracheal tube and its concentration adjusted as required to maintain an areflexive state. Surgery began with a midline scalp incision and the exposure of the underlying skull. Skull and cortical landmarks were used to determine the location of the right auditory cortex, and a craniotomy was performed. The dura mater was opened over the middle ectosylvian gyrus, and the chronic recording array was implanted in the primary auditory cortex (A1) using a micromanipulator. Recording sites on the array connected with a flexible cable terminating in a

percutaneous connector mounted on the skull near the midline. A stainless-steel protective cylinder (1.5 cm in diameter) was placed over the connector. The exposed brain surface was covered with silicone rubber (Kwik-sil, World Precision Instruments) and then with methacrylate cement. Stainless-steel screws were inserted into the skull near the midline to anchor the methacrylate cement and the cylinder. After approximately two weeks of recovery, we began physiological recordings for a period of several weeks to several months.

Experimental apparatus, stimulus generation, and data acquisition.

Experiments were conducted in a double-walled, sound-attenuating booth (Industrial Acoustics; inside dimensions: 2.6 x 2.6 x 2.5 m) lined with 60-mm-thick absorbent foam (SONEXone). A circular hoop, 1.2 m in radius, supported 8.4-cm-diameter two-way loudspeakers in the horizontal plane at 0° and 40° contralateral relative to the electrode placement in the animal's right hemisphere. During recording, the animal sat or stood on a raised pedestal adjusted in height to center the cat's head in the array of the loudspeakers. A harness restricted the animal to the pedestal but allowed free movement of the limbs and head.

Stimulus generation and data acquisition used System III hardware from Tucker-Davis Technologies (Alachua, FL). Custom MATLAB software (Mathworks; Natick, MA) on a Windows-based computer controlled the stimulus presentation, acquired the neural waveforms, and allowed on-line monitoring of responses. Sounds were generated at a sample rate of 97,656 s^{-1} with a 24-bit precision. Loudspeakers were calibrated in the absence of the cat using a precision ½" microphone (ACO Pacific) positioned at the center of the chamber at the normal location of the animal's head. Golay codes were used as broadband probe sounds (Zhou et al., 1992). The calibration procedure for broadband stimuli yielded a 1029-tap finite-impulse-response correction filter for each speaker. The filters flattened and equalized the responses of

the loudspeakers such that, for each loudspeaker, the standard deviation of the magnitude spectrum across the .2-25 kHz calibrated passband was <1 dB. The responses rolled off by 10 dB from 25 to 40 kHz. Tonal stimuli were calibrated using pure-tone bursts in 1/24 octave intervals.

Extracellular neural spike activity was recorded with N-Form 32-channel chronic recording arrays from Modular Bionics (Berkeley, CA). Each array consisted of four parallel shanks, each containing eight recording sites. The shanks were either of equal length at 3 mm or staggered lengths, with two shanks at 2.5 mm and two shanks at 3.5 mm, arranged on corners of a rectangle .8 μm or 1.0 mm in the medio-lateral dimension and .8 μm or 1.5 mm in the rostro-caudal dimension. Recording sites were spaced in 250 μm intervals along each shank. The sites consisted of the cut ends of 25-μm-diameter platinum wires that were coated in activated iridium. Waveforms were recorded simultaneously from 32 sites using high-impedance headstages and multichannel amplifiers from Tucker-Davis Technologies. Waveforms were filtered, digitized at a 25 kHz sampling rate, and stored to computer disk for off-line analysis.

Experimental procedure

Frequency response areas (FRAs) were measured using pure tones. Tones were 100 ms in duration with 5 ms raised-cosine onset and offset ramps, presented at a repetition rate of ~1.7/s from the contralateral 40° loudspeaker. Study of the set of 32 recording sites in each animal began with a coarse estimate of FRA using 1/3-oct steps of frequency and 10-dB steps of sound level. The frequency that yielded the lowest threshold at each site was taken as that site's characteristic frequency (CF). Once a range of CFs was acquired for all active sites, FRAs were measured at a higher resolution consisting of tones typically 1 octave below and 1 octave above the estimated CF range in 1/6- or 1/12-octave steps in frequency and steps of 5 dB in level, typically from -30 to 70 dB SPL. Each combination of frequency and level was presented once in

a random order, and then again in a different order, and so on for a total of 10 presentations of each stimulus condition. In addition to the 100-ms tones used for FRA measures, sustained responses of neurons in 9 cats were tested with long-duration tones, 5 s in duration. In those measures, tones were presented only at the sound level that elicited a maximum response, and frequencies were in 1/6-octave steps from 1/2 octave below to 1/6 octave above the previously measured CF.

Responses of neural synchrony to periodic sounds were tested with trains of clicks. The click trains were 1 s in duration, presented at rates of 5 to 320 s^{-1} every 1.5 s. Click trains were presented from 0 or contralateral 40° loudspeaker locations; usually both locations were tested in separate blocks of trials.

Data analysis

We aimed to compare spectro-temporal sensitivity in the auditory cortex of alert cats with that in previously published reports studies of the awake marmoset (Lu et al., 2001; Wang et al., 2005; Bartlett et al., 2011). For that purpose, qualitative measures of response are patterned largely after those described by those previous reports

Data analysis began with off-line identification of neural action potentials ("spike-sorting"), as described previously (Middlebrooks, 2008). Responses were classified as well-isolated single units when they met the following criteria: (1) the majority of inter-spike intervals were >1 ms; (2) the waveform appearance was consistent upon visual inspection; (3) the histogram of spike amplitudes showed a peak that was distinct from other activity. Multiple-unit recordings consisted of spikes from two or more undifferentiated neurons. Except when stated otherwise, "unit" refers collectively to single- and multiple-unit recordings. Sound-evoked unit

responses were recorded at 105 sites in 12 array placements. Non-responsive sites were assumed to be located in non-responsive cortical layers or outside of targeted auditory areas.

Frequency sensitivity was quantified as FRAs that consisted of mean spikes rates as a function of sound frequency and level. Consistent responses to pure tones were obtained from 102 units in 12 awake cats. The sound-level and frequency selectivity of the FRA for each unit were quantified by characteristics of the level profile at the best frequency (BF) and frequency profiles at multiple sound levels. Prior to any analysis of FRA properties, the spontaneous rate was subtracted from the neural response rate, and a threshold was applied corresponding to 20% of the maximum response rate. Analyses of FRAs were conducted for the time range of 10–110ms post stimulus onset; that time window allowed for ~4-ms travel time from the sound source to the cat and a minimum latency for neural condition from the ears to the cortex. The characteristic frequency for each unit was computed by finding the frequency that elicited a reliable response at the lowest sound level and at a level 10 dB higher; the lower of those two levels was taken as the threshold. The best frequency for a unit was computed by taking the mean response across all levels and calculating a response-weighted centroid for the frequency tuning curve. The best level for a unit was then found by computing Hann-weighted level profile across 3 frequencies centered on the BF. The best level was taken as the sound pressure level at the peak of this level profile. The level profile was further characterized by the monotonicity index. The monotonicity index was calculated as the spike rate at the highest tested sound level divided by the maximum spike rate across all levels tested. Prior to the calculation of the monotonicity index, the spontaneous rate was subtracted, and a threshold correspond to 20% of the maximum response rate was applied. Monotonicity index values could range from 0 to 1: a

value of 0 indicated a low spike rate at the highest level tested, and a value of 1 indicated that the spike rate at the highest level was the maximum spike rate.

Frequency sensitivity of units was represented by the bandwidth computed from frequency contours measured at constant sound levels. The bandwidth at a particular sound level was evaluated by computing the area of the spike-rate-weighted frequency profile at that level, forming the rectangle having the same area with height equal to the maximum spike rate, and taking the width of that rectangle. Bandwidths were computed at the best level, the maximum tested sound level, and at values 10 and 40dB above threshold. In instances at which there was no response at a particular sound level, the bandwidth was recorded as 0 oct. Following Sadagopan and Wang (2008), we also computed a shape index. The shape index was taken as the bandwidth at the maximum level presented, divided by the bandwidth at the best level. The mean spontaneous rate was removed, and a threshold correspond to 20% of the maximum response rate was applied prior to the calculation of bandwidth and shape index values.

A sustained response index was computed to characterize the time course of response to unmodulated tones. The sustained response index was defined as the spike rate at the best frequency and best level in the second half of the tone duration (60 – 110 ms) divided by the spike rate in the initial part of the stimulus duration (10-60 ms) for short duration (100ms) tones. For long duration tones, a long duration sustained index was defined as the spike rate in the second half of the tone duration (2510 ms – 5010 ms) as a proportion of the spike rate of the initial part of the stimulus duration (10 ms to 60 ms). Prior to the calculation of sustained response index values for short and long duration tones, the mean spontaneous rate was subtracted from the response; rates that were negative after subtraction of the spontaneous rate

were set to 0. The 20% threshold applied for FRA tuning analysis was not applied in the calculation of the sustained response index for short and long duration tones.

We evaluated coding of temporal properties of stimuli by quantifying the spike rates and spike timing of responses to click trains at various rates. Responses of units to the click trains were tested by comparing spike rates in the 100-ms interval prior to sound onset with rates in the 1000-ms interval beginning 10 ms after the click-train onset (10ms-1010ms). Spike rates in the two intervals were compared with a two-tailed Wilcoxon rank sum test. Also, a Kruskal-Wallis test was used to test whether response rates in the 10-1010ms-post-onset interval varied significantly with click rate. Units that showed significance in either test ($p<.05$) and showed adequate spike isolation were considered for further analyses; 105 units met those criteria. Analysis of stimulus synchrony of spikes was based on the response interval from 100 – 1010ms post stimulus onset; that time window excluded the response to the first click in each click train. For analysis of synchrony, each spike was treated as a unit vector oriented with respect to the stimulus phase. Vector strength was calculated by taking the sum of the unit vectors and calculating the mean length of the resultant (Goldberg & Brown, 1969). Significant synchrony was indicated through the Rayleigh statistic—the Rayleigh statistic was calculated using the equation $2nr^2$ (Mardia, 1972), where r is the vector strength and n is the number of spikes. A Rayleigh statistic criterion of 13.8 indicated synchronous firing with $p < 0.001$. Significant synchronized response to click trains at rates 5 s^{-1} or higher was observed in 84/105 units, of which 16 were well isolated single units, and 68 were multi-unit sites. The synchronization boundary was defined as the highest click rate to which a neuron synchronized significantly.

Many neurons that failed to synchronize to high click rates could code those click rates with systematic increases in sustained spike rates. A Kruskal-Wallis test was applied to functions

of spike rates versus click rates. When significant, a Bonferroni-corrected *post-hoc* analysis tested for significant increases in spike rates elicited by pairs of increasing click rates. Out of 105 units, 52 represented spike rates by significant nonsynchronous spike-rate coding. The dynamic range of spike-rate coding by each unit gave the range of click rates over which increases in click rates resulted in significant increases in unit spike rates. The bottom of the dynamic range (also referred to as the rate boundary) was given by the lowest click rate beyond which an increase in rate elicited a significant increase in spike. The top of the dynamic range was given by the click rate at the peak of the spike-rate versus click rate function above the rate boundary. The breadth of the dynamic range was given by the difference in octaves between the top and bottom of the range. The depth of spike-rate modulation by click rates was given by the range in spike rates across the dynamic range of click rates as a percentage of the range of spike rates across all click rates.

Results

We measured spectral response properties of neurons in the primary auditory cortex using pure tones 100 ms in duration and varying in frequency and sound level. We measured the ability of neurons to represent rates of periodic stimuli using click trains presented at rates in ½-oct steps from 5 to 320 clicks per second (cps). We recorded responses from the primary auditory cortex of 12 awake cats.

Frequency Selectivity

Across 12 awake cats, we observed eighteen single units and 84 multi-unit sites, a total of 102 units, that had reliable responses to tones. The frequency and sound-level sensitivity of units were represented by FRAs, which recorded mean spike rate as a function of sound frequency and sound level. We classified FRA types as V-, I-, and O-shaped based on visual inspection (following Ramachandran et al., 1999). That classification was confirmed by quantitative measures, presented below. Representative examples of FRAs from one animal are shown as contour plots in Figure 2.1. The V-shaped FRAs (as in Figure 2.1a) showed a generally increasing response magnitude and broadening frequency tuning associated with increasing sound levels. In this example, the BF (7.8 kHz) was substantially lower in frequency than the CF (10.6 kHz), a 0.45-oct difference. There were other instances of differences that great, but across all units BFs averaged only 0.1±0.3 oct lower than CFs. Across all units, median BF values differed significantly from median CF values ($p=2.4e-3$, sign = 24, Sign Test). The I-shaped FRAs (e.g., Figure 2.1b) showed narrow frequency tuning that was essentially constant in bandwidth with increasing sound levels above threshold. Both V- and I-shaped FRAs maintained responses at the highest tested sound levels. The bandwidths at

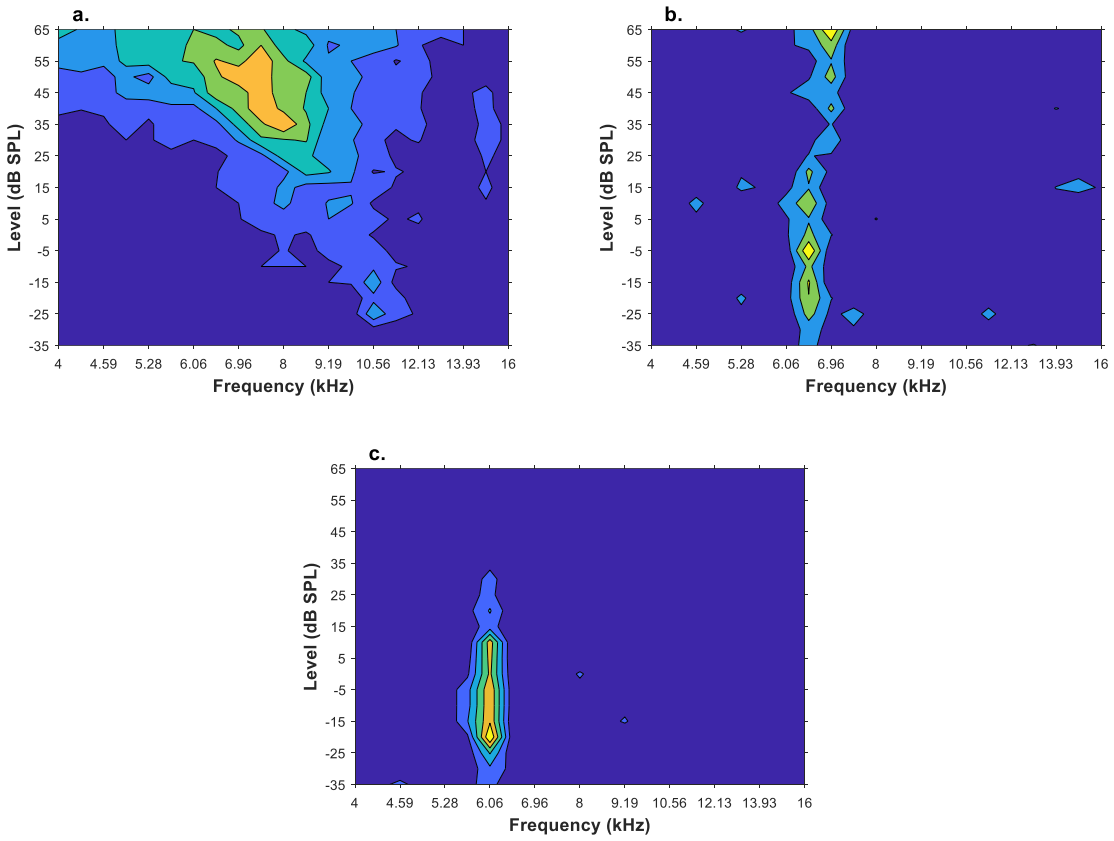

Figure 2.1. Example FRAs from one animal. Frequency response areas (FRAs) from one animal plotted as contour lines. A V-, I-, and O-type response can be seen in figures A, B, C, respectively. Spike rate (color) is plotted as a function of sound frequency and sound level. The V-shape FRA (a) had a best frequency (BF) value of 7.8 kHz, and a characteristic frequency (CF) value of 10.6 kHz. The I-shape FRA (b) had a BF value of 6.5 kHz, and a CF value of 6.5 kHz. The O-shape FRA (c) had a BF value of 6.1 kHz, and a CF value of 6.1 kHz. Units An0104, An0127, An0126.

the highest level were distributed continuously from I- to V-shape FRAs precluding a quantitative distinction between those FRA types. For that reason, V and I FRAs are denoted hereafter as "V/I". The O-shape FRAs (e.g., Figure 2.1c) were characterized by sharp frequency tuning at a particular best level and a response that declined markedly at higher sound levels. The non-monotonic response magnitude as a function of increasing sound level was the principal defining feature of O-shape FRAs, as quantified below.

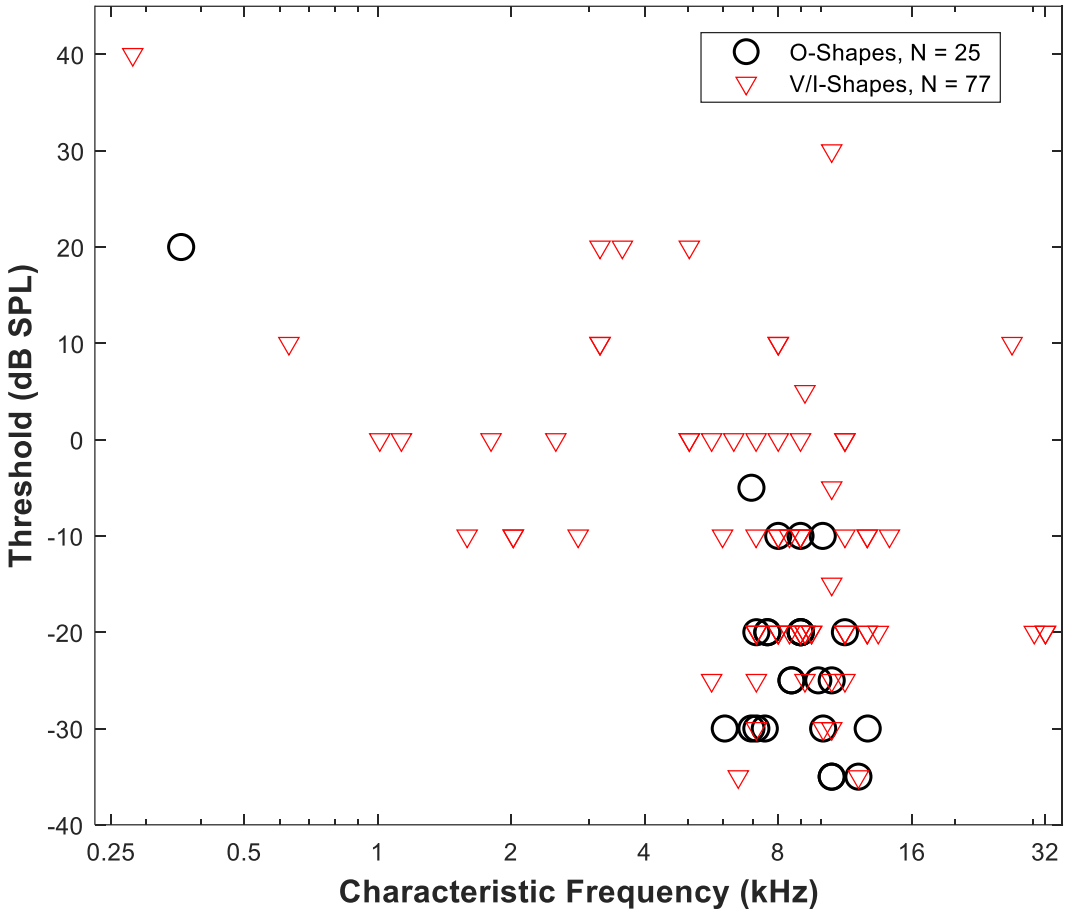

Figure 2.2. Threshold as a function of characteristic frequency. Threshold (dB SPL) values plotted as a function of the characteristic frequency values (kHz). In this and all figures, black circles represent O-shape FRAs, and red triangles represent V/I-shape FRAs. O-shape FRAs had a median threshold value of -25 dB SPL, and a median characteristic frequency value of 8.98 kHz. V/I-shape FRAs had a median threshold value of -10 dB SPL, and a median characteristic frequency value of 8.48 kHz.

Figure 2.2 displays threshold and CF values for V/I- and O-shape FRAs. O- and V/I-shape FRAs had similar distributions of CF values ($p=0.23$, $KS2stat = 0.23$, Kolmogorov-Smirnov Test). Our sample of CFs was largely concentrated within ± 1 oct of 8 kHz (across all units, CF median = 8.6 kHz, geometric mean = 6.9 kHz). That distribution reflects our placement of recording probes on the crown of the ectosylvian gyrus, which is the typical location of the ~8-kHz area of the area-A1 tonotopic map. Also, we avoided electrode placements in rostral A1, where CFs are higher, because such placements might have strayed over the border into the

anterior auditory area (area AAF). The O- and V/I-shape FRAs differed substantially in their distributions of threshold values – the lowest O and V/I thresholds overlapped, but the range of V/I thresholds extended to higher values (p = 4.3e-3, KS2stat = 0.39, Kolmogorov-Smirnov test). The median O unit threshold value was -25 dB compared to a median of -10 dB for V/I unit thresholds.

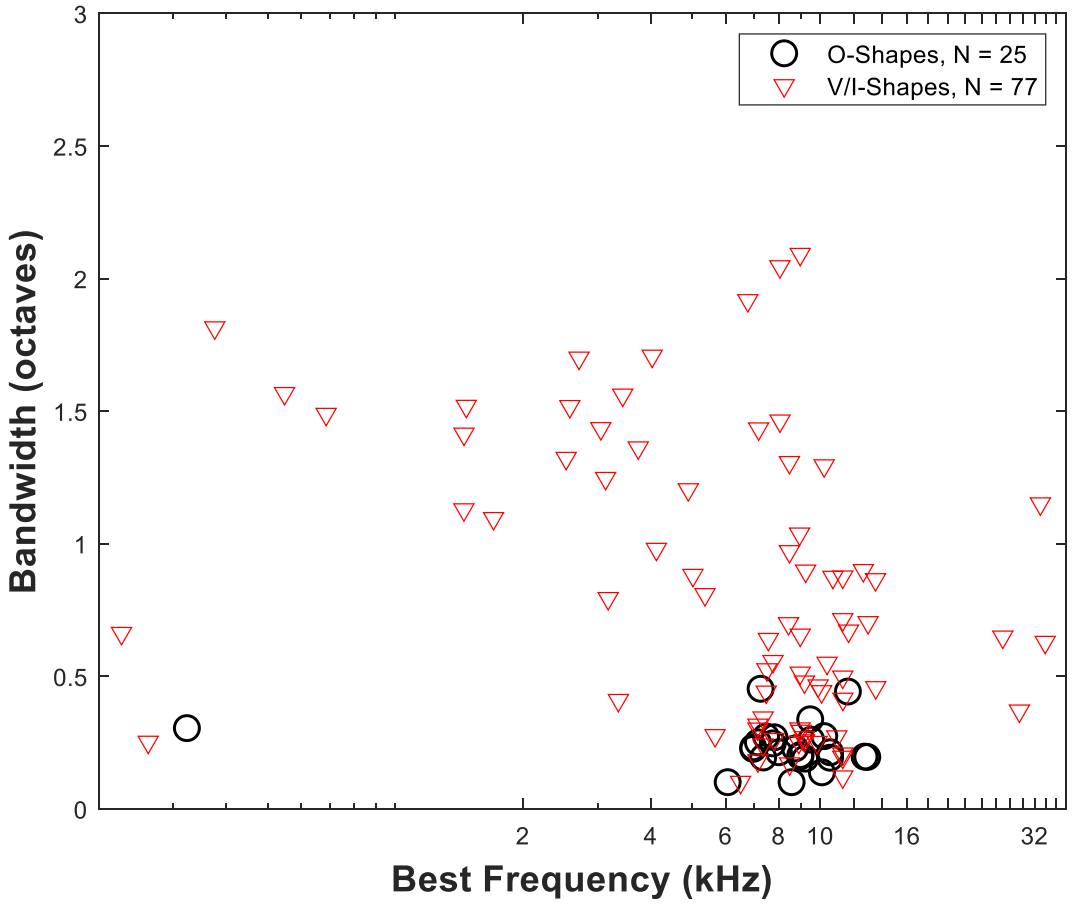

Figure 2.3. Bandwidths as a function of best frequency. Distribution of bandwidth (in octaves) at best level values as a function of best frequency (kHz) values for O- and V/I-shape FRAs. O-shape FRAs had a median best frequency value of 8.73 kHz, and a median bandwidth value of 0.23 oct. V/I-shape FRAs had a median BF value of 8.05 kHz, and a median bandwidth value of 0.67 oct.

We represented the frequency selectivity of units by the bandwidth of each unit computed at its best level; see Methods for the computation of bandwidth. Figure 2.3 illustrates bandwidths as a function of best frequency. The distributions of such bandwidths differed significantly between O and V/I units ($p<10^{-7}$, KS2 stat= 0.68). Nearly all the O units in our sample had BFs in the range of 6-12 kHz (median= 8.7 kHz) and bandwidths narrower than 0.3 oct (median= .23 oct). Some of the V/I units had bandwidths as narrow as those of O units, but the range of V/I

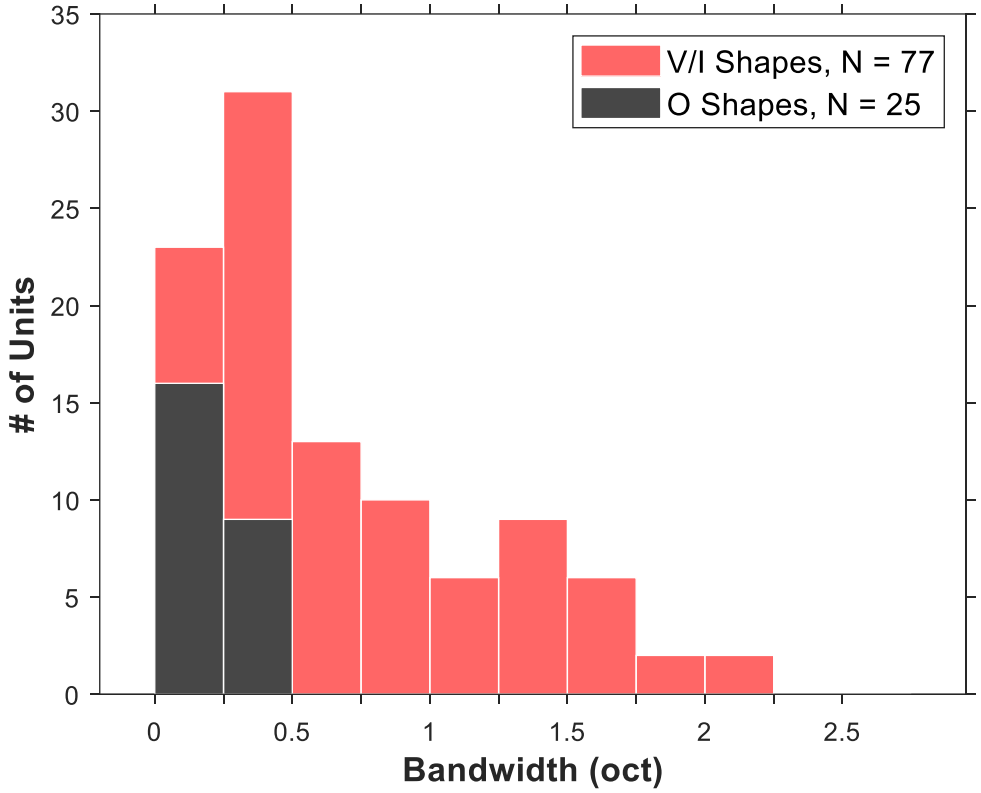

Figure 2.4. Distribution of bandwidths at best level. A stacked Histogram of bandwidth at best level values (in octaves) for O-shape FRAs (black bars) and V/I-shape FRAs (red bars). O-shape FRAs had a median bandwidth value of 0.23 octaves, and V/I-shape FRAs had a median bandwidth value of 0.67 octaves.

bandwidths extended to ~2 oct (median= .67 oct); the median BF of V/I units was 8.0 kHz. The distribution of bandwidth at best level values is shown in Figure 2.4. The median bandwidth of O units was significantly narrower than that of V/I-shape units (p=7.1e-9, ranksum = 543, Wilcoxon Rank-sum).

We observed a correspondence of O- and V/I-shaped FRAs (classified by visual inspection) with particular ranges of bandwidths and monotonicity index values (Figure 2.5). The monotonicity index is a ratio of the response rate at the maximum sound level divided by the

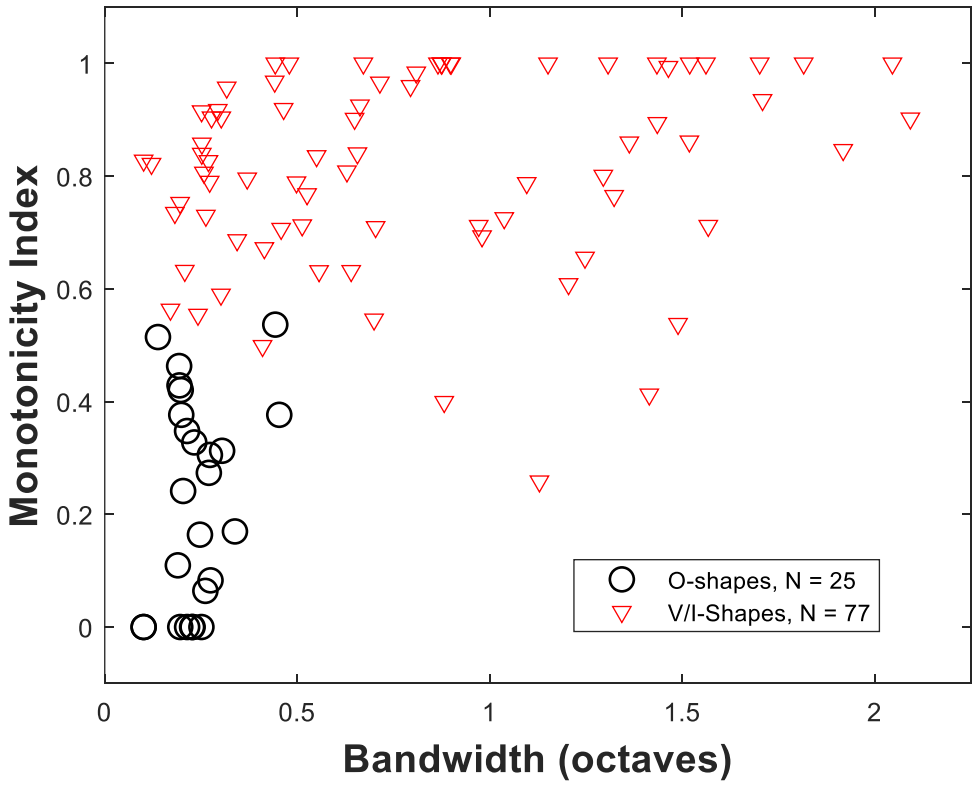

Figure 2.5. Monotonicity Index values as a function of bandwidth. Monotonicity index values plotted as a function of bandwidth at best level values. O-shape FRAs had a median monotonicity index value of 0.24, and V-shape FRAs had a median value of 0.84.

response rate at the best level (see Methods). The O units in our sample had monotonicity values less than ~.5 (median = .24) and most had bandwidths (measured at best levels) ≤ .3 oct. The V/I units had generally higher monotonicity indices (V/I median = 0.84) and bandwidths that ranged from ~.1 to broader than 2 oct. The differences in monotonicity index observed here were to be expected, as non-monotonic level sensitivity was a defining characteristic of the O-shape FRAs. The O units generally responded to narrower ranges of sound level (median range of effective levels = ~47 dB) compared to V/I units (median level range =~59dB); those ranges of effective levels were significantly different for O and V/I units (p = 5.8e-4, ranksum = 845, Wilcoxon-

Rank Sum). A small number of units did not precisely fit those criteria in that they had monotonicity values <0.5 but bandwidths >0.5 oct —those were units judged to be V shapes that showed somewhat patchy FRAs.

A previous study of the marmoset auditory cortex used a "shape index", defined as a ration of the bandwidth at the maximum level presented divided by the bandwidth at the best level, to characterize FRAs (Sadagopan & Wang, 2008). Shape index values near 0 indicated

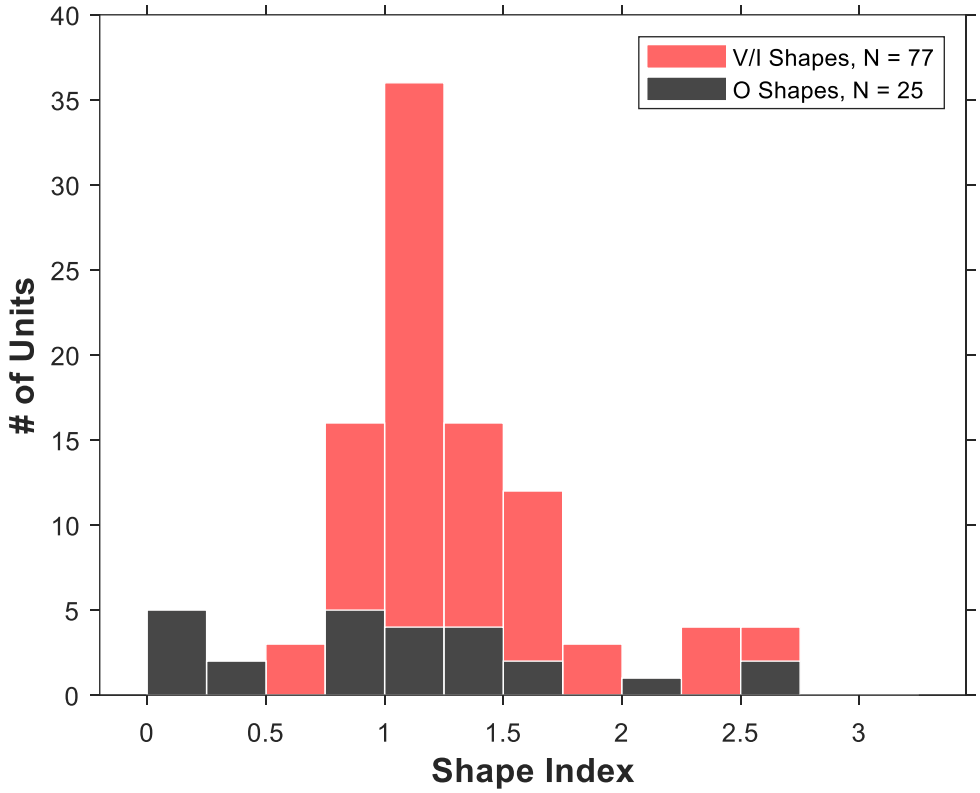

Figure 2.6. Distribution of shape index values. A stacked histogram of shape index values for O-shape FRAs (black) and V/I-shape FRAs (red). O-shape FRAs had a median shape index value of 1.05, and V/I-shape FRAs had a median shape index value of 1.13.

narrowing frequency tuning at high levels (indicative of O-shape FRAs), whereas shape index values of 1 or greater indicated tuning that broadened at high sound level (indicative of V-shape FRAs). In the marmoset study, shape indices displayed a bi-modal distribution, with modes centered near 0 and 1. In contrast, the distribution of shape indices in the present study had a

single mode near 1 (Figure 2.6). The majority of the V and I units had shape indices ≥ 1. The lowest shape indices belonged to O units, but about half of O units showed shape index values ≥1. We think that the presence of O units showing high-valued shape indices represented a difficulty in measurement. That is, O units showed non-monotonic level sensitivity, meaning that responses to high sound levels showed little or no response, thereby confounding computation of bandwidth at high sound level and, hence, a shape index. Bandwidth values for units that showed

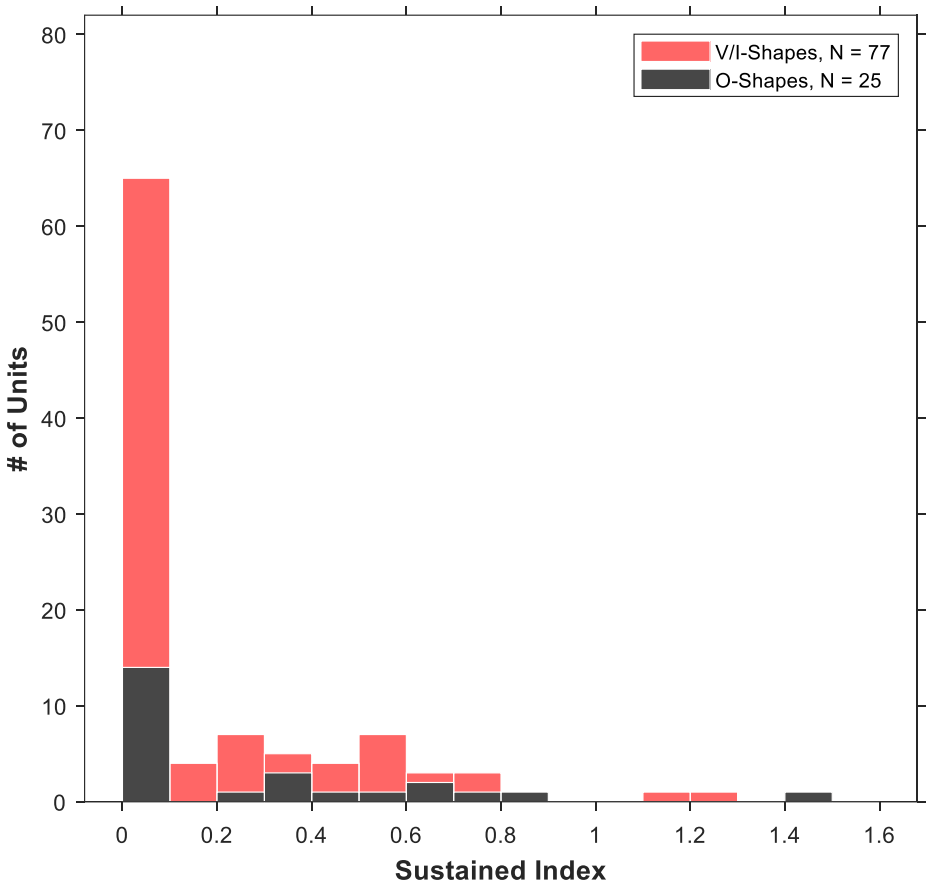

Figure 2.7. Distribution of sustained index values. A stacked histogram of sustained index values for O-shape FRAs (black) and V/I-shape FRAs (red). The median sustained index value for O-shape FRAs was 0.08, and the median value for V/I-shape FRAs was 0.

no response to the highest tested level were undefined; we assigned those units shape indices of 0. In some other O units, a few scattered responses to high-level sounds gave the false appearance of broad frequency tuning, thereby producing an erroneously large shape index. The

shape index did not provide a useful quantitative means of distinguishing O or V/I shape FRAs in this study.

Studies in anesthetized cat cortex have shown primarily phasic responses to the onsets of sound stimuli (Eggermont, 1991), whereas we observed a variety of responses ranging from phasic to tonic in the awake cat cortex. We quantified the temporal dynamics of the frequency response of units by calculating a sustained index. The sustained index was defined as the response rate in the latter half of the stimulus (60 – 110 ms relative to stimulus onset, allowing 10 ms for acoustic travel time and ear-to-cortex latency) divided by the response rate in the initial part of the stimulus duration (10 ms – 60 ms). A sustained index of zero would indicate no spikes in the latter half of the stimulus duration, and a sustained index value of 1 indicated equal spike rates during initial and latter halves of the 100-ms stimulus. For the calculation of the sustained index, responses for each unit were taken at the BF and best level. Figure 2.7 displays the distribution of sustained index values for V/I- (median sustained index value = 0) and O-shape FRAs (median value = .08). Sustained index values differed significantly between the two populations ($p=0.048$, ranksum = 1500, Wilcoxon Rank-Sum). To further investigate the sustained response properties of cortical neurons, we also presented long duration tones to 9 awake cats. These tones were 5 s in length and presented at the best level of a unit. Tones were presented at the best frequency (previously determined from FRA analysis) and in a small range above and below the best frequency in 1/6 octave increments. We applied those stimulus conditions to 43 units that responded to tones. Long-duration sustained responses were quantified as the response rate in the latter half of the 5-s stimulus duration (2510ms – 5010ms) divided by the response rate in the onset response (10ms – 60 ms). Figure 2.8 displays the

distribution of long duration sustained index values. The median sustained index value for all units was 0.13. All units tested in the long duration condition were multiple units.

Inspection of PSTHs suggested that, in many instances, sustained responses were limited to frequencies close to units' BF. To investigate this further, we calculated the bandwidth at best level in different parts of the sound duration for O and V/I units. We observed a sharpening in

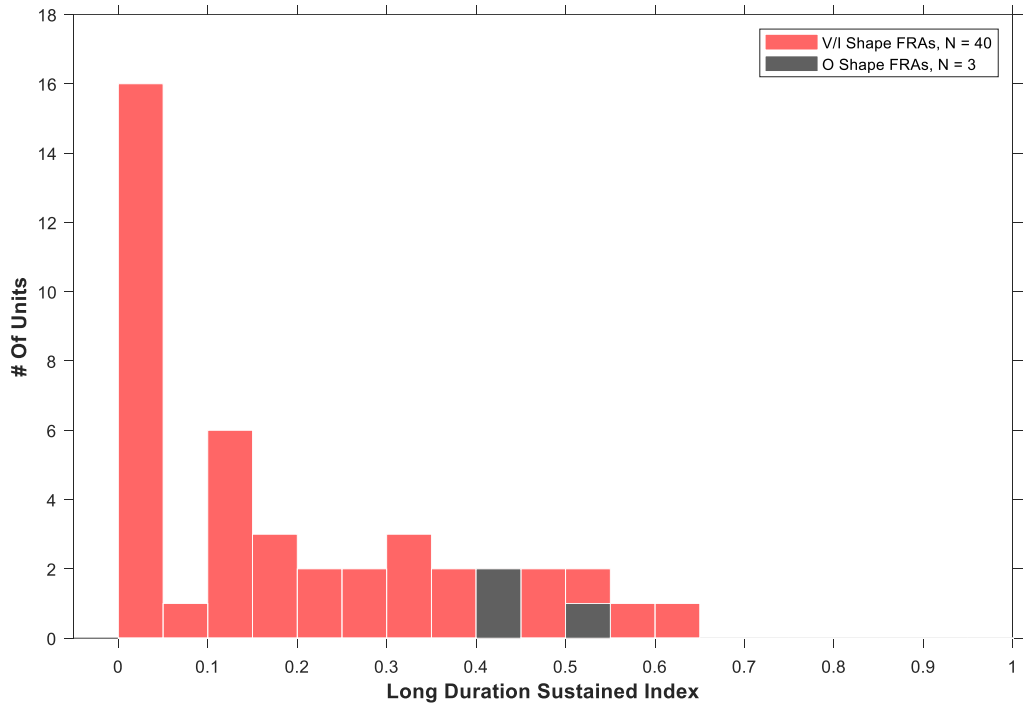

Figure 2.8. Distribution of sustained index values—long duration tones. A histogram of sustained index values for units presented with long duration (5s) tones. All observed units were deemed to be multi-unit, and the median sustained index value for all units was 0.13. V/I-Shape FRAs had a median long duration sustained index value of 0.12, and O-shape FRAs had a median value of 0.41.

the frequency tuning bandwidth of V/I unit responses in the latter half of the sound duration whereas O unit responses maintained a sharp tuning throughout the sound duration. Figure 2.9 represents an example of a V/I unit that displays sharpening of its frequency tuning bandwidth. Figure 2.9a shows a PSTH, with frequency and sound level shown on the vertical axis; all tested

levels are shown at one frequency, then repeated at the next frequency, and so on. The sustained index of this unit was 0.33. Sharpening of bandwidth can be observed in the PSTH of this unit during the latter half of the sound duration (as in Fig 2.9a), and in the FRAs computed in early and late ranges of the sound duration (as in Fig 2.9b and 2.9c, respectively). Across the

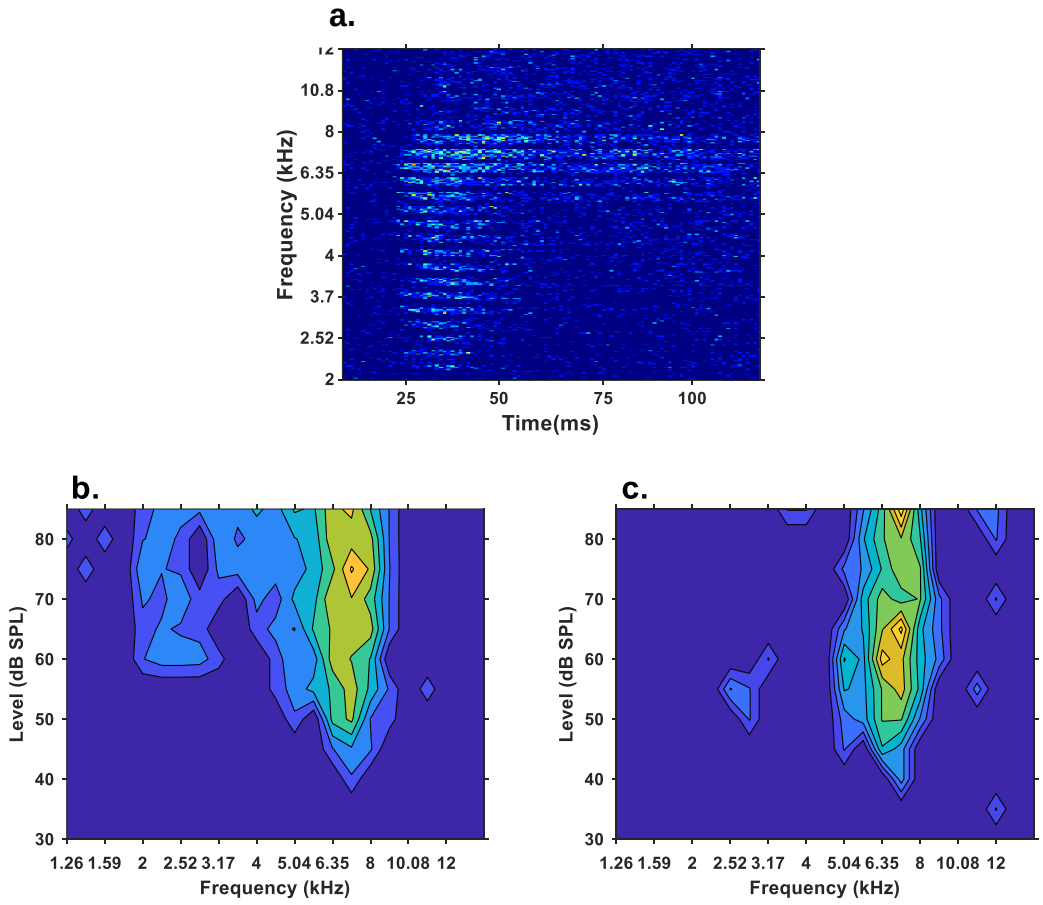

Figure 2.9. Example of narrowing bandwidth in sustained response. Example of a sustained V/I-shape FRA which displayed narrowed bandwidth in the latter part of the stimulus duration. Figure 2.9a plots the PSTH of this unit; mean spike rate is plotted as color for presented frequencies (y-axis), with each frequency row combining all levels tested. The stimulus duration is plotted on the x-axis. The sustained index value for this unit was 0.33. Figure 2.9b displays the FRA of this unit, plotted as contour lines, restricted to the time period of 10ms-60ms post stimulus onset. The bandwidth value in the 10ms-60ms time period was 1.0 octaves. Figure 2.9c displays the FRA of this unit for the time period of 60ms – 110 ms i.e., the latter portion of the stimulus duration. The bandwidth value in the latter portion was 0.56 octaves—this unit had a 44% narrower bandwidth value in the latter portion of the stimulus duration. Unit Ma04-16.

population of V/I units, bandwidths decreased ~44% in the latter part of the response (Figure 2.10; median bandwidth of V/I units for first half = 0.73 oct, and in the latter half = 0.41 oct; p =

7.7e-6, ranksum = 4100, Wilcoxon Rank-Sum one-tailed test). In contrast, O unit bandwidth values remained essentially unchanged (median first half = 0.22 oct latter half = 0.24 oct) and were not significantly different in the first and latter halves (p=0.68, ranksum = 604, Wilcoxon Rank-Sum).

Most units observed in our data included spikes from more than one neuron. Out of 102 units for which FRAs were analyzed, 18 were well-isolated single units (~18%). Of the single units, ~33% (6/18) displayed O-shaped FRAs, compared to ~23% of multi-unit sites (19/84). Single unit sites did not differ significantly from multi-unit sites in their monotonicity index

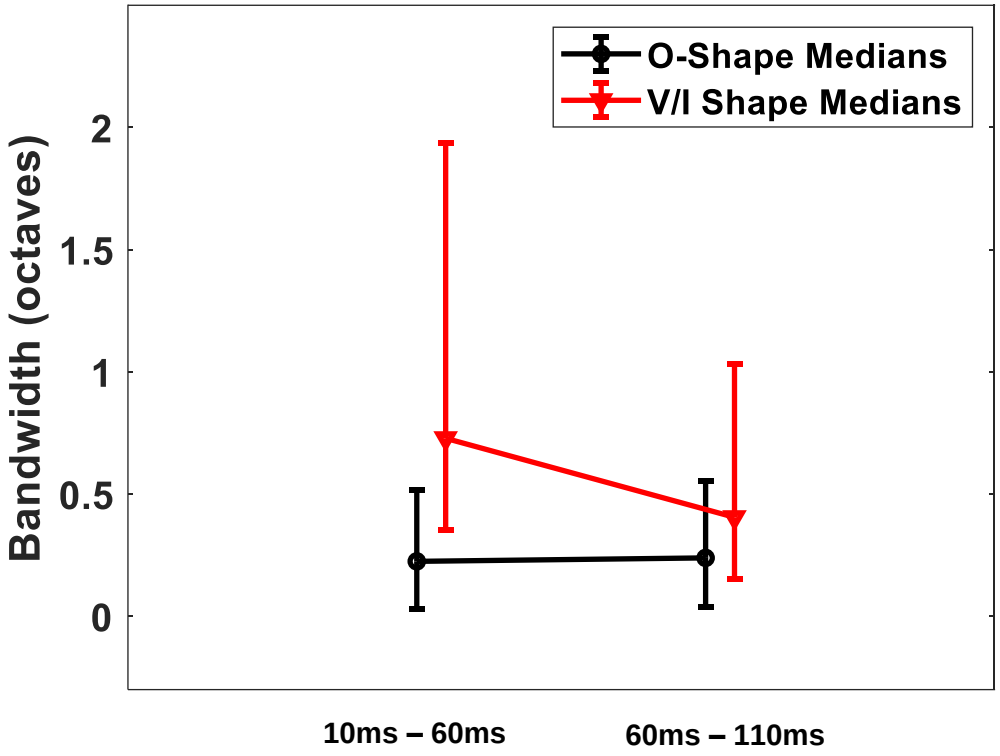

Figure 2.10. Sharpening of V/I-shape bandwidths in sustained response. Median bandwidth at best level values plotted for the onset period (10ms – 60ms post stimulus onset) and sustained period (60 – 110ms post stimulus onset) for O-shape FRAs (black) and V/I-shape FRAs (red). O- and V-shape medians are plotted with error bars representing interquartile range. Median bandwidth value for O-shape FRAs during the onset portion was 0.22 oct, and V/I-shape FRAs had a median value of 0.73 oct. In the sustained period, O-shape FRAs had a median value of 0.24 oct, and V/I-shape FRAs had a median value of 0.41 oct. O unit medians did not differ between onset and sustained periods, while V/I-shape unit bandwidths became significantly narrower (p=7.7e-6, ranksum=4136, single-tailed Wilcoxon Ranksum).

values (p = 0.19, ranksum = 824, Wilcoxon Rank-Sum), or their bandwidth at best level (p = 0.90, ranksum = 912, Wilcoxon Rank-Sum). That we did not observe a significant difference in the response properties of single units when compared to multi-unit sites suggests that neighboring neurons tended to have similar frequency and level sensitivity.

Click-Rate Sensitivity

We measured the ability of neurons to represent the rates of periodic stimuli by their synchronous firing patterns and by their non-synchronized tonic spike rates. Significant responses to click-train stimuli were observed in 105 units. Of those, 24 were deemed to be well isolated single units, and 81 were multi-unit sites. Significant synchrony to click rates 5 cps or

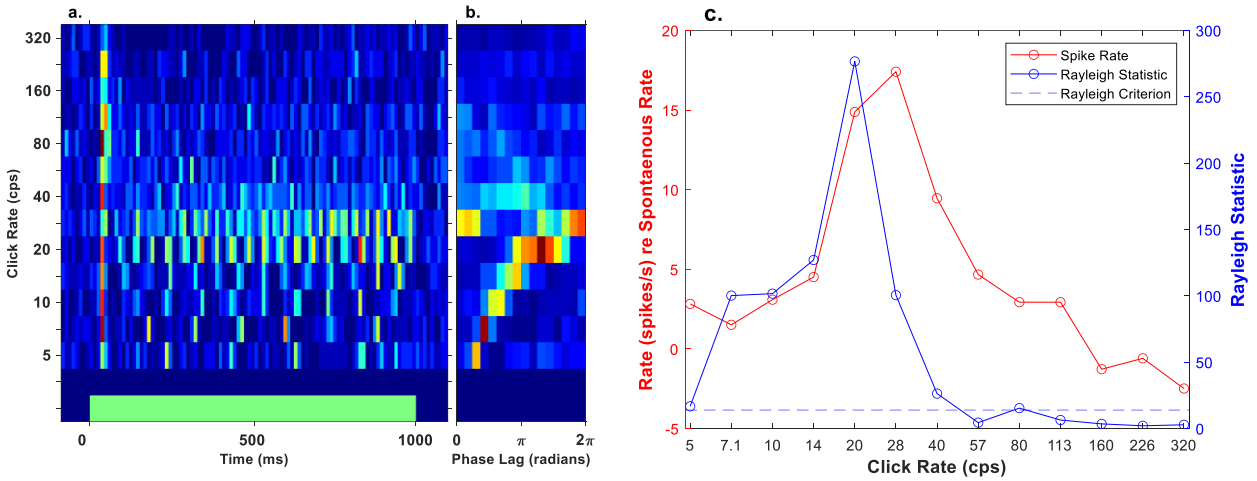

Figure 2.11: Phase locking to high click rates in one unit. Figure 2.11a displays the PSTHs of a unit with a synchronization boundary of 49.5 cps. Click rates are plotted on the y-axis, and spike rate is denoted by color. The green bar corresponds to the stimulus duration. Figure 2.11b illustrates the period histograms of this unit. The y-axis denotes click rate (cps), and the x-axis denotes the phase angle lag (in radians). Strength of spikes accumulated at each phase angle lag is denoted by color. Figure 2.11c displays the spike rate of this unit relative to the spontaneous rate (red curve) on the left y-axis, and the Rayleigh statistic (blue solid curve) on the right y-axis, as a function of the click rate. The dashed blue line represents the Rayleigh criterion value of 13.8 and is plotted on the right y-axis. Rayleigh statistic values above the criterion line denote significant synchrony (p<.001). Unit An01_4017.

higher was observed in 84/105 units (80%)—16/84 were well isolated single units, and 68/84 were multi-unit sites. Figure 2.11 shows an example of a unit synchronized to click trains. Figure 2.11a plots the PSTHs of this unit at each of the tested click rates, and Figure 2.11b shows the

corresponding period histograms. This unit displayed a prominent onset response across all click rates, followed by tonic stimulus-synchronized responses to click trains with rates up to 40 cps. The period histograms (Fig. 2.11b) plot the mean spike rate of this unit expressed relative to the phases of the click trains. Accumulation of spikes at particular phase lags was indicative of phase-locked synchronous firing. The peak value of each period histogram in this unit shifted in phase lag with increasing click rates up to 40 cps, consistent with a constant delay between the cochlea and the cortex. Figure 2.11c represents the synchrony and spike rate of the same unit, with measurement restricted to the post-onset times of 100 ms to 1010 ms, i.e., excluding the rate-insensitive onset response. The red curve and left axis show the mean tonic spike rate relative to the spontaneous firing rate. The solid blue line and the right axis represent the Rayleigh statistic, which is a measure of synchrony and spike rate (see Methods). Values of the Rayleigh statistic ≥ 13.8 were taken as statistically significant ($p<.001$). The synchronization boundary of each unit was the interpolated click rate at which the Rayleigh statistic crossed the criterion line, ~49.5 cps in this example. This unit shared response characteristics with other observed synchronized units — synchrony to low click rates, often increasing with somewhat higher click rates, followed by the synchrony fading at even higher click rates.

The spike rate of this unit peaked at 28 cps, after which the rate declined with increasing click rates (Fig. 2.11c). It is interesting to note that the tonic rate of this unit remained above the spontaneous rate in response to click rates up to 113 cps, where synchrony was non-significant. In many other instances, we observed a prominent suppression of spike rate to well below the spontaneous rate. Figure 2.12 illustrates an example of a unit showing stronger suppression to higher click rates. The spike rate of this peaked at 14.1 cps, which was a click rate higher than

that for peak synchrony (at 7.1 cps), and the spike rate dropped below the spontaneous rate for click rates > 40 cps.

Most of the synchronized units in this study (61/84, ~73%) showed synchrony to click rates limited to < 40 cps, but we observed examples of synchrony to click rates as high as 226 cps. Figure 2.13 represents the response of one high-synchronization unit. The PSTH of this unit (Fig. 2.13a) displays a strong onset response across presented click rates, and strong synchronized firing

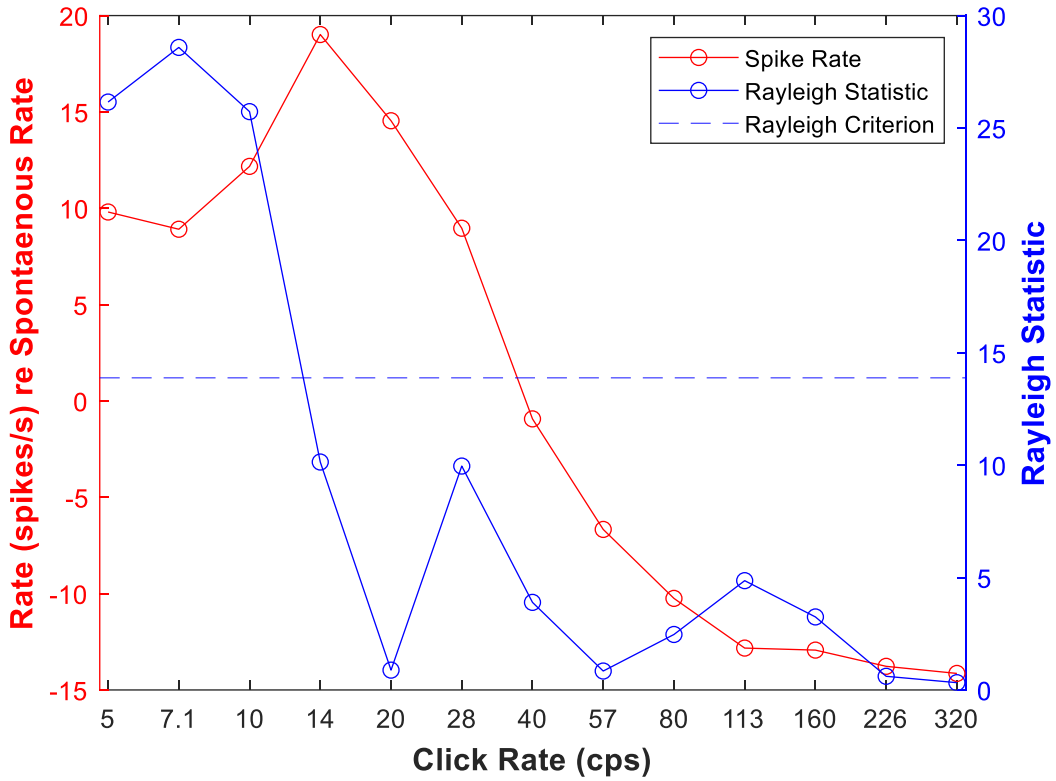

Figure 2.12. Strong suppression of spike rate in one unit. Figure 2.12 displays the spike rate of a unit displaying strong suppression of spike rate. This unit has a synchronization boundary of 13.2 cps. The format of this figure is identical to that of figure 2.11C. Unit He6_4019.

to rates up to 57 cps; synchrony at rates above 57 cps is not visible at the resolution of this PSTH time scale. This unit also displayed a strong offset at the higher click rates, and suppression at click rates ≥ 40 cps. The period histograms (Fig. 2.13b) display an accumulation of spikes at particular phase lags up to 113 cps, and an accumulation is faintly evident at 160 cps. The plot of the Rayleigh

statistic shows that this unit had a synchronization boundary of 167.2 cps (Fig. 2.13c). The spike rate of this unit stayed near the spontaneous rate for click rates up to 28 cps and was suppressed to below the spontaneous rate beginning at ~40 cps (Fig. 2.13c). However, the remaining spikes showed synchrony to click rates up to the synchronization boundary. The gray curve in Figure 2.13c displays the spike rate of the response limited to the time window directly following the stimulus offset i.e., 1000ms – 1100ms. This unit displayed an offset response close to the spontaneous rate to clicks up ~57 cps, followed by a sharp increase to click rates up to 160 cps, followed by a decrease at higher click rates.

The distribution of synchronization boundaries of well isolated single units and multi-unit sites that displayed significant synchrony in their response to presented click rates is illustrated in

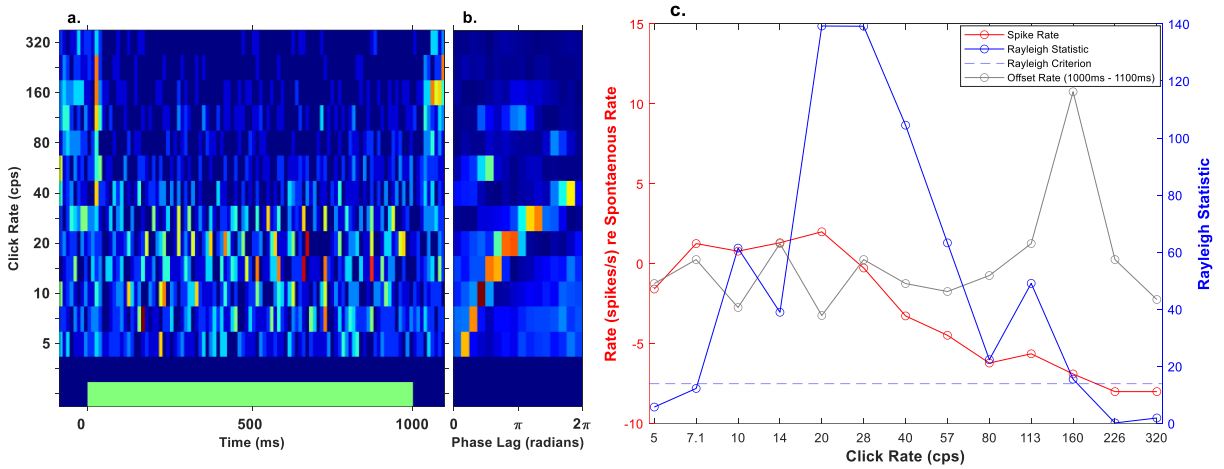

Figure 2.13 Phase locking to very high click rates in one unit. PSTHs for a unit with a synchronization boundary of 167.2 cps. The gray curve is plotted against the left y-axis and denotes the spike rate of this unit limited to the time window of 1000ms – 1100ms, i.e., the offset rate. Otherwise, the format is identical to that of Figure 2.11.

Figure 2.14. The solid blue curve indicates the percentage of multi-unit sites that synchronized to each click rate, and the solid red curve indicates the percentage of synchronized well isolated single units; values are percentages of the populations that synchronized to click rates ≥5 cps, a total of 84 units. The median synchronization boundary for all synchronized units was 28.4 cps. Synchrony to rates above 16.5 cps was observed in 64/84 units (~76%), and synchrony to rates

above 40 cps was observed in 23/84 units (~27%). The median synchronization boundary for well isolated single units (16/84) was 34 cps, and the median value for multi-unit sites (68/84) was ~28 cps. Single- and multi-unit sites did not differ significantly in their median synchronization boundaries (p = 0.75, ranksum = 651, Wilcoxon Rank-Sum), and had similar distributions (p = 0.38, ks2stat = 0.20, Kolmogorov-Smirnov two-tailed test).

About half of all units (52/105, ~50%) represented spike rates by nonsynchronous rate coding. That is, they showed a non-synchronized tonic response that increased in spike rate over a range of increasing click rates. An example of this type of unit is shown in Figure 2.15. The PSTHs of this unit display strong firing to click rates > 160 cps, with the strongest rate occurring

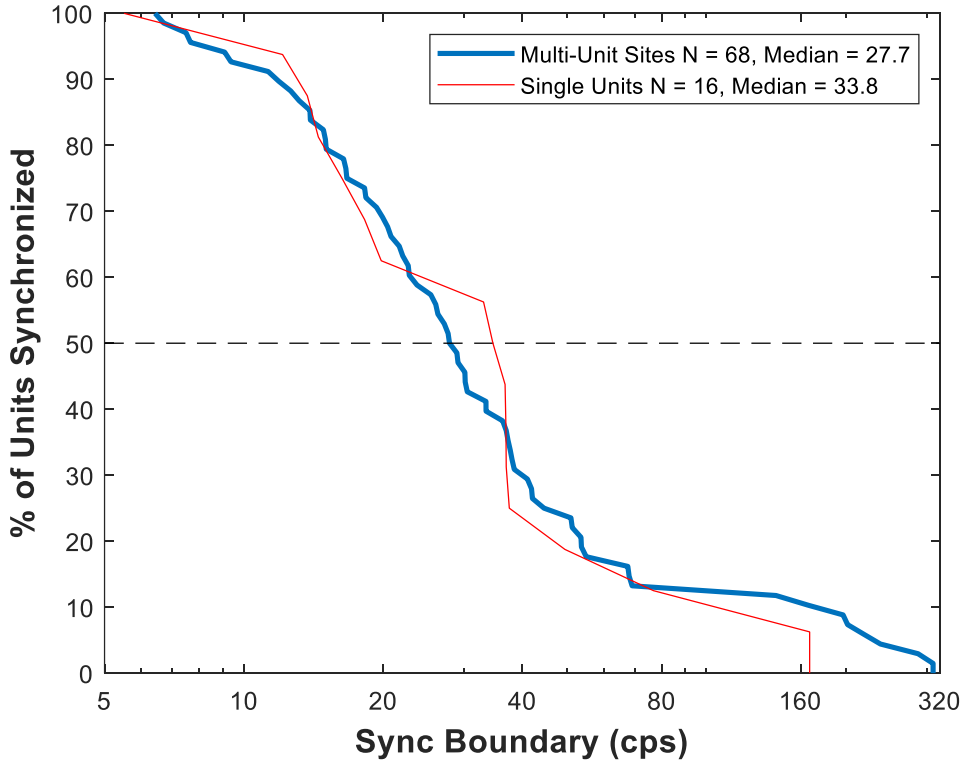

Figure 2.14. Synchronization boundaries for all synchronized units. Figure 2.14 displays the percentage of units that displayed synchrony to each of the presented click rates (x-axis). This plot is limited to the 84 units that synchronized to click rates of 5 cps or higher. The solid blue curve represents the synchronization boundaries for multi-unit sites, and the solid red curve represents the synchronization boundaries for well isolated single units. The dashed black line represents the median point i.e., 50% of units synchronized. The median synchronization boundary for multi-unit sites was 27.7 cps, and the median boundary for single unit sites was 33.8 cps.

at the highest click rate presented. This unit also displays a click-rate-dependent onset response—the onset response is present at all presented click rates but gets stronger at rates > 28 cps. The period histograms (Fig 2.15b) display accumulation of spikes to phase lags up to 14 cps, indicating phase-locked synchronous firing up to that click rate. Strong non-synchronous firing is observed regardless of phase angle lag at click rates ≥ 160 cps, indicative of non-synchronous rate coding. This unit displayed a firing rate close to its spontaneous rate for click rates up to 40 cps (Fig 2.15c), and the Rayleigh statistic displayed significant synchrony to click rates between

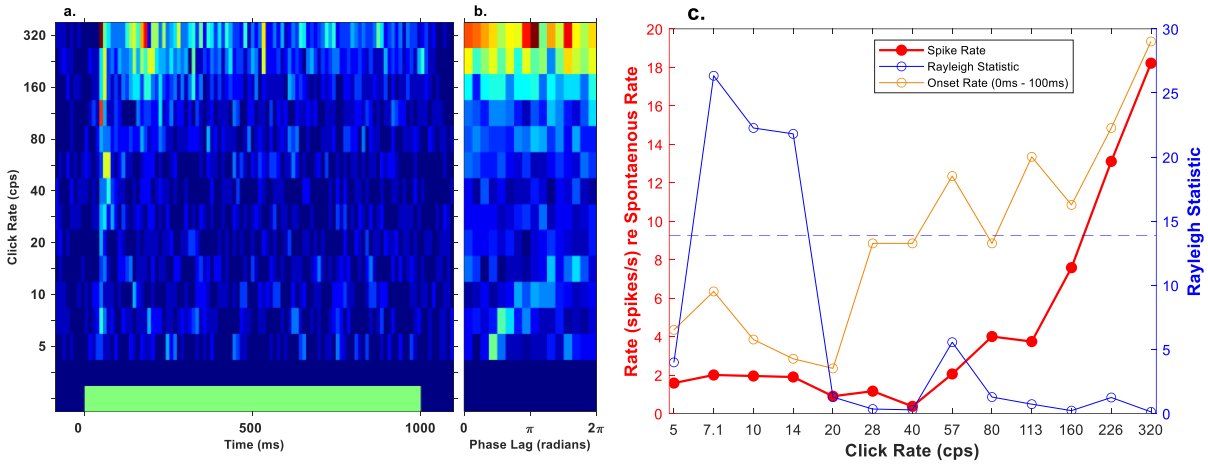

Figure 2.15. Synchronous and non-synchronous rate coding in one unit. Figure 2.15 displays the PSTHs (a), and period histograms (b) of a unit that displayed non-synchronous rate coding. The orange curve represents the spike rate of this unit limited to the time window directly following stimulus onset i.e., 0ms – 100ms, and is plotted on the left y-axis. Otherwise, the format of this figure is identical to figure 2.11. This unit had a dynamic range value of 2.5 oct, and a modulation of 88%. Unit Ra09_0027.

~7.1 to ~16 cps. The firing rate of this unit increased sharply in response to click rates > 40 cps and continued to increase to successively higher click rates. The orange curve in Figure 15c displays the spike rate of this unit in the time window directly following stimulus onset i.e., 0ms – 100ms. The onset rate can be observed to be increasing to click rates > 20 cps, suggesting that this unit integrated inputs over a time scale on the order of 40ms. It is interesting to note that although this unit displayed non-synchronous coding, it also displayed synchronous phase-locked firing to low click rates. Indeed, most units (31/52, ~60%) that displayed non-synchronized rate coding also displayed synchrony to click rates at or above 5 cps.

Some of the units that showed non-synchronized rate coding displayed a non-monotonic dependence on click rate: spike rates of 37/52 units peaked at ≤ 225 cps and declined to an average of ~86% at the highest click rates. Figure 2.16 illustrates one such unit. The PSTHs of this unit (Fig 2.16a) display strong firing to click rates between 113 cps and 226 cps, and weaker firing at 80 cps and 320 cps. The period histograms (Fig 2.16b) similarly display the strongest firing by this unit occurred to spike rates between 113 cps and 226 cps. Further, no clear accumulation was observed at any specific phase angle for any of the presented click rates,

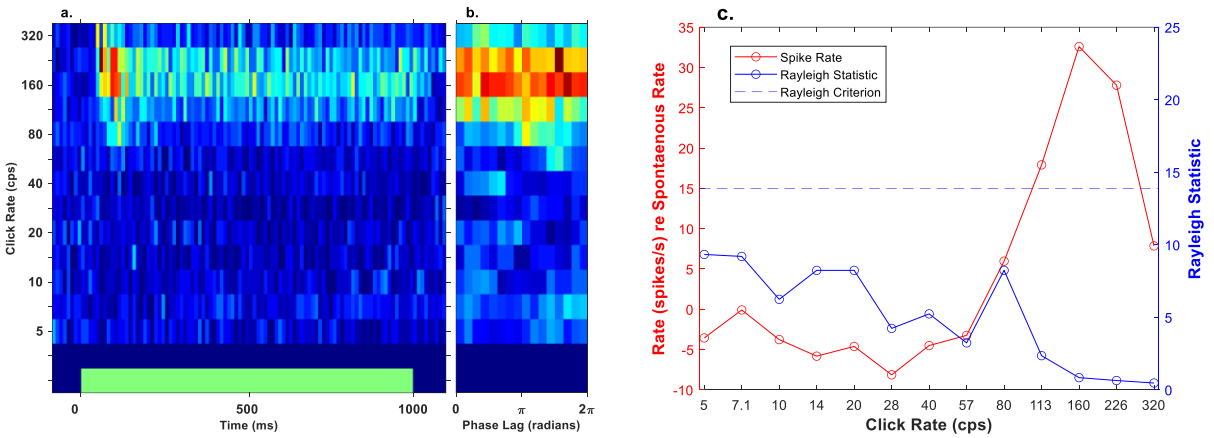

Figure 2.16. Non-synchronized rate coding in one unit. Figure 2.16 plots the PSTHs (a), period histograms (b), and spike rate re spontaneous as a function of click rate (c) in the convention of Figures 2.11, 2.13, and 2.15, of a unit displaying non-synchronous rate coding. This unit had a dynamic range value of 2 oct, and a modulation of 91.9%. Unit Ka02_4012.

indicating that this unit did not display a strong phase-locked response. This unit displayed suppressed tonic firing below the spontaneous rate to click rates < ~57 cps, followed by a monotonic increase to increasing click rates up to ~160 cps (Fig. 2.16c). A strong onset response can also be observed to click rates ≥ 80 cps. Unlike the unit represented in Figure 2.15, the spike rate of this unit decreased from its peak to click rates higher than 160 cps. This unit was somewhat unusual in that even its onset response was rather sensitive to the rates of click trains—that is, there was no indication of a typical onset response that is independent of click

rate. This type of click-rate dependent onset response was observed in 12/105 (~11%) of all units.

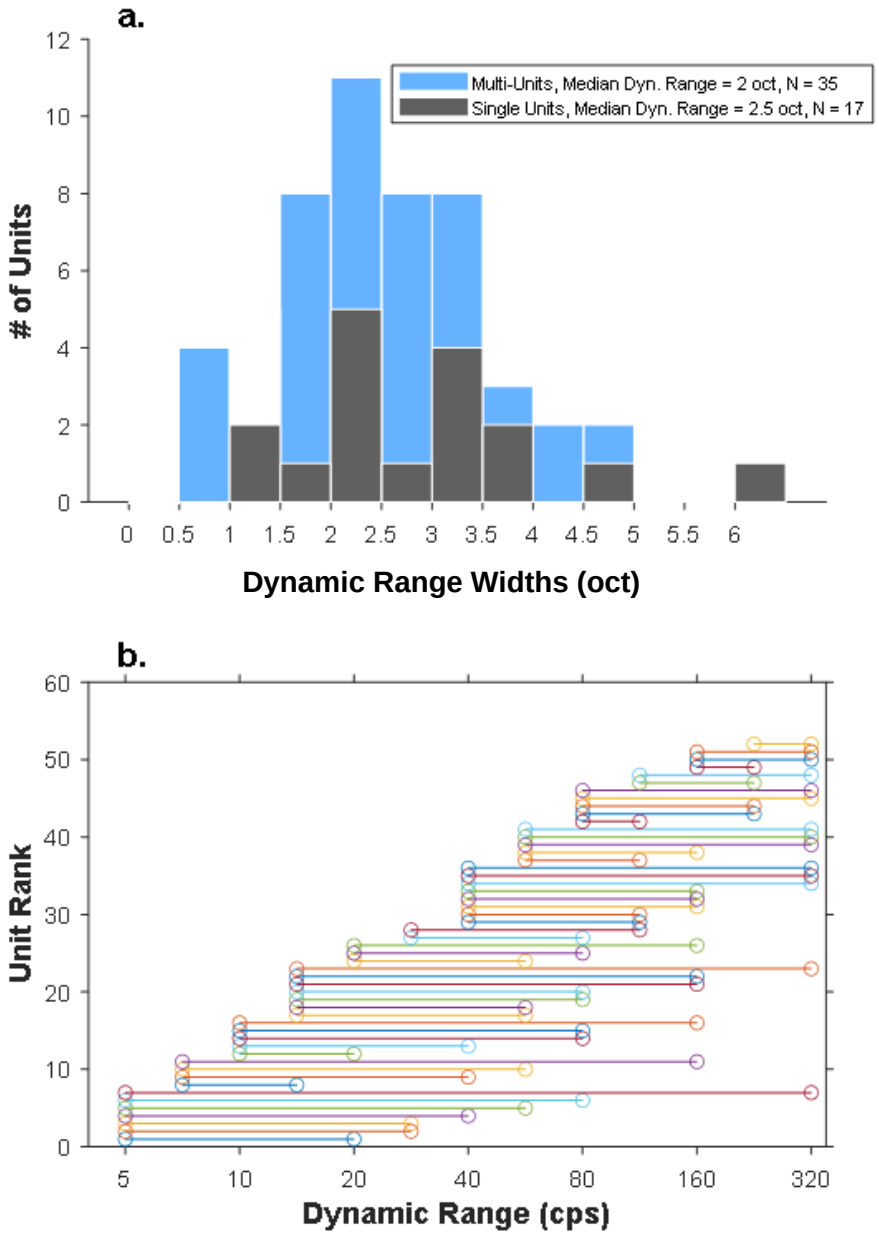

Figure 2.17: Dynamic range for non-synchronized responses. Figure 2.17(a) plots the distribution of dynamic range width values for multi-unit sites (blue) and well isolated single units (black) that displayed non-synchronous rate coding, as a stacked histogram. In Figure 2.17(b), the dynamic range values are presented for each unit as a horizontal line. For each unit, the left and right points represent the lower and upper click rates (respectively) for which the unit displayed non-synchronous rate coding. The units are plotted on the y-axis ranked by their lower dynamic range boundaries.

We observed a wide variation in the ranges of click rates that elicited non-synchronized rate coding. To quantify this range, we calculated a dynamic range value. The dynamic range of

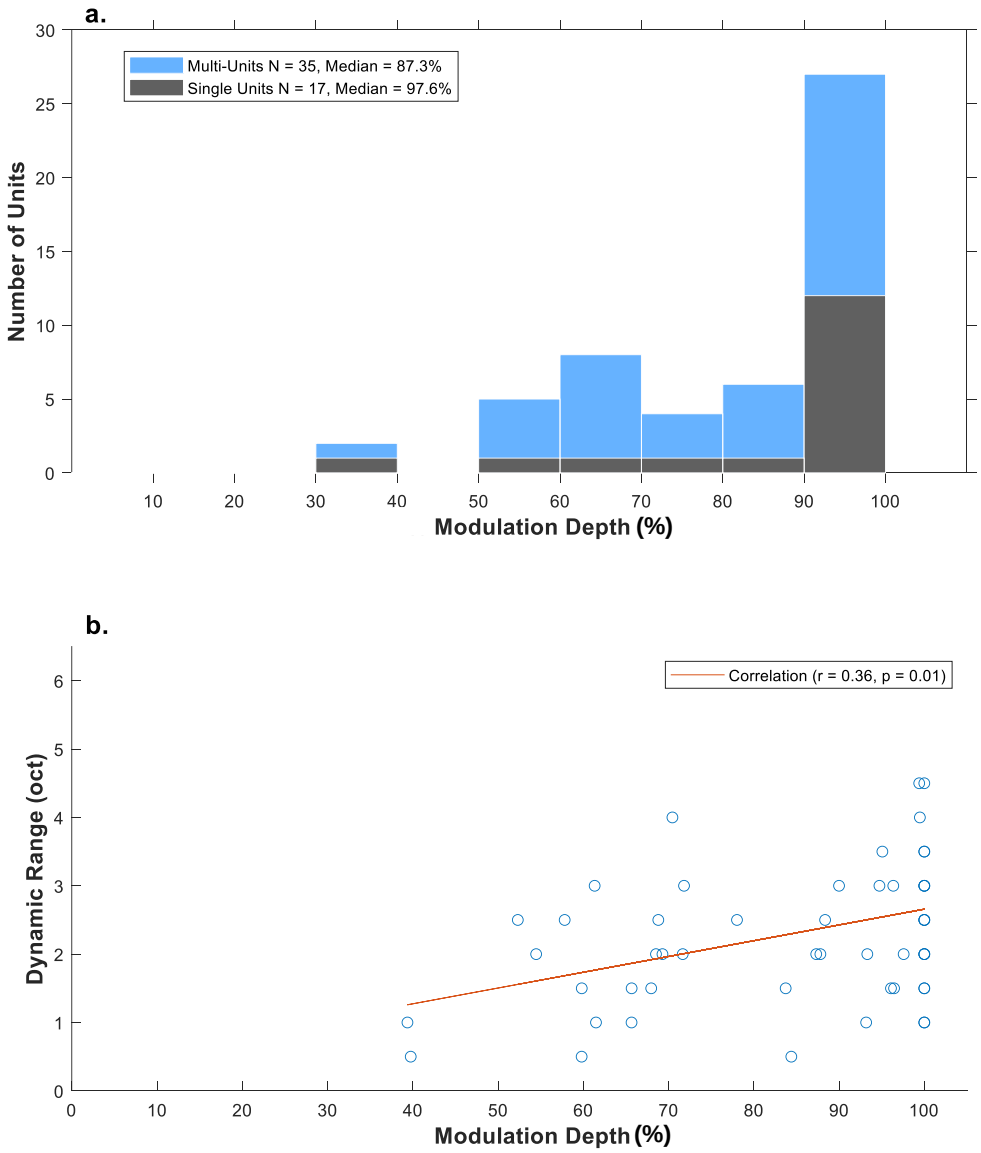

Figure 2.18: Modulation depth for non-synchronized responses. A stacked histogram of the distribution of modulation depth values for multi-unit sites (blue) and well isolated single units (black) is plotted in Figure 2.18(a) for units that displayed non-synchronous rate coding. The median modulation depth for multi-unit sites was 87.3%, and the median value for single units was 97.6%. Figure 2.18(b) plots the dynamic range values (in octaves) as a function of the modulation depth values for all units that displayed non-synchronous rate coding (N = 52). The red line represents the correlation value between these two measures. These two measures were positively correlated (r = 0.36, p = 0.0062).

non-synchronized rate coding for each unit was given by the range of click rates over which increases in click rates resulted in significant increases in unit spike rates. The dynamic ranges of the units shown in Figures 2.15 and 2.16, 2.5 oct and 2 oct respectively, were around the mode of the distribution of our sample whereas other units had dynamic ranges that spanned most of the 6-oct tested range of click rates. Figure 2.17 (a) plots the distribution of widths of dynamic ranges (in octaves) for non-synchronous coding multi-unit sites (in blue), and well isolated single units (in black). The median dynamic range for multi-unit sites that displayed non-synchronous coding was 2 octaves. Of the 24 well isolated single units observed in this study, 17 showed non-synchronous coding. The median dynamic range for single units was 2.5 oct. The difference in the median dynamic range values for single- and multi-unit sites was not significant ($p = 0.10$, ranksum = 532, Wilcoxon Rank-Sum). Overall, the distribution of dynamic range values observed highlights a variety of rate coding possible within this population for the range of click rages presented. Figure 2.17(b) plots the dynamic range values of each non-synchronous coding unit as a line, illustrating the range of click rates encoded by this population. It is important to note that non-synchronized rate coding did not occur only at high rates—every click rate in the range of 5 to 320 cps fell within the dynamic range of at least 7 of this sample of 52 units. To further quantify non-synchronous rate coding, we also examined the depth of modulation of the tonic firing rates across the range of click rates at which non-synchronous rate coding took place. Figure 2.18(a) plots the distribution of the modulation depth values for multi-unit sites (blue) and well isolated single units (black). The median modulation depth value for all units was 93.3%, the median for multi-units was 87.3%, and the median for well isolated single units was 97.6%. Single- and multi-unit sites did not differ in their median modulation depth values ($p = 0.12$, ranksum = 849, Wilcoxon Rank-Sum). These values indicated that click rates generally had a

profound impact on the firing rates of non-synchronized units. Figure 2.18(b) plots the dynamic range values in octaves as a function of modulation depth values. These two values were significantly correlated ($r = 0.36$. $p = 0.01$) which indicated that to some degree, deeper modulation of the tonic firing rate supported a broader dynamic range value.

Discussion

We evaluated spectral and temporal coding properties of neurons in the primary auditory cortex in 12 awake cats. Study of spectral sensitivity demonstrated sharp frequency tuning, including the presence of O-shape FRAs that responded to a small range of frequencies and levels. Temporally dynamic responses in V/I-shape FRAs were also observed—these units displayed sustained firing throughout the length of the 100-ms stimulus duration, particularly for frequency ranges narrowing around the BF. Further, we observed units that displayed firing sustained throughout tones as long as 5 s. Study of the temporal coding properties of the primary auditory cortex demonstrated synchronous firing to click rates as high as 226 cps, as well as non-synchronized rate coding in response to all presented click rates. Previous investigations in the cat primary auditory cortex have largely been conducted under anesthetized conditions. In preparations using anesthesia, spectral tuning has been observed to be broad, and units typically respond only to the onset of sound. Units in the anesthetized cortex have rarely been observed to synchronize to click rates > 20 cps, and non-synchronized rate coding has not been observed under anesthesia in the cat primary auditory cortex. Our results demonstrate a wide array of spectral and temporal coding properties present in the awake cat auditory cortex.

Spectral Coding

We observed sharp spectral tuning including FRAs with their neural excitation limited in both frequency and sound level (i.e., O-Shape FRAs). This type of frequency tuning has been observed in the ascending auditory pathway in unanesthetized but decerebrate conditions in the cat. In the dorsal cochlear nucleus (DCN), Young & Brownell, 1976 observed Type IV units with FRAs restricted in tuning to frequency and sound level which closely resembled what are now referred to as O-shape FRAs. They also observed Type II/III units, which more closely

resembled V-shape FRAs. Young and Brownell also measured frequency tuning under barbiturate anesthesia by comparing the activity of units first under the decerebrate condition, and then with the addition of a barbiturate anesthetic. The addition of the barbiturate anesthesia caused inhibitory responses surrounding the receptive fields of units with Type IV FRAs to become excitatory, such that frequency tuning became wider with increasing sound level. This type of response closely resembled a Type II/III FRA. Type IV FRAs were not observed in the anesthetized preparation. In a similar unanesthetized but decerebrate preparation, Ramachandran et al (1999) observed V-, I-, and O-shape FRAs in the central nucleus of the inferior colliculus (ICC). The majority of units observed by Ramachandran et al. in the ICC were O type (71/134), a smaller number of units were I Type (47/134), and V type responses only accounted for a small group of units (16/134).

In previous studies of the awake primary auditory cortex, Sadagopan and Wang (2008) observed sharp spectral tuning, including I- and O-shape FRAs in single units in response to pure tones in the marmoset. Sadagopan and Wang (2008) classified a majority of units (~64%) as O type, whereas we classified ~25% of units as O type in the current study. Aside from the lower proportion of units having O-type FRAs in cats, many of the properties of FRAs were remarkably similar between the marmoset and cat cortex—for example, the median bandwidth at best level value for O type units in the awake marmoset was 0.25 octaves, compared to 0.23 octaves in the awake cat cortex in this study. Similarly, the median bandwidth value for V and I type units in the awake marmoset was observed to be 0.52 octaves, compared to 0.67 octaves in this study. Sharp spectral tuning has also been observed in the awake auditory cortex of awake macaque monkeys (Recanzone et al., 2000). Recanzone et al., did not observe clear O-shape FRAs, but did find I-shape FRAs in the response of neurons in area A1 of the awake macaque.

Investigations in the anesthetized cat cortex have shown that most A1 units have broad frequency tuning (Moshitch et al., 2006; Schreiner & Sutter, 1992; Sutter & Schreiner, 1991). Sutter and Schreiner (1991, 1992) observed that frequency tuning bandwidths changed as a function of the mediolateral position along isofrequency contours of A1. Specifically, they observed units that exhibited multi-peaked FRAs, which contained two or more excitatory frequency ranges, were common in the dorsal part of A1. In Schreiner and Sutter (1992), they found that units located centrally in area A1 of anesthetized cats had narrower bandwidths. Specifically, they observed a mean bandwidth of 0.31 octave for single units, and 0.57 for multi-unit sites, in the central region of A1 for tones presented 40 dB above threshold. In the dorsal region of A1, single units had a mean bandwidth value of 0.88 octave and multi-unit sites had a mean bandwidth value of 0.98 octave. In ventral A1, single units had a mean bandwidth value of 0.40 octave, and multi-unit sites had a mean bandwidth value of 0.95 octaves. Across all regions of A1, the mean bandwidth values were 0.50 for single units, and 0.80 for multi-unit sites. In the present experiment, our electrode placement was targeted towards an area more ventral than the dorsal part of A1 tested by Sutter and Schreiner (1991), and likely comparable to the central and ventral regions of area A1 tested by Schreiner and Sutter (1992). It is possible that we did not observe multi-peaked FRAs in the awake cat cortex due to the placement of electrodes in this study. Sutter and Schreiner (1991, 1992) studied the auditory cortex of cats using a barbiturate anesthetic. In comparison, Moshitch et al. (2006) observed the properties of cat auditory cortical neurons in a preparation using a gas anesthetic (Halothane). Under Halothane anesthesia, researchers observed broad frequency tuning, including V-shape FRAs in the primary auditory cortex of cats. Mean bandwidth values were 1.2 octaves for tones 10 dB SPL above threshold, and 4 octaves for tones 40 dB SPL above threshold—these values are higher than those observed

by Schreiner and Sutter (1991, 1992) using barbiturate anesthesia. In the awake cat auditory cortex, we observed mean bandwidth values to be narrower than what has been observed in previous anesthetized preparations. In our sample, median bandwidth at best frequency and best level values were 0.23 octaves for O-shape FRAs and 0.67 octaves for V/I-shape FRAs.

Previous studies in anesthetized cortex have also shown primarily phasic responses to tones limited to tone onsets (Eggermont 1991). Most anesthetized studies in which units in the primary auditory cortex displayed a phasic response were conducted using barbiturate or ketamine anesthetics. There is evidence to suggest that the type of anesthetic can influence the response properties of cortical neurons. Specifically, Moschitch et al., (2006) used a halothane-based anesthetic and observed sustained activity in cortical neurons in response to pure tones 115 ms in duration. To analyze changes in FRA shape through the stimulus duration, Moschitch et al., also defined a compactness value as the area bounded by the tuning curve of a unit divided by the squared length of the perimeter of the tuning curve. Units with low compactness values had diffuse FRAs, with many weak responses distributed over a range of frequency and levels. Moschitch et al. observed an overall reduction in the compactness value over the stimulus duration, suggesting that tuning curves became more diffuse. In the awake cat cortex, we observed responses ranging from phasic to sustained, with units displaying activity to the entirety of the stimulus duration. We further observed a subset of units that also responded to long duration tones (5s) with a sustained response. This agrees with previous studies of the awake auditory cortex in marmosets (Wang et al., 2005), wherein units were found to respond to the entirety of the duration of unmodulated tones 5s in duration. We further analyzed changes in the FRA shape through the stimulus duration for 100 ms pure tones. We observed a sharpening in the frequency tuning of V/I-shape FRA responses, based on the decrease of bandwidth at best

level values, during the latter half of the response. O-shape FRAs maintained their sharp frequency tuning throughout the duration of the response. These findings suggest that V/I units could serve in a detection-activation role, wherein V/I units sample a larger part of the frequency space and can therefore detect more a wider range of sound frequencies and levels at the onset of sound. In the latter part of the stimulus duration, these units display a sharpening in their spectral tuning, which in turn likely leads to a finer-scale representation of stimuli. A similar result has previously been observed in the awake marmoset cortex (Sadagopan and Wang, 2008), wherein they observed a ~25% percent sharpening in V/I unit bandwidths in the marmoset cortex, compared to ~44% in the cat cortex in in this study. This type of mechanism may therefore be a conserved property of the awake mammalian auditory cortex.

Temporal Coding

The median synchronization boundary observed in this study in the awake cat cortex was 28.4 cps, and we observed about ~25% of the population had synchronization boundaries > 40 cps. In anesthetized conditions, previous studies have shown the median synchronization boundary of A1 neurons in their ability to synchronize to click trains to be as high as 25 cps (Lu et al, 2000), but most studies show median values < 20 cps (Eggermont, 1991, 1998; Gaese & Ostwald, 1995; Phillips, 1989). The variation observed in synchronization boundary values in past studies could partly be explained by the type of repetitive or periodic stimuli used, as well as the analysis used to determine synchronization boundary values. Synchronization boundary values in this study, as well as in Lu et al., 2000, were calculated through analyzing vector strength as a measure of synchrony. Previous studies have often used modulation transfer functions and a best modulation frequency measure to quantify synchronization to successive stimuli (Eggermont 1991, 1998; Gaese and Ostwald 1995; Schreiner & Raggio, 1996).

Eggermont (1991) explored the effects of different analysis techniques on the synchronization boundary value using a single data set. In that study, researchers presented click trains ranging from 1 cps to 32 cps and recorded the response of cortical neurons in cats anesthetized with ketamine. They observed synchronization boundaries ranging from 3 cps in an analysis of the rate modulation transfer function calculated as an average of the spike rates attributed to the first, second, and last click train in a series, to 24 cps when using vector strength (which is close to the analysis technique used in our study), to greater than 32 cps when the rate modulation transfer function was based on the average spike rate to all presented clicks in a click train, for the same data set. Lu et al. (2000) examined synchrony to click trains in the auditory cortex of cats anesthetized with ketamine. Wide- and narrowband clicks were presented at rates between 10 cps and 333 cps and click trains had a duration of 600 or 1000 ms for both types of clicks. They observed a median synchronization boundary of ~25 cps in the response of anesthetized cortical neurons, and 75% of the observed units synchronized to rates < 40 cps. Along with the type of analysis used, the relatively high synchronization boundary values observed in anesthetized cortical neurons in Lu et al., 2000 could be partially explained by the recording parameters used in their study. Specifically, all units observed were deemed to be multi-unit responses. Further, a small number of units in their study had exceptionally high synchronization boundaries ~100 cps. They suggested that their multi-unit recordings may have been contaminated by post-synaptic potentials of thalamocortical afferents.

Studies conducted in awake cortex in the cat (Dong et al., 2013), and in the awake marmoset (Lu et al., 2001) show synchrony to higher rates. Dong et al., for example, observed the response of cortical neurons of awake cats in on-task and off-task conditions. Cats in this study were trained to discriminate between click rates of 12.5 cps and 50 cps. They found a

subset of cortical units that reliably displayed a synchronized response to click rates presented at 12.5 cps and 50 cps in both on-task and off-task conditions. In the awake marmoset, synchrony was observed to click rates as high as 333 cps, and the median synchronization boundary was ~47 cps. Our results in this study are in accordance with previous studies conducted in awake preparations and add evidence to the idea that synchrony to higher click rates is a general property of the awake auditory cortex. Further, these findings suggests that previous observations of limited synchrony in anesthetized preparations were likely a result of anesthesia used in the studies.

In addition to synchronized responses, we also observed non-synchronized rate coding in the response of auditory cortical neurons in awake cats. Rate coding was observed in about half of all units in this study in response to click rates. This type of non-synchronized rate coding has previously only been observed in the awake marmoset cortex (Lu et al., 2001), and has not been observed under anesthetized conditions. To further quantify to extent of rate coding possible in the awake cortical neurons, we also calculated a dynamic range value. This measure highlighted a wide variety in the response of cortical neurons that displayed non-synchronized rate coding. Specifically, we observed that rate coding was not limited in response to higher click rates. Rather, every click rate presented was encoded by more than 10% of our sample of non-synchronized rate-coding units. These results demonstrate that a dual mechanism of temporal coding is present in the awake cat cortex. Specifically, we observed that units could represent click rates through stimulus synchronized responses of the tonic firing rate, and through non-synchronized rate coding. The responses observed in these data, including units with synchrony to fast click rates, as well as units that exhibit non-synchronous coding to low click rates, suggest

that these mechanisms work together to encode a wide range of rates of temporally varying stimuli in the awake cat cortex.

The results in this study replicate, for the first time in cats, the spectral and temporal coding properties previously seen in awake marmosets. It has been suggested that the coding properties observed in the awake marmosets are specializations for the marmoset's well developed vocal repertoire. Marmoset vocalizations include repetitive phrases at rates of 6-9 s^{-1}, with each phrase containing 2-3 frequency modulation sweeps at different frequencies ranging from 7-8 kHz (Nagarajan et al., 2002; Wang et al., 1995). Cat vocalizations are comparatively less complex (Farley et al., 1992; Gehr et al., 2000), featuring at least 6 call types but lacking the repetitive structure and frequency sweeps contained in the marmoset twitter call. Though these animals have a different vocal repertoire, the spectral and temporal coding properties observed in the awake cat in this study suggest that these features are likely a general property of the mammalian auditory cortex. Further, a review of previous studies suggests that these observations have likely not been observed in the cat auditory cortex due to the influence of anesthesia. Sadagopan and Wang (2008) also classified most units observed in the awake marmoset cortex as single units, however we observed both multi-unit and well isolated single units in this study. The overlap in spectral and temporal coding properties suggests sharp spectral tuning, including O-shape FRAs, is not restricted to well isolated single units and that neighboring neurons in the auditory cortex have similar response properties. In summary, we observed response properties in the awake auditory cortex that have previously only been observed in the awake marmoset cortex. These include sharp spectral coding including I- and O-shape FRAs in the awake cat auditory cortex. Measurements of tuning also revealed sustained responses, and a sharpening of the tuning bandwidth in the latter part of the stimulus duration for

V/I-shape FRAs. We also observed neurons that displayed synchronous responses to rates as high as 226 cps. Moreover, we observed that about half of the units in this study displayed non-synchronous rate coding.

Chapter 3
Stream Segregation in the Idle Awake Auditory Cortex

Introduction

Listeners have a remarkable ability to discriminate between interleaved sound sequences from two or more sources in a process referred to as "stream segregation" (Bregman, 1990). Spatial separation of sound sources has been shown to be a robust cue for stream segregation (Middlebrooks and Onsan, 2012; Javier et al., 2016). Middlebrooks and Bremen (2013) demonstrated that neurons in the anesthetized cat cortex preferentially synchronized to one of two competing sound sources when sound sources were separated in space. In that way, such neurons demonstrated stream segregation using spatial cues with spatial acuity that rivals what has been observed in behavior (humans: Middlebrooks and Onsan, 2012; cats: Javier et al., 2016; Chapter 1).

Middlebrooks and Bremen (2013) observed that most neurons in the anesthetized cat cortex responded poorly to trains of nose bursts with an aggregate rate as high as 10 s^{-1}. Nevertheless, neurons could synchronize to one of two competing trains of noise bursts when those noise bursts were separated in source location. These noise bursts were spectrally identical and interleaved in time, such that each train of noise bursts had a presentation rate of 5 s^{-1}, and when co-located the resulting stimulus had a presentation rate of 10 s^{-1}. Those authors suggested that the failure of cortical neurons to respond to high stimulus rates in anesthetized conditions was due to forward suppression. That is, the response to the second of two identical noise bursts was suppressed. When sound sources were separated in location, neurons that displayed a preferential response to one of the source locations tended to have a suppressed response to the less-preferred source location in competing conditions. Forward suppression has been previously

observed in the response of cortical neurons in the anesthetized cat presented with pairs of tones (Brosch & Schreiner, 1997).

In this chapter, we sought to examine whether forward suppression would occur in the response of neurons in the primary auditory cortex of awake cats when they are presented with competing streams of noise bursts, and whether that forward suppression would result in stream segregation. We first began by examining the ability of awake cat cortical neurons to synchronize to trains of noise bursts with rates varying from 5 s^{-1} to 40 s^{-1} presented from a single source. In Chapter 2, we observed neurons in the awake cat cortex synchronized to trains of clicks with presentation rates higher than what has been previously observed in the anesthetized cortex. Here, we similarly observed that neurons in the awake cortex displayed synchrony to trains of noise bursts at rates higher than what has been previously observed in the anesthetized cortex. Indeed, some neurons synchronized to the highest rate of noise bursts presented (40 s^{-1}). To examine whether neurons in the awake cortex demonstrated stream segregation in non-task conditions, we then presented awake cats with trains of noise bursts interleaved in time and differing in source location. These trains of noise bursts were spectrally identical, varied in source location, and had an aggregate presentation rate of 10 s^{-1}, similar to stimuli used in our psychophysical studies (Javier et al., 2016) and to some of the stimuli used by Middlebrooks and Bremen (2013). Unlike the results from the anesthetized cortex, we did not observe significant discrimination in the response of awake cat cortical neurons to one of two competing sound sources differing in location. We observed that neurons in the awake cortex were able to synchronize to the aggregate sound rate of both trains of noise bursts, regardless of location. A small population of neurons did display a preference to one of two competing trains of noise bursts, but we did not observe forward suppression through a decrease in response to the

non-preferred stream. These results suggest that unlike results from the anesthetized preparation, forward suppression may not occur to enhance stream segregation based on source location in the response of neurons in the primary auditory cortex of awake cats that are not engaged in a stream-segregation task.

Methods

Overview

Extracellular spike activity was recorded with multi-channel recording arrays chronically implanted in the primary auditory cortex (area A1) of 14 cats. Fourteen cats were presented with trains of noise bursts that varied in rate and had a fixed location in space. Nine cats from this population also were presented with fixed-rate interleaved trains of noise bursts that varied in source location; seven of the 9 cats were previously trained in a spatial stream segregation task (Javier et al., 2016; Chapter 1). This population of cats is the same as mentioned in chapter 2. The results in this report were obtained entirely during awake, non-task conditions for both types of stimuli. The response pedal and automatic feeder were removed from the apparatus, and the cat was given small amounts of food intended to keep it alert and oriented toward the center of the coordinate system.

Animal Preparation

All procedures were conducted in accordance with the National Institute of Health guidelines and with the approval of the Institutional Animal Care and Use Committee for the University of California—Irvine. Fourteen domestic shorthair cats (*Felis catus)*, 9 males and 5 females, were presented with trains of noise bursts varying in rate and presented in free-field from a fixed location (0° azimuth). Nine of the cats, 5 males and 4 females, were presented with interleaved trains of noise bursts. Interleaved trains of noise bursts were fixed in rate (5 s^{-1} for each train) and varied in source location along azimuth. All cats were obtained from a breeding colony at the University of California at Davis. Each animal was implanted with a chronic multi-site recording array in the auditory cortex using aseptic procedures. Surgical procedures and details of the implant used are described in Chapter 2.

Single-source trains of noise bursts fixed in source location and varying in rate were generated by gating a continuous Gaussian noise source generated by the RZ6 digital signal processor (Tucker-Davis Technologies). Each noise burst was 20 ms in duration, gated with a raised cosine function with 1 ms rise and fall times, and presented at 60 dB SPL. Trains of noise bursts were 1s in duration, filtered at 0.4-25 kHz, and presented at rates from 5 to 40 s^{-1}; 40 s^{-1} was the highest burst rate that permitted an appreciable gap between the 20-ms-duration bursts. Sound sources were fixed at 0° or contralateral 40° sound speaker locations; usually both locations were tested in separate blocks of trials. All sound locations were located in the horizontal plane. Contralateral and ipsilateral refer to the location of the sound speaker in reference to the multi-channel recording array in the cat's right hemisphere.

Interleaved trains of noise bursts varying in source location and fixed in rate consisted of band-pass noise bursts filtered at 0.4-25 kHz and presented at a rate of 5 s^{-1}. Pairs of such trains were interleaved in time, resulting in aggregate burst rates of 10 s^{-1}. Those noise-burst trains parameters correspond to those used in previous psychophysical studies in humans (Middlebrooks and Onsan, 2012) and cats (Javier et al., 2016; Chapter 2). Noise-burst trains in this condition were presented as interleaved competing A and B trains in an alternating ABAB… pattern; when A and B sources were co-located in space, the stimulus was an undifferentiated continuous sequence of noise bursts with an aggregate rate of 10 s^{-1}. The A and B noise burst trains were identical in long-term spectrum and only varied in source location; the A source was always located at 0° in azimuth, and the B sources varied in location from ± 60, 40, 20, 10, and 0°. We also presented a B source only condition, in which noise bursts were presented from the B source alone at a rate of 5 s^{-1}, varying in location, without the presence of the interleaved A

source sequence. Interleaved trains of sound bursts had a total duration of 3400 ms. All stimuli were presented at 60 dB SPL and repeated 20 times for each B source location.

Data Analysis

Data analysis began with off-line identification of neural action potentials as previously described in Middlebrooks (2008), as well as in Chapter 2. For trains of noise bursts varying in rate, sound-evoked unit responses were recorded at 162 sites in 14 array placements. For interleaved trains of noise bursts, sound-evoked unit responses were recorded at 88 sites in 9 array placements.

Sensitivity to noise bursts with varying rates

We evaluated the representation of noise burst stimuli by quantifying the spike rates and spike timing of neurons in response to trains of noise bursts at various rates. Response of units to the burst trains was tested through a comparison of spontaneous spike rates in the 100-ms interval prior to sound onset with stimulus-driven rates in the 1000-ms interval beginning 10 ms after the noise burst train onset (10ms – 1010ms). Spike rates (in spikes per second) in the two intervals were compared with a two-tailed Wilcoxon rank sum test and with a Kruskal-Wallis test to determine whether response rates in the 10-1010ms-post-onset interval varied significantly from the spontaneous rate and/or varied with stimulus burst rate. Units that showed significance in either test ($p<.05$) and showed adequate spike isolation were considered for further analysis. For the noise burst train stimuli, 107 units met those criteria. Analysis of stimulus synchrony was based on the time interval from 100 – 1010 ms post stimulus onset, which excluded the response to the first noise burst in each train of noise bursts. Analysis of synchrony was conducted in an identical manner to the analysis described in Chapter 2. Briefly,

significant synchrony was indicated through the Rayleigh statistic, which was calculated through an analysis of the vector strength and spike rate. Significantly synchronized response to noise burst trains at rates of 5 s^{-1} or higher were observed in 92/107 units, of which 10 were well isolated single units, and 82 were multi-unit sites. The synchronization boundary was defined as the interpolated highest noise burst rate at which a neuron responded with a Rayleigh statistic >13.8, which indicates $p<.001$.

Competing sound streams

We evaluated the representation of competing-sound stimuli by first identifying units that had a significant sound-evoked response. We conducted a comparison of the spontaneous spike rates in the 100 ms time window prior to sound onset with the time window of 10-3410 ms post-stimulus-onset. Rates in these two windows were analyzed through a Wilcoxon Rank-Sum test to determine whether spike rates in the 3400 ms time window post sound onset varied significantly from the spontaneous rate; 88 sites met this criterion. Of these 88 observed units, 8 were observed to be well-isolated single units, and 80 were deemed to multi-unit sites. Analysis of competing-sound stimuli was conducted through a measurement of rate-azimuth functions (RAFs), which were expressed as the mean number of spikes synchronized to each 20 ms sound burst as a function of the location of the B sound source. We observed that spikes usually fell within 50 ms after each noise burst onset—we therefore counted spikes in the 8-58 ms time windows after each noise burst onset; the 8 ms offset allowed for a minimum latency from ear to cortex. This analysis was used to attribute spikes to sound bursts in the A and B sound sources.

To measure the discrimination of sound-source locations by trial-by-trial neural spike counts, we used a procedure based on signal detection theory (Green and Swets, 1966; Macmillan & Creelman, 2005) similar to Middlebrooks and Bremen (2013). We compiled spikes

counts for all repetitions that were synchronized to the A and B sources and formed an empirical receiver operating characteristic (ROC) curve based on the trial-by-trial distributions of spikes counts elicited on all trials by the two stimuli. The area under the ROC curve described the probability of correct discrimination of the stimuli, which was expressed as a *z*-score and multiplied by $\sqrt{2}$ to obtain the discrimination index, *d'*. If 100% of the spike rates elicited by one stimulus were greater than those elicited by the other stimulus, *d'* was written as ±2.77, corresponding to 97.5% correct discrimination. In the plot of *d'* versus azimuth, the interpolated separation at which the plot crossed $d' = \pm 1$ was taken as the threshold for significance. Positive *d'* values denoted more spikes synchronized to the more-contralateral source.

Results

We measured the ability of neurons to represent the rates of periodic noise bursts by their synchronous firing patterns. We evaluated trains of 20 ms Gaussian noise bursts presented from 0° azimuth. Burst rates were 5 to 40 bursts per second (bps) varied parametrically in 5 bps increments. We recorded responses from the primary auditory cortex of 14 awake cats. In 9 of those cats, we also measured the ability of cortical neurons to segregate streams of competing noise bursts differing in source location. Competing streams were spectrally identical, interleaved in time, and presented at 5 bps each for an aggregate rate of 10 bps.

Sensitivity to trains of noise bursts with varying rate

Significant response to trains of noise bursts varying in rate were observed in 107 units. Of the 107 units, we observed synchronized responses to trains of noise bursts with rates 5 bps or higher in 92 units, 10 of which were well isolated single units and 82 of which were multi-unit sites. Figure 3.1 displays an example of a unit synchronized to trains of noise bursts. Figure 3.1a plots the PSTHs of this unit at each presented rate, and Figure 1b displays the corresponding period histograms. This unit displayed a prominent onset response to all presented click rates; such rate-insensitive onset responses were observed in most synchronized units (87/92, ~95%). Subsequent analysis of spike synchrony was limited to the post-onset times of 100 to 1050 ms, which excluded this onset response. Stimulus-synchronized responses to trains of noise bursts up to 15 bps can also be observed in the PSTHs. Figure 3.1b displays the period histograms, which plot the mean spike rate of this unit as a function of spike time relative to the phases of the noise-burst trains. In this format, robust synchrony can be observed in burst rates up to 20 bps, and a fainter response can be observed at 25 bps. Figure 3.1c displays the synchrony and spike rate of the same unit as a function of noise-burst rate. The red curve, referred to the left y-axis, displays

the spike rate of this unit in response to the presented burst rates (x-axis). The solid blue line, referred to the right y-axis, displays the Rayleigh statistic, a measure of synchrony. The synchronization boundary of each unit was the interpolated burst rate at which the Rayleigh statistic crossed the criterion line of 13.8 (represented in Fig. 3.1c by a dashed blue horizontal line). For this unit, the synchronization boundary was 24.9 bps. The tonic spike rate of this unit was elevated above the spontaneous rate for noise burst rates up to 40 bps, well above the synchronization boundary.

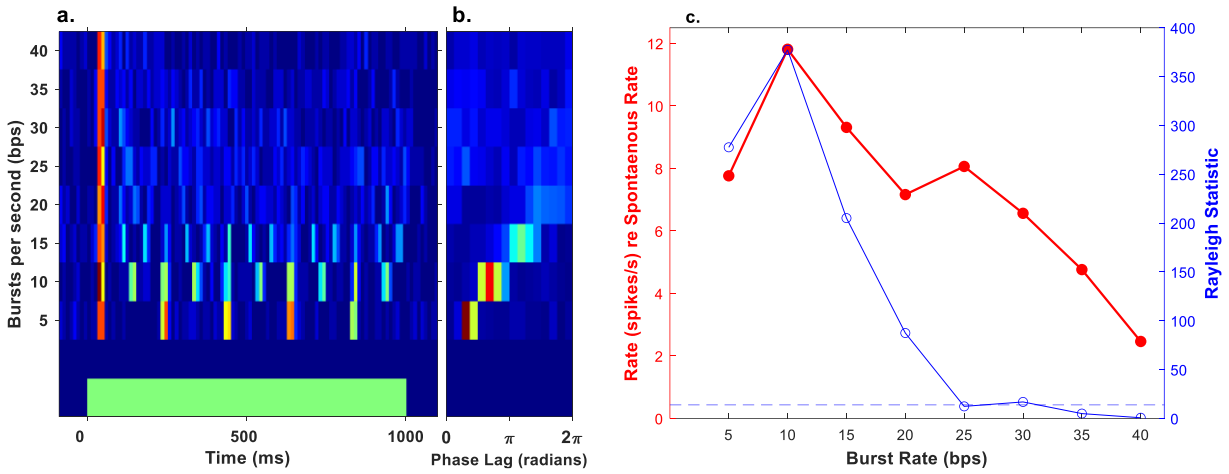

Figure 3.1 Synchronous response to noise burst trains in one unit. Figure 3.1a displays the PSTHs of a unit with a synchronization boundary of 24.9 bps. Noise burst rates are plotted on the y-axis, and spike rate is denoted by color. The green bar corresponds to the stimulus duration. Figure 3.1b illustrates the period histogram for the unit. The y-axis denotes pulse rate (pps), and the x-axis denotes the phase angle lag (in radians). Strength of spikes accumulated at each phase angle lag is denoted by color. Figure 3.1c displays the spike rate of this unit relative to the spontaneous rate (red curve) as a function of the pulse rate on the left y-axis. The Rayleigh statistic (blue curve) is plotted on the right y-axis, and the dashed blue line represents the Rayleigh criterion (13.8). Values of the Rayleigh statistic above the Rayleigh criterion indicate significant synchrony to burst rates ($p<.001$). UitKa02_0_11.

The unit displayed in Figure 3.1 had a synchronization boundary near the median of the population (23.1 bps), but some units displayed synchronous firing to the highest rates tested; i.e., 40 bps. Out of 92 units, 28 had synchronization boundary values > 35 bps, including 15 units that displayed significant synchrony to the highest presented noise burst rates. These 15 units did not have a defined synchronization boundary, as they displayed significant synchronization to all rates presented. Figure 3.2 displays the PSTHs (Fig. 3.2a), period histograms (Fig. 3.2b), and

spike rate (Fig. 3.2c) of one such unit. The PSTHs of this unit (3.2a) display substantial spontaneous activity, followed by an onset response and tonic activity to all presented rates; the synchrony of spikes at the highest rates cannot be appreciated because of limited temporal resolution of the PSTH format. The period histograms (Fig. 3.2b) display an accumulation of spikes at particular phase lags to rates up to 40 bps. The mean phase lag of this unit increased linearly with increasing linear steps of burst rates, consistent with a constant group delay of 26.4 ms from the ear to the recording site in the cortex. The unit displayed synchrony and spike rates that increased as rates of noise bursts increased up to 30 bps and then declined as burst rates were increased to the highest tested rate (Fig. 3.2c). It is interesting to note that the overall tonic response rate of this unit was suppressed below its spontaneous rate at most tested noise-burst rates, even though the stimulus-driven spikes were well synchronized to the stimulus bursts.

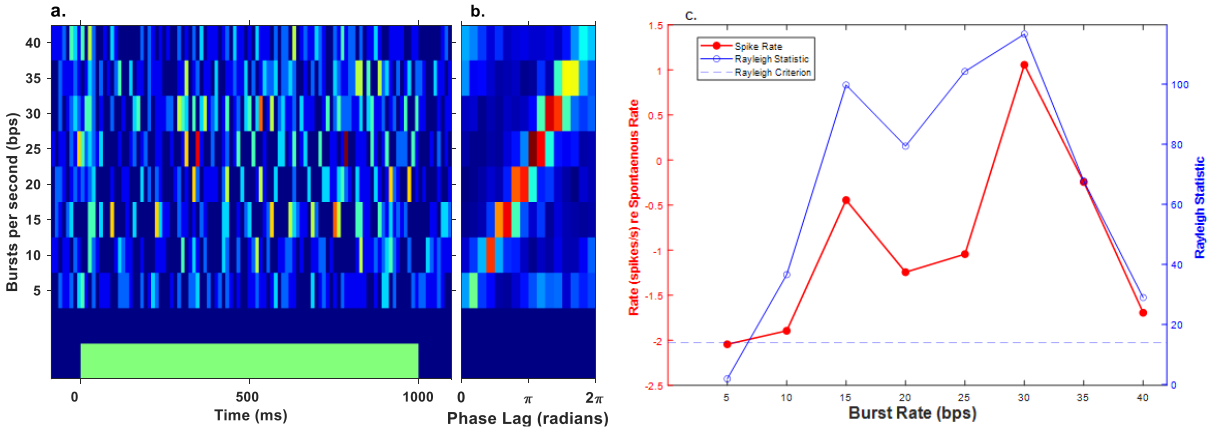

Figure 3.2. Synchronous response to high noise burst rates in one unit. Figure 3.2 displays the spike rate of a unit with synchrony to the highest noise burst rate presented. The format of this figure is identical to that of figure 3.1. Unit An01_027.

Figure 3.3 displays the distribution of synchronization boundaries of single- and multi-unit sites as a stacked histogram. Units that displayed significant synchrony to all tested rates are denoted by synchronization boundaries of "≥40". The median synchronization boundary for well-isolated single units (10/92) was 27.9 bps, and the median value for multi-unit sites (82/92)

was 22.2 bps. Nearly all of the synchronized units (89/92, ~97%) had a synchronization boundary value >10 bps. Well isolated single units and multi-unit sites did not differ significantly in their median synchronization boundaries (p = 0.29, ranksum = 560, Wilcoxon Rank-Sum), and had similar distributions (p = 0.59, ks2stat = 0.25, Kolmogorov-Smirnov two-tailed test). That the median synchronization boundary for single units was (non-significantly) higher than for multi-unit sites indicates that the synchrony that was observed to fairly high burst rates likely was not due to a volley of responses of multiple neurons.

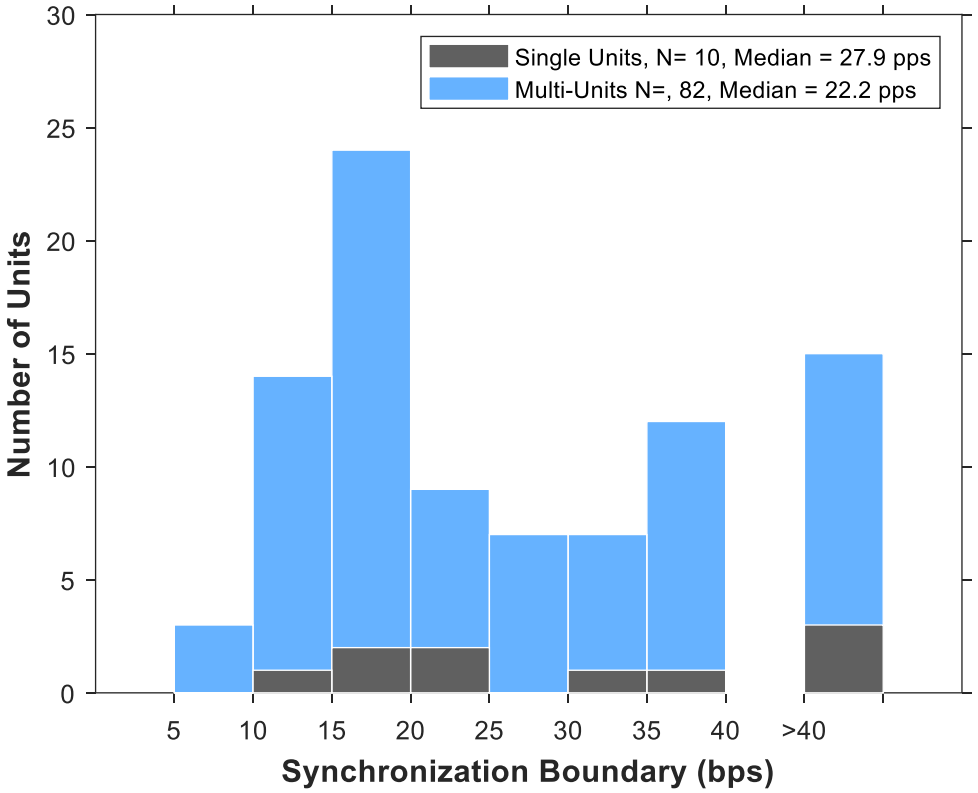

Figure 3.3: Synchronization boundaries for noise burst stimuli. Figure 3.3 displays a stacked histogram of synchronization boundary values for well isolated single units and multi-unit sites. Black bars represent well isolated single units, and blue bars represent multi-unit sites. Units which displayed synchrony to burst rates higher than 40 bps had undefined synchronized boundaries and are represented by the bar on the far right.

Figure 3.4 displays the grand mean normalized spike rate across all synchronized units expressed as spikes per second (red curve) and spikes per noise burst (black curve) as a function of the burst rate. Spikes rates were highest for burst rates up to a peak of 15 bps, followed by a gradual decline in spike rates to increasing noise burst presentation rates. The two magenta

points display grand mean normalized spikes per noise burst data from anesthetized cats (Middlebrooks and Bremen, 2013) for rates of 5 and 10 bps. Synchrony in units in the anesthetized cortex declined rapidly when the burst rate was increased from 5 to 10 bps, whereas we observed a peak in the spikes per burst for noise bursts presented at 15 bps and a gradual decline toward 40 bps. That units in the awake cortex were able to synchronize to rates higher than units in the anesthetized cortex mirrors our previous observation of synchrony to higher click rates in awake conditions (Chapter 2).

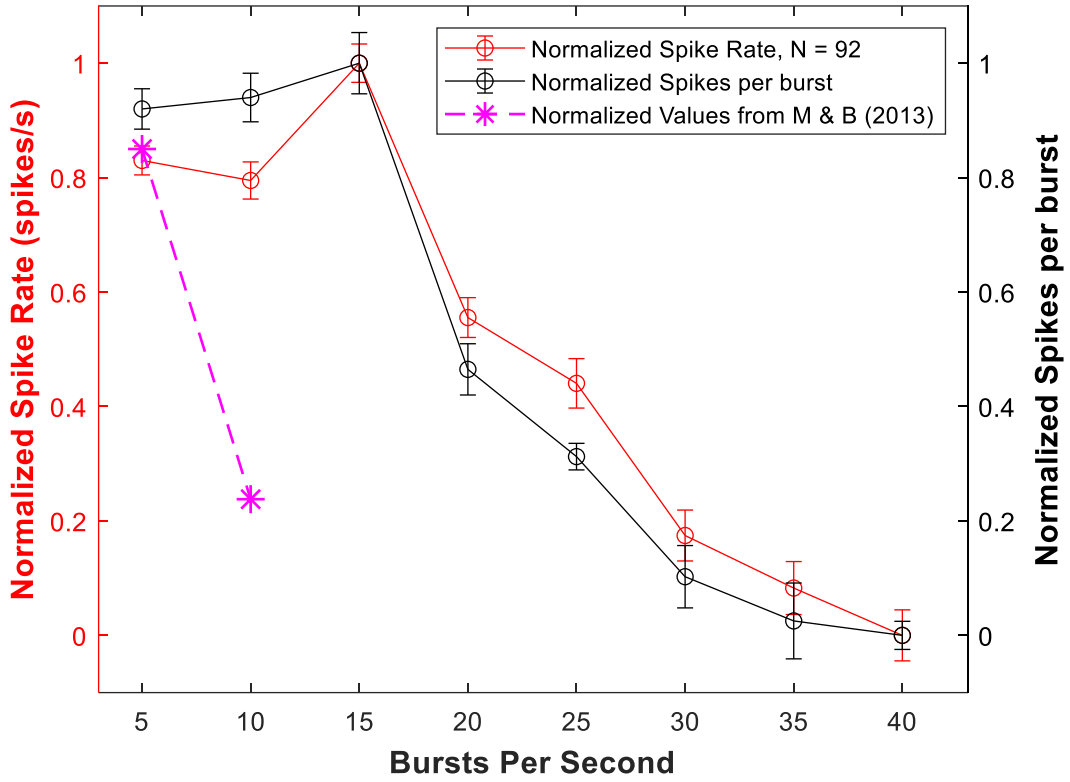

Figure 3.4. Grand mean spike rates across all synchronized units. Figure 3.4 displays normalized grand mean spike rate across all synchronized units are displayed as a function of the burst rate on the left y-axis (red curve). Spike rates for all synchronized units were normalized before averaging across all trials for each noise burst presentation rate. On the right y-axis, normalized grand mean spikes per burst (black curve) are displayed as a function of the burst rate. Data points from an anesthetized preparation (Middlebrooks and Bremen, 2013) are also presented in magenta on the right y-axis. These represent the normalized grand mean spikes per burst for units in the primary auditory cortex of cats under anesthesia.

Stream segregation in non-task conditions

We evaluated the response of cortical neurons in 9 cats to competing interleaved streams of noise bursts in an alternating ABAB… stimulus pattern; the cats were awake but were not participating in an auditory task and. In our stimulus, the A source (i.e., the target) was always located at 0° azimuth, and the competing B source (i.e., the masker) varied in location in azimuth from trial to trial. Spikes counts synchronized to bursts in either stream were quantified for each of the B locations. Each source produced a noise burst stream at a rate of 5 bps, resulting in an aggregate rate of 10/s across A and B streams.

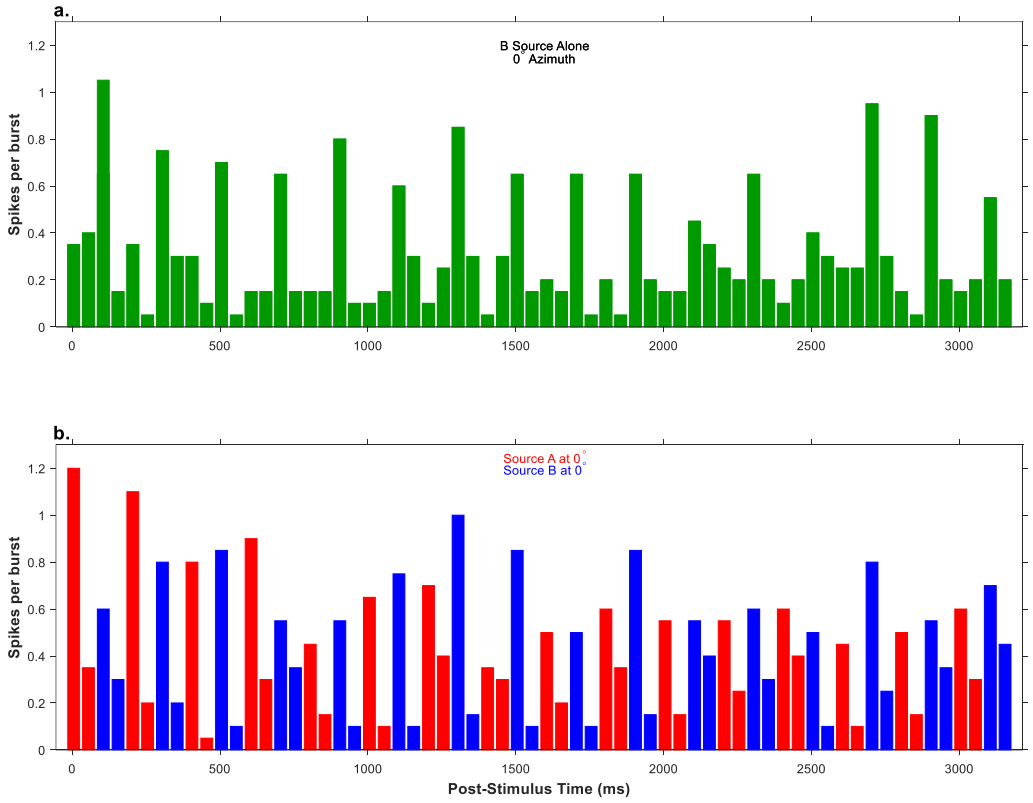

Figure 3.5. Response of one unit to single source and competing sequences. PSTHs of a multi-unit site. Plotted are the responses to sound sequences from a single-source location (Fig. 3.5A) and to competing sequences from the same location (Fig 3.5b.). Responses are spikes per sound burst in 50 ms bins, averaged over 20 trials. In both the single and competing conditions, sound sources were located at 0 degrees azimuth. In the bottom column, colors indicate spikes rates synchronized to the A source (red) and B source (blue). Unit An_01_10.

Most units in our study displayed synchrony to both sources in competing conditions and synchrony to the B sound source presented alone. Figure 3.5 shows a PST histogram for the responses from a multi-unit site for conditions in which the B source was presented alone (Fig. 3.5a), and when A and B sources were presented as competing streams, with both sources located at 0° azimuth (Fig. 3.5b). Data are plotted in 50 ms time bins. This unit displayed synchrony to the B source alone condition, with most spikes falling within 50 ms of sound onset from the B source. The burst rate in this condition was 5 bps. In Fig. 3.5a, this synchrony can be observed through the increased spikes per burst in every 4th bar, which aligns with the onset of each burst from the B source. In the competing condition (Fig. 3.5b), the unit exhibited synchrony to both A (red bars) and B (blue bars) sound sources. Similar to the B source alone condition, spikes fell within the first 50 ms after the onset of the burst from source, indicated by the increased spikes per burst rate of every 2^{nd} bar. The noise burst rate in Fig. 3.5b is double that of Fig 3.5a.,10 bps, yet the number of spikes per burst is about the same in both conditions, indicating synchrony to both sources in the competing condition.

We used rate azimuth functions (RAFs) to analyze units displaying a significant response to competing noise-burst stimuli. Significant responses were observed in 88 units across 9 array placements. Of those, 8 were well isolated single units, and 80 were multi-unit sites. Figure 3.6 illustrates the RAFs for three multi-unit sites from one animal. The x-axis in each panel indicates the B source location contralateral (C) or ipsilateral (I) relative to the placement of the recording electrode in the cat's right hemisphere. The vertical dashed line indicates the A source location, which was always fixed at 0°. In the left column (Figures 3.6A, 3.6C, and 3.6E), the y-axis indicates mean spikes per burst for each sound source; the data in Fig. 3.6E are from the unit represented in Fig. 3.5). The green curve indicates spikes synchronized in conditions where the B

source was presented alone, without a competing A source stream. The blue curve represents spikes synchronized to noise bursts from the B source as a function of B source location. The blue curve can be observed to run parallel, and in some cases coincide with, the green curve since they are synchronized to the same sound source. The red curve represents response to the A source, fixed at 0°, as the B source location was varied. Any variation in the A curve as a function of B location would reflect an interaction between sounds from A and B sources. Responses synchronized to A and B sources were roughly equal in the condition in which the B source was co-located with the A source at 0° and equal to the B-alone condition, suggesting these units were able to synchronize to both streams in competing conditions. In the figure, the most conspicuous effect of B-source location on the response of the A source at 0° is seen in Figure 6C, in which a shift of the B source from 0° to ipsilateral 60° resulted in a decrease of ~11% in the response to the A source.

To measure the accuracy to which spike counts discriminated between the A and B sources in competing conditions, we computed a discrimination index, *d'*, which is plotted in Figure 3.6 in the right column (Figs. 3.6b, 3.6d, and 3.6f). The dashed black lines indicate threshold values for the *d'* analysis; we took values of < -1 or >+1 to indicate significant synchrony to a sound source. The solid black curves in Figs. 3.6B, 3.6D, and 3.6F indicate the discrimination index for A and B sources based on B-source location in azimuth. Positive *d'* values indicated stronger responses to the more contralateral source location, which can be observed in the Fig. 3.6c through higher spikes per burst for spikes synchronized to the B source (blue curve). The figures in the right column are paired with the units displayed in the left column, such that Fig. 3.6b illustrates the discrimination index for the unit displayed in Fig. 3.6a, Fig. 3.6d displays the discrimination index for the unit in Fig. 3.6c, and so on. In nearly all

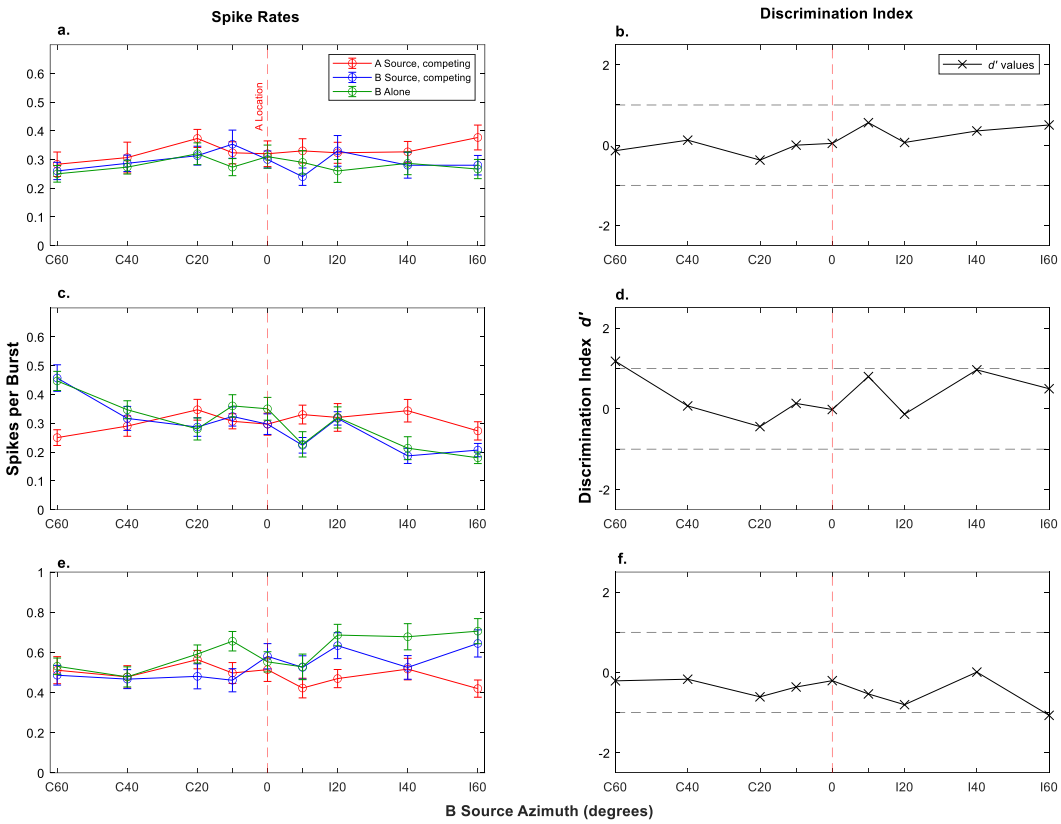

Figure 3.6. Rate-Azimuth Functions from one animal. RAFs from one animal for spikes synchronized to A source and B source bursts. The figures in the left column (Figs. 3.6A, C, and E) represent the spikes per burst for each location and each sound source. The x-axis plots the B source location, and the red dashed line indicates the A source location for each condition. For all trials, the A source was fixed at 0° in azimuth. The red curve represents mean spikes synchronized to A source across all trials, with standard error. The blue curve represents mean spikes synchronized to the B source across all trials. The green curve represents the mean spikes synchronized to the B source location in a condition where the B source location was presented alone i.e., with no competing A source. The figures in the right column (Figs. 3.6B, D, and F) represent the discrimination index values for the units represented in the right column. Units in the right column are paired with the discrimination values plotted in the right column in each row. In each right column figure, the y-axis plots the discrimination index *d'*. Dashed black lines represent the significance threshold of ±1 for *d'* values—locations where *d'* (black line) crosses the threshold indicate significant discrimination in the neural responses. Units An01_21 (A), An01_31(C), An_01_10 (E).

instances, *d'* fell within a range of approximately ±1, indicating that these units failed to show significant spatial stream segregation.

Spatial segregation for various B source locations was quantified by computing the *d'* for discrimination of trial-by-trial spike synchrony to competing A and B sources. Out of 88 units that displayed a significant response to competing sound bursts, 16 units (~18%) displayed *d'*

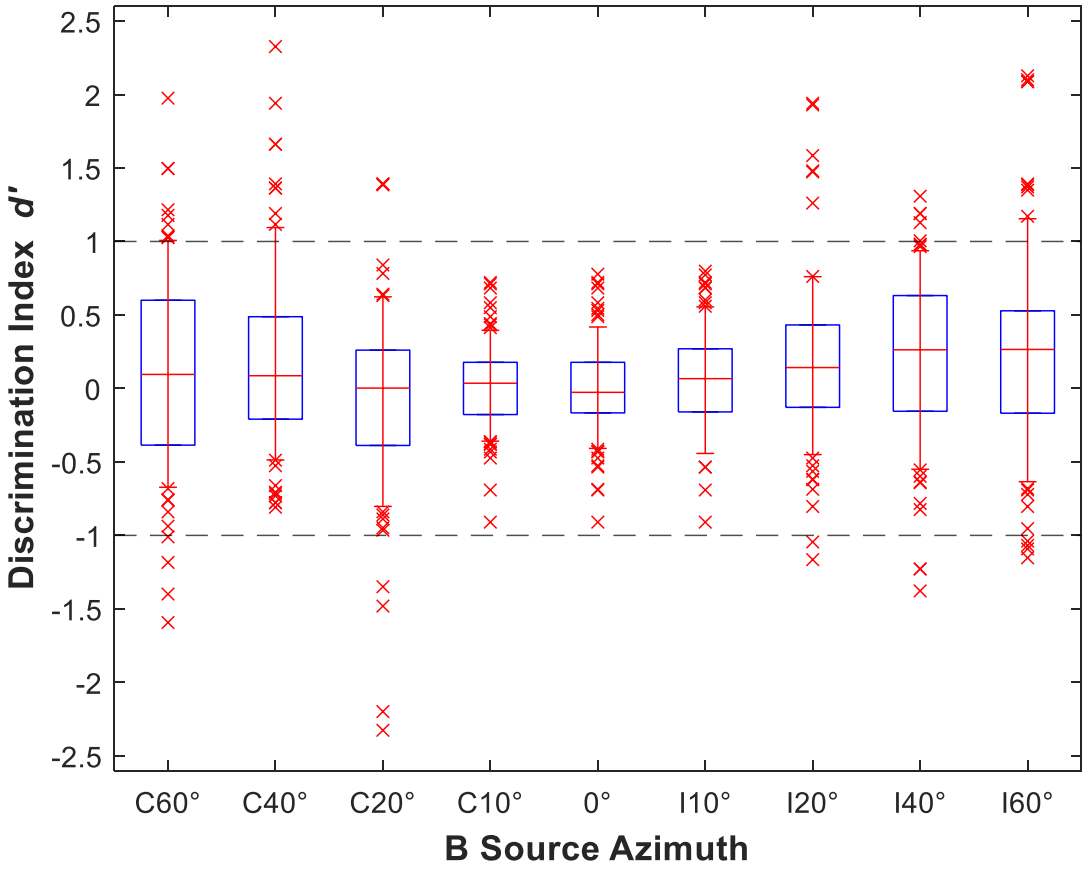

Figure 3.7. Distribution of *d'* values in competing conditions. The horizontal line in each box represents the median *d'* value all units. Upper and lower edges of each box represent the 75th and 25th quartiles for each distribution. Vertical red lines represent 90% of the distribution of data; the upper edge represents the 90th quantile, and the lower edge of the line represents the 10th quantile of the data. Horizontal dashed black lines represent threshold values for significant discrimination.

values greater than +1 or less than –1 indicating significant segregation of A and B sources for at least one B source location. Of these 18 units, 2 were well isolated single units, and 16 were multi-unit sites. Out of the 18 units that displayed significant *d'* values, 8 units displayed segregation to more than one B source location. The minimum separation between A and B sources that resulted in significant discrimination across all units was 20°. Figure 3.7 displays the distribution of *d'* values for the B-source locations. In each box, the red line indicates the median, and the bottom and top edges of the box indicate the 25th and 75th percentiles, respectively. The whiskers indicate the 10th and 90th percentiles. The dashed black lines indicate

the discrimination index threshold values of ± 1. There was a weak but significant tendency for the absolute values of *d'* to increase with increasing separation between A and B sources ($X^2_{(8,792)}$ = 21.4, p = 6.1e-3, Kruskal-Wallis). Figure 8 displays the grand means for the spikes per burst for all units tested. The black curve, referred to the right y-axis, represents averaged *d'* values for each B-source location. The majority of units observed in this study did not display significant discrimination between A and B sources and were able to synchronize to noise bursts in both interleaved streams.

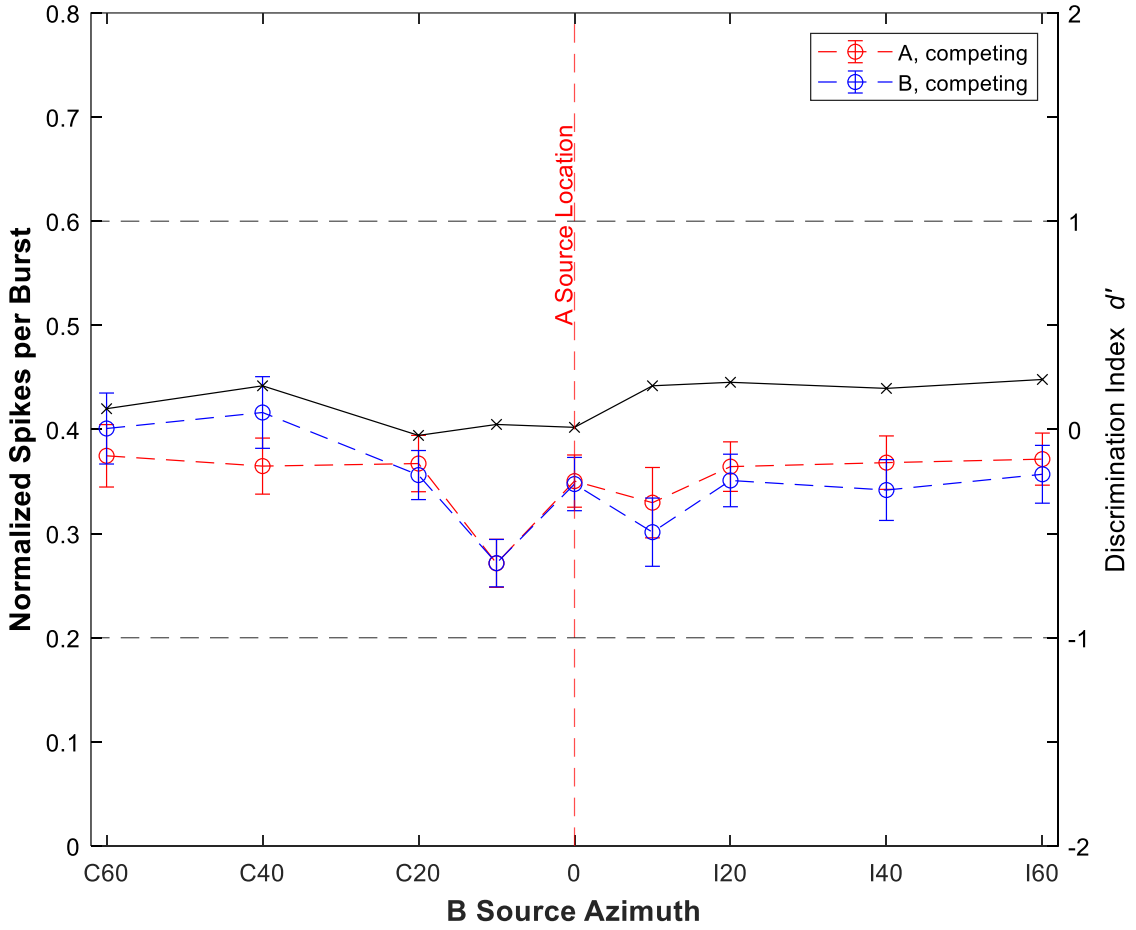

Figure 3.8. Grand means of trial-by-trial spikes per burst for spike synchronized to A and B sources in competing conditions. The black curve represents average *d'* values for each B source location.

To characterize the extent of forward suppression occurring in the response of cortical units in competing conditions, we computed an attenuation measure following Middlebrooks and Bremen (2013). Middlebrooks and Bremen defined attenuation the following equation:

$$RA(\theta_A, \theta_B) = RSgl(\theta_A) - Atten\ X\ RSgl(\theta_B)$$

where *RA* represents the spike counts synchronized to the A source as a function of A and B locations, θ_A, and θ_B, respectively. $RSgl(\theta)$ represents the spike count elicited by a single source at location θ, and *Atten* is the attenuation factor computed for each unit. The expression states that the predicted spike count synchronized to A or B for a location B in competing conditions is the single-source spike count at the location B location attenuated by a scalar, times the single-source spike count at the location of the competing sound. Middlebrooks and Bremen found an attenuation value of 0.68 ± 0.16 (mean ± standard deviation) in the anesthetized cortex for the 10 bursts per second condition when A and B sources were co-located (Middlebrooks and Bremen, 2013). In the awake cortex, we observed a mean attenuation value of only 0.18 ± 0.031 across all units when A and B sources were co-located at 0°. The substantially lower attenuation observed in the awake cortex accords with the strong response to a 10-bps train of noise bursts, as shown in Fig. 3.4. Further, the small attenuation value observed in the awake cortex could account for the tendency of the synchrony to the B source in competing conditions to closely follow the synchrony B source in B-alone conditions (e.g., Fig. 6c), as well as the general lack of enhancement for stream segregation observed across all units.

Discussion

We evaluated the ability of neurons to encode trains of noise bursts in the primary auditory cortex of 14 cats in awake conditions. Study of entrainment of neural spikes to noise bursts demonstrated synchronous firing of some units to rates as high as 40 bursts per second. That rate of synchrony in awake conditions was substantially higher that rates previously observed under anesthesia. We further evaluated the ability of neurons to synchronize to interleaved competing noise bursts varying in spatial separation in the primary auditory cortex of 9 cats in awake conditions. Study of competing sound sources revealed most neurons in non-task conditions displayed synchrony to both competing streams, regardless of spatial separation. That is, there was minimal evidence of segregation of competing streams of noise bursts by neurons in the unanesthetized auditory cortex. This contrasts with anesthetized preparations, in which neurons in the primary auditory cortex show a robust ability to segregation between two interleaved competing sound sources (Middlebrooks and Bremen, 2013).

Representation of noise bursts with varying rate

In our study of coding of varying rates of noise bursts in awake conditions, we observed a median synchronization boundary of 22.9 s^{-1} to noise burst trains in the response of cortical neurons in cats not engaged in a task. The majority of units in our study (82/92) synchronized to rates >10 bps, and 15 units were able to synchronize to rates as high as the highest presented rate (40 bps). These findings are markedly higher than what has been observed in anesthetized preparations. Middlebrooks and Bremen (2013) presented trains of noise bursts to anesthetized cats and recorded the response of neurons in the primary auditory cortex. They observed that most units in the anesthetized cortex in this study were able to respond with spikes synchronized to burst rates of 5 bps, but stimulus-synchronized spike numbers were reduced in response to

higher rates of 10 bps in the majority of neurons. Our results coincide with our previous finding (STP chapter) regarding the ability of neurons in the cat cortex in awake preparations to synchronize to trains of click stimuli with rates higher than what has been observed in anesthetized preparations.

Spatial tuning in the cat auditory cortex

Middlebrooks and Bremen (2013) characterized the spatial tuning of neurons in the anesthetized cat cortex. They observed spatial tuning in the synchronized responses to sound bursts presented at rates of 2.5 and 5 bps, with units typically showing a preference for the contralateral hemifield. The spatial sensitivity of units was represented through their RAFs, which were then characterized by the widths of equivalent rectangular receptive fields (ERRFs) and the modulation of spike rate based on B source location in azimuth (modulation depth) for each unit. Middlebrooks and Bremen reported an overall median ERRF width of 148.7° across all units. In our study, the median ERRF width for all units was 116.1°. This discrepancy is likely due to the inclusion of the ±80° source locations in azimuth in the Middlebrooks and Bremen study. In simulated conditions, the addition of the ±80° source locations in the calculation of the ERRF values in the awake condition led to a distribution with a median value of 147.1°. Middlebrooks and Bremen (2013) also reported a median modulation depth of 35.3% across all units. In the awake cortex, we observed a median modulation depth value of 44.1%. Some of the discrepancy observed between the anesthetized condition in Middlebrooks and Bremen and the present study could be explained by the free head movement allowed in the awake condition. Indeed, during visual monitoring of the cats in the single source condition, we often observed the cats moving their heads during the 3.4-s train of noise bursts to look at the sound source location in each trial. The free head movement would likely introduce confounds to

the measure of ERRFs from trial to trial, causing them to likely be smaller than in head-fixed positions. Spatial tuning in awake non-task conditions has also been previously characterized in our laboratory (Lee & Middlebrooks, 2011). Lee and Middlebrooks observed a median ERRF width value of 185° in the spatial tuning of cortical neurons in awake non-task conditions. We note that the experimental design in that study precluded stimulus-directed changes in head orientation. Also, the earlier study included measurements for locations spanning 360° in azimuth. In the current study, measurements spanned 120° in azimuth, making comparison of spatial sensitivity between the two studies difficult.

Stream segregation in psychophysics and physiology

Previous psychophysical results have explored the role of the stimulus duration and stimulus rate in stream segregation (for review, see Moore and Gockel, 2002). Stream segregation in human psychophysics has been commonly studied using tone sequences. A common type of stimuli used in streaming experiments consists of two tones with different frequencies, presented as triplets in an ABA… pattern (Bregman et al., 2000; van Noorden, 1975)). When heard as a single stream of tone sequences, this pattern produces the percept of a "gallop" rhythm. In other conditions, the A and B tones are heard as distinct A and B streams, with the A tones appearing at twice the rate of the B tones. In the study by van Noorden (1975) using these stimuli, a high incidence of streaming (with sufficient frequency separation between A and B tones) was observed at rates between 4 and 10 presentations of tone bursts per second, with performance improving for rates up to 20 s^{-1}. In Bregman et al., (2000), researchers altered temporal and frequency characteristics of this ABA… pattern and observed that that rate of presentation of triplets was the strongest temporal property, and on par with frequency differences, in allowing listeners to segregate A and B streams in this auditory task. In

comparison, temporal features of stimuli such as the duration of each tone had a minimal impact on stream segregation performance. In general, presentation rates between 4 and 10 bursts per second have been typically used in streaming experiments, and stream segregation performance increases with increasing rates. (e.g., Cusack et al., 2004; Vliegen & Oxenham, 1999). Stream segregation is not typically tested for rates higher than 20 bursts per second, as subjects typically display an inability to fuse the competing stimuli and can only perceive two distinct streams.

Stream segregation with spatial cues has been studied in cortical physiology in anesthetized conditions (Middlebrooks and Bremen, 2013). In their study, Middlebrooks and Bremen presented interleaved streams of noise bursts varying in spatial separation, and recorded responses from the primary auditory cortex of cats in an anesthetized preparation. Noise bursts were 5 ms in duration and presented at aggregate rates of 5 or 10 bps. Competing streams were presented in an ABAB… pattern, and sound source locations were varied in azimuth, including the location of the A source. Here, we focus on the condition of that paper in which one of the competing sources was fixed at 0° and the aggregate sound-burst rate was 10/s. In anesthetized conditions, cortical neurons reliably displayed stimulus-synchronized spike rates to single-source conditions. When a competing interleaved sound source was added, however, the majority of neurons preferentially synchronized to one of the two streams, and displayed significant discrimination ($d' > 1$). This was marked by an increase in the spike per burst rate for responses to the preferred source location, accompanied by a decrease in the response to the non-preferred location. In contrast, the majority of neurons in awake conditions in the present study did not display preferential synchrony to the A or B streams with spatial separation. Most neurons in our awake preparation synchronized to both competing streams regardless of spatial separation, and only a small number of units displayed significant discrimination (18/88, ~20%) at any spatial

separation. Middlebrooks and Bremen (2013) further observed a general increase in stream segregation with increasing spatial separation. Neurons in the anesthetized cortex reliably displayed significant discrimination to one of two competing streams with a spatial separation as low as 10-20° in azimuth, and *d'* values typically increased with larger separation between the A and B sources. In the awake condition, we observed a weak but significant increase in discrimination between the two streams with increasing spatial separation. However, stream segregation in the awake cortex was much less prevalent, and discrimination index values were much lower than in the anesthetized preparation. In Chapter 2, we observed that the majority of units in our sample had characteristic frequency values around 8 kHz. This matches the frequency range in which cats in previous studies have been shown to perform well in psychophysical measures of stream segregation using spatial cues (Javier et al., 2016). In their study, Javier and colleagues observed that cats consistently performed with better accuracy in high-pass conditions, where noise bursts were filtered to the 4-25 kHz frequency band, compared to low-pass conditions (0.4-1.6 kHz frequency band). These findings suggested that cats performed worse when interaural level cues were limited in low-pass stimuli. In their study, performance in the high-pass condition matched performance of the broadband condition (.4 – 25 kHz frequency band), suggesting that feline listeners were able to rely on high frequency ILD cues in the broadband condition in order to successfully perform the stream segregation task. In the anesthetized cortex, Middlebrooks and Bremen observed that among units with a characteristic frequency of 8 kHz, more than 75% had *d'* values greater than 1 for 20° separations at the pair of locations that displayed the highest *d'* values. Comparatively, in the awake condition we observed few units that displayed significant discrimination among the two presented streams, even at the largest spatial separation (60°).

Middlebrooks and Bremen (2013) fit their data successfully with a parameter free linear model, a key element of which was forward suppression. Forward suppression (referred to as *Atten* by Middlebrooks and Bremen) refers to the suppression of the response to the second of 2 sounds that are similar in spectrum or source location. Forward suppression is evident as a decrease in spike rate with increasing stimulus burst rates. In the Middlebrooks and Bremen model, forward suppression had the effect of enhancing spatial sensitivity in the response of neurons in the anesthetized cortex. Middlebrooks and Bremen reported that a doubling of burst rate from 5 to 10 bps resulted in 68% decrease in the number of synchronized spikes per burst in the anesthetized cortex. In the awake cortex, we only observed a decrease of 18% due to forward suppression at those rates. The reduction in forward suppression in the awake cortex observed in this current study likely accounts for the weak stream segregation observed in the response of cortical neurons.

Though this current report was modeled after the design of the report of Middlebrooks and Bremen (2013), there were differences in the duration of individual noise bursts, as well as the way the animal was positioned during the presentation of the stimuli. Noise bursts in the current study were 20 ms in duration, as compared to 5 ms in duration in the Middlebrooks and Bremen (2013) study. Six of the nine cats used in this study had previously been trained for a behavioral spatial stream segregation task (Javier et al., 2016; Chapter 1). The noise bursts in the behavioral task were 20 ms in duration, and we chose to maintain that for the study of interleaved sound bursts in non-task conditions. It is unlikely that the length of noise bursts contributed to the lack of stream segregation observed in the awake cortex. Previous studies have explored the length of stimulus duration and found that longer durations are likely to facilitate and enhance stream segregation in psychophysical measures (van Noorden, 1975). That is, the

longer burst durations in the present study compared to those in Middlebrooks and Bremen (2013) should have, if anything, strengthened stream segregation by cortical neurons. In tests of spatial stream segregation in human psychophysics, measures of spatial acuity using 10-, 20-, and 40-ms burst durations showed no significant difference between the 10- and 20-ms bursts and increased acuity for the 40-ms bursts (Middlebrooks and Onsan, 2012). Further, cats have been shown to behaviorally segregate streams of noise bursts with as little as 10° spatial separation with 20 ms noise bursts (Javier et al., 2016; Chapter 1). The current study also differed in the positioning of the cat during stimulus presentation. Specifically, in the anesthetized preparation, the cat's head was fixed in position, whereas the awake cats in the current study had free range of motion in their head and limbs. Although the head orientation could change during a trial, that would not have affected the separation of A and B sources. However, the free head movement, as well as the awake non-task design of the study, may have allowed cats to not attend to the presentation of the stimulus, which in turn may have diminished the stream segregation response of the cortical neurons.

It is surprising that Middlebrooks and Bremen (2013) observed robust stream segregation in the response of cortical neurons under anesthesia at spatial separations that agree with human and cat psychophysics results (human: Middlebrooks and Onsan, 2012; cat: Javier et al., 2016), whereas we observed little or no stream segregation in awake conditions at a similar time scale. Stream segregation has been demonstrated in the response of cortical neurons in awake preparations in studies where stimuli varied in their frequency rather than spatial location (Fishman et al., 2001). Fishman et al., for example, observed stream segregation in the response of cortical neurons in macaques presented with competing streams of noise differing in frequency in a similar ABAB… interleaved pattern in non-task conditions. In their stimuli, one

source was presented at a predetermined best frequency for a neuron, and the other source was varied in frequency in different conditions. They observed that neurons in the awake macaque cortex displayed significant discrimination between the two streams of noise in conditions at rates of 20 s^{-1} and 40 s^{-1}, but not at rates of 5 s^{-1} and 10 s^{-1}. Fishman et al. (2001) suggested that forward suppression was enhancing the segregation of competing streams in the response of awake neurons in the macaque cortex when tone bursts were presented at higher rates. Similar to the results we observed in the awake cat cortex, Fishman et al. found minimal forward suppression and weak stream segregation at rates of 10 s^{-1} in the macaque cortex. These findings are in stark difference to findings from the anesthetized cortex and psychophysics. In the anesthetized cat cortex, strong forward suppression and robust stream segregation was observed at rates between 5 s^{-1} and 10 s^{-1} (Middlebrooks and Bremen, 2013). Results from psychophysics experiments have demonstrated that stream segregation typically occurs at rates of 5 s^{-1}, is prominent at rates of 10 s^{-1}, and increases with increasing rate up to 20 s^{-1} (van Noorden, 1975; Bregman et al., 2000). In the awake cat cortex, we observe diminishing synchrony and strong suppression to noise bursts at rates 20 s^{-1} and higher (Fig. 4). We therefore think it is likely that stream segregation might have been observed in the awake cat cortex had we tested interleaved stimuli at higher rates, such as 20 s^{-1} or 40 s^{-1}. Nevertheless, cortical streaming in awake non-task conditions at rates $\geq$ 20 s^{-1} does not account for the psychophysical streaming that has been observed at rates of 5 s^{-1} to10 s^{-1} in both humans (van Noorden, 1975; Middlebrooks and Onsan, 2012) and cats (Javier et al., 2016; Chapter 1). It is possible, therefore, that another mechanism such as selective attention may help facilitate stream segregation in the awake cat cortex at rates used in this study in on-task conditions.

Selective attention has been shown to modulate neural responses in stream segregation tasks at the level of the auditory cortex (Bidet-Caulet et al., 2007; Lakatos et al., 2013). In Bidet-Caulet, 2007, researchers observed the neural responses of the auditory cortex through intracranial electroencephalography (EEG) in human subjects performing a stream segregation task. The stimuli consisted of two concurrently played amplitude modulated streams differing in modulation rate and carrier frequency. Subjects were tasked with attending to one of the two streams and detect randomly introduced noise bursts superimposed onto the target stream. Synchrony to the target and masker streams were studied through the steady-state potentials of populations of neurons in the auditory cortex. Researchers found cortical neurons were able to represent both competing streams. Further, when tasked with stream segregation during on-task conditions, researchers found an enhancement of the synchrony in the cortical neurons to the attended stream, as well as diminished response to the competing streams. Researchers were also able to ask the subjects to switch their attention between streams and observe a similar reversal in the synchrony of the neurons in the steady-state potential response. This study demonstrates that selective attention can modulate neuronal firing to enhance representation of the target stream and diminish the representation of competing streams in on-task conditions. In Lakatos et al., 2013, researchers observed the response of cortical neurons in the primary auditory cortex of awake macaque monkeys as the monkeys performed a stream segregation task. The stimuli in this study competing concurrent bursts of pure tones. Each stream was presented with a fixed frequency either a recording site's best frequency, or a frequency 2 octaves below or above the best frequency. Within the presentation of each stream, small deviations were produced in a random manner every 3-9 second. These deviations consisted of frequency shifts to the tone bursts, on the order of 2-4 semitones. Researchers observed that neurons in the primary auditory

cortex showed enhanced synchrony and a larger magnitude of response to the attended stream when subjects were on-task and discriminating between the two streams of tones. They further observed that during on-task conditions, synchrony to the competing unattended stream diminished significantly. In the current study, it may be that selective attention is necessary to enhance the representation of the target stream and facilitate stream segregation.

The results in this study demonstrate that cortical neurons in the awake cat can synchronize to Gaussian noise bursts with much higher rates than what has been previously observed in the anesthetized cortex. Further, we observed that when presented with two competing streams of interleaved noise bursts with an aggregate rate of $10s^{-1}$, the majority of neurons are able to synchronize to both streams even when the sound sources are separated in spatial location in azimuth. Overall, we observed minimal discrimination of competing streams in the response of awake neurons in the cat auditory cortex, and substantially less forward suppression active in the awake cortex in competing stream conditions, compared to anesthetized conditions. Previous work has demonstrated robust spatial stream segregation in psychophysics by cats with the same stimuli parameters used in this study (Javier et al., 2016; Chapter 1). It may be that in on-task conditions, mechanisms such as selective attention or forward suppression will modulate the neuronal responses and facilitate stream segregation in the response of neurons in the primary auditory cortex.

Summary and Future Directions

Summary

Listeners have the remarkable ability to perceptually group relevant sequences of sounds amidst competing sources in complex auditory environments. This phenomenon has been referred to as "stream segregation". Physical separation of sound has been observed to be a robust factor in facilitating stream segregation. Human listeners, for example, can perceptually segregate between competing sounds with as little as ~8° of spatial separation. In the cat animal model, behavioral measures demonstrate that feline listeners are similarly able to perform stream segregation with as little as ~10° of spatial separation between competing sound sources. Neural correlates of stream segregation have also been observed in the primary auditory cortex of anesthetized cats (Middlebrooks and Bremen, 2013). Neurophysiological measures of the anesthetized cat cortex demonstrate that cortical neurons can similarly synchronize to one of two competing streams with as little as ~10° of spatial separation. The goal for this dissertation is to evaluate the neural correlates of spatial stream segregation, and to evaluate the spectral and temporal coding properties of the primary auditory cortex, in the cat animal model in the absence of anesthesia. The cat animal model has been extensively studied in auditory research and are especially well suited for tasks with spatially varying stimuli due to their robust sound localization abilities. Further, their well-developed auditory cortex is easily accessible on the surface of the brain, making them ideal candidates for neurophysiological recordings. In chapter 1, I demonstrate that cats can successfully perform a spatial stream segregation task with median threshold of ~9.8° of spatial separation between sound sources. These findings match studies using the same task in cats (Javier et al., 2016), and a similar task in human listeners (Middlebrooks and Onsan, 2012). In Chapter 2, I observe that cortical units in the awake primary

auditory cortex of cats display a wide array of coding properties to stimuli varying in frequency and rate. Specifically, I observed properties that are rarely seen in anesthetized preparations and have only been observed in the marmoset animal model. These properties include frequency tuning restricted in both frequency and level. I also observed sustained and temporally dynamic responses to tonal stimuli, including sharpening of tuning bandwidths in the duration of the stimulus. For stimuli varying in rate, I observed synchronous firing to click trains as fast as 226 clicks per second. I further observed non-synchronous coding, in which units displayed increasing firing rates with increasing click rates. These findings have support the hypothesis that the variety of coding observed is a generally present in the awake auditory cortex, and not a species-specific specialization for the marmoset. In Chapter 3, I observed that neurons in the awake primary auditory cortex could synchronize to trains of noise bursts as high as 40 bursts per second, which contrasts with findings in anesthetized preparations. I further found cortical neurons in the awake auditory cortex were able to synchronize competing interleaved sound bursts regardless of spatial separation between sound sources. These findings contradict what has been previously observed in the response of cortical neurons in the anesthetized cortex, and behavioral measures of awake cats engaged in a stream segregation task. This dissertation highlights the neurophysiological properties of the awake cat auditory cortex and can serve as a basis for future studies exploring the neural correlates of stream segregation.

Future Directions

More study is needed to understand the neural basis of stream segregation when animals are engaged in a behavioral task. Prior work has demonstrated that selective attention can modulate the spatial tuning sensitivity of cortical neurons in awake conditions. Lee and Middlebrooks, 2011, observed a sharpening of spatial sensitivity when animals were engaged in

a spatial localization task, compared to spatial tuning in off-task conditions. Studies have also demonstrated that selective attention can modulate neural responses in stream segregation tasks in cortical neurons. Bidet-Caulet and colleagues (2007) demonstrated that cortical neurons in humans performing a stream segregation task had an enhancement of the synchrony to the attended stream, accompanied by a diminished response to competing streams. We may observe a similar mechanism occurring in on-task conditions in a spatial stream segregation task—one in which cortical neurons show an enhancement to the synchrony of the attended stream, coupled with a diminishing representation of the competing stream.

Recent studies have explored the role of oscillatory activity in the cortex as a potential mechanism for stream segregation using stimuli varying in rhythm. Lakatos and colleagues (2013) observed oscillatory interacting and driving the response of neurons in the primary auditory cortex when macaque monkeys performed a stream segregation task. In their observations, different neural oscillations worked to enhance synchrony in the response of cortical neurons to an attended stream and diminish synchrony to competing streams. An exploration of oscillatory activity may reveal a similar mechanism when animals are engaged in a stream segregation task using spatial cues. Further, neural oscillations may shed light into interactions between cortical areas, and further our understanding of the role of cortical regions outside of the primary auditory cortex in the process of stream segregation. Overall, the work in this dissertation provides insights into the properties of the auditory cortex, and mechanisms underlying spatial stream segregation.

References

Bartlett, E. L., Sadagopan, S., & Wang, X. (2011). Fine frequency tuning in monkey auditory cortex and thalamus. *Journal of Neurophysiology*, *106*(2), 849–859. https://doi.org/10.1152/jn.00559.2010

Bidet-Caulet, A., Fischer, C., Besle, J., Aguera, P.-E., Giard, M.-H., & Bertrand, O. (2007). Effects of selective attention on the electrophysiological representation of concurrent sounds in the human auditory cortex. *The Journal of Neuroscience: The Official Journal of the Society for Neuroscience*, *27*(35), 9252–9261. https://doi.org/10.1523/JNEUROSCI.1402-07.2007

Bregman, A. (1990). *Auditory Scene Analysis: The Perceptual Organization of Sound*. The MIT Press.

Bregman, A. S., Ahad, P. A., Crum, P. A., & O'Reilly, J. (2000). Effects of time intervals and tone durations on auditory stream segregation. *Perception & Psychophysics*, *62*(3), 626–636. https://doi.org/10.3758/bf03212114

Brosch, M., & Schreiner, C. E. (1997). Time course of forward masking tuning curves in cat primary auditory cortex. *Journal of Neurophysiology*, *77*(2), 923–943. https://doi.org/10.1152/jn.1997.77.2.923

Cheung, S. W., Bedenbaugh, P. H., Nagarajan, S. S., & Schreiner, C. E. (2001). Functional Organization of Squirrel Monkey Primary Auditory Cortex: Responses to Pure Tones. *Journal of Neurophysiology*, *85*(4), 1732–1749. https://doi.org/10.1152/jn.2001.85.4.1732

Cusack, R., Decks, J., Aikman, G., & Carlyon, R. P. (2004). Effects of Location, Frequency Region, and Time Course of Selective Attention on Auditory Scene Analysis. *Journal of Experimental Psychology: Human Perception and Performance*, *30*(4), 643–656. https://doi.org/10.1037/0096-1523.30.4.643

Dong, C., Qin, L., Zhao, Z., Zhong, R., & Sato, Y. (2013). Behavioral modulation of neural encoding of click-trains in the primary and nonprimary auditory cortex of cats. *Journal of Neuroscience*, *33*(32), 13126–13137. https://doi.org/10.1523/JNEUROSCI.1724-13.2013

Eggermont, J. J. (1991). Rate and synchronization measures of periodicity coding in cat primary auditory cortex. *Hearing Research*, *56*(1–2), 153–167. https://doi.org/10.1016/0378-5955(91)90165-6

Eggermont, J. J. (1998). Representation of spectral and temporal sound features in three cortical fields of the cat. Similarities outweigh differences. *Journal of Neurophysiology*, *80*(5), 2743–2764. https://doi.org/10.1152/JN.1998.80.5.2743

Farley, GlennR., Barlow, StevenM., Netsell, R., & Chmelka, JamesV. (1992). Vocalizations in the cat: Behavioral methodology and spectrographic analysis. *Experimental Brain Research*, *89*(2). https://doi.org/10.1007/BF00228249

Fishman, Y. I., Reser, D. H., Arezzo, J. C., & Steinschneider, M. (2001). Neural correlates of auditory stream segregation in primary auditory cortex of the awake monkey. *Hearing Research*, *151*(1), 167–187.

Gaese, B. H., & Ostwald, J. (1995). Temporal Coding of Amplitude and Frequency Modulation in the Rat Auditory Cortex. *European Journal of Neuroscience*, *7*(3), 438–450. https://doi.org/10.1111/j.1460-9568.1995.tb00340.x

Gehr, D. D., Komiya, H., & Eggermont, J. J. (2000). Neuronal responses in cat primary auditory cortex to natural and altered species-specific calls. *Hearing Research*, *150*(1–2), 27–42. https://doi.org/10.1016/s0378-5955(00)00170-2

Goldberg, J. M., & Brown, P. B. (1969). Response of binaural neurons of dog superior olivary complex to dichotic tonal stimuli: Some physiological mechanisms of sound localization. *Journal of Neurophysiology*, *32*(4), 613–636. https://doi.org/10.1152/jn.1969.32.4.613

Green, D. M., & Swets, J. A. (1966). *Signal detection theory and psychophysics.* John Wiley.

Heil, P., Rajan, R., & Irvine, D. R. F. (1992). Sensitivity of neurons in cat primary auditory cortex to tones and frequency-modulated stimuli. I: Effects of variation of stimulus parameters. *Hearing Research*, *63*(1–2), 108–134. https://doi.org/10.1016/0378-5955(92)90080-7

Javier, L. K., McGuire, E. A., & Middlebrooks, J. C. (2016). Spatial Stream Segregation by Cats. *Journal of the Association for Research in Otolaryngology: JARO*, *17*(3), 195–207. https://doi.org/10.1007/s10162-016-0561-0

Kajikawa, Y., De La Mothe, L., Blumell, S., & Hackett, T. A. (2005). A comparison of neuron response properties in areas A1 and CM of the marmoset monkey auditory cortex: Tones and broadband noise. *Journal of Neurophysiology*, *93*(1), 22–34. https://doi.org/10.1152/jn.00248.2004

Lakatos, P., Musacchia, G., O'Connel, M. N., Falchier, A. Y., Javitt, D. C., & Schroeder, C. E. (2013). The Spectrotemporal Filter Mechanism of Auditory Selective Attention. *Neuron*, *77*(4), 750–761. https://doi.org/10.1016/j.neuron.2012.11.034

Lee, C.-C., & Middlebrooks, J. C. (2011). Auditory cortex spatial sensitivity sharpens during task performance. *Nature Neuroscience*, *14*(1), 108–114. https://doi.org/10.1038/nn.2713

Lu, T., Liang, L., & Wang, X. (2001a). Temporal and rate representations of time-varying signals in the auditory cortex of awake primates. *Nature Neuroscience*, *4*(11), 1131–1138. https://doi.org/10.1038/nn737

Lu, T., Liang, L., & Wang, X. (2001b). Temporal and rate representations of time-varying signals in the auditory cortex of awake primates. *Nature Neuroscience*, *4*(11), 1131–1138. https://doi.org/10.1038/nn737

Lu, T., & Wang, X. (2000). Temporal discharge patterns evoked by rapid sequences of wide- and narrowband clicks in the primary auditory cortex of cat. *Journal of Neurophysiology*, *84*(1), 236–246. https://doi.org/10.1152/jn.2000.84.1.236

Macmillan, N. A., & Creelman, C. D. (2005). *Detection theory: A user's guide* (2nd ed). Lawrence Erlbaum Associates.

Macmillan, N. A., & Kaplan, H. (1985). *Detection theory: A user's guide*. Psychology Press.

Mardia, K. (1972). *Statistics of Directional Data*. Academic Press.

Middlebrooks, J. C. (2008). Auditory cortex phase locking to amplitude-modulated cochlear implant pulse trains. *Journal of Neurophysiology*, *100*(1), 76–91. https://doi.org/10.1152/jn.01109.2007

Middlebrooks, J. C., & Bremen, P. (2013). Spatial Stream Segregation by Auditory Cortical Neurons. *Journal of Neuroscience*, *33*(27), 10986–11001. https://doi.org/10.1523/JNEUROSCI.1065-13.2013

Middlebrooks, J. C., & Onsan, Z. A. (2012). Stream segregation with high spatial acuity. *The Journal of the Acoustical Society of America*, *132*(6), 3896–3911. https://doi.org/10.1121/1.4764879

Moore, B., & Gockel, H. (2002). *Factors Influencing Sequential Stream Segregation* (Vol. 88).

Moshitch, D., Las, L., Ulanovsky, N., Bar-Yosef, O., & Nelken, I. (2006). Responses of neurons in primary auditory cortex (A1) to pure tones in the halothane-anesthetized cat. *Journal of Neurophysiology*, *95*(6), 3756–3769. https://doi.org/10.1152/jn.00822.2005

Nagarajan, S. S., Cheung, S. W., Bedenbaugh, P., Beitel, R. E., Schreiner, C. E., & Merzenich, M. M. (2002). Representation of Spectral and Temporal Envelope of Twitter Vocalizations in Common Marmoset Primary Auditory Cortex. *Journal of Neurophysiology*, *87*(4), 1723–1737. https://doi.org/10.1152/jn.00632.2001

Philibert, B., Beitel, R. E., Nagarajan, S. S., Bonham, B. H., Schreiner, C. E., & Cheung, S. W. (2005). Functional organization and hemispheric comparison of primary auditory cortex in the common marmoset (Callithrix jacchus). *Journal of Comparative Neurology*, *487*(4), 391–406. https://doi.org/10.1002/cne.20581

Phillips, D. P. (1989). Timing of spike discharges in cat auditory cortex neurons: Implications for encoding of stimulus periodicity. *Hearing Research*, *40*(1–2), 137–146. https://doi.org/10.1016/0378-5955(89)90107-x

Ramachandran, R., Davis, K. A., & May, B. J. (1999). Single-Unit Responses in the Inferior Colliculus of Decerebrate Cats I. Classification Based on Frequency Response Maps. *Journal of Neurophysiology*, *82*(1), 152–163. https://doi.org/10.1152/jn.1999.82.1.152

Recanzone, G. H., Guard, D. C., & Phan, M. L. (2000). Frequency and Intensity Response Properties of Single Neurons in the Auditory Cortex of the Behaving Macaque Monkey. *Https://Doi.Org/10.1152/Jn.2000.83.4.2315*, *83*(4), 2315–2331. https://doi.org/10.1152/JN.2000.83.4.2315

Sadagopan, S., & Wang, X. (2008). Level Invariant Representation of Sounds by Populations of Neurons in Primary Auditory Cortex. *Journal of Neuroscience*, *28*(13), 3415–3426. https://doi.org/10.1523/JNEUROSCI.2743-07.2008

Schreiner, C. E., & Raggio, M. W. (1996). Neuronal responses in cat primary auditory cortex to electrical cochlear stimulation. II. Repetition rate coding. *Journal of Neurophysiology*, *75*(3), 1283–1300. https://doi.org/10.1152/jn.1996.75.3.1283

Schreiner, C. E., & Sutter, M. L. (1992). Topography of excitatory bandwidth in cat primary auditory cortex: Single-neuron versus multiple-neuron recordings. *Journal of Neurophysiology*, *68*(5), 1487–1502. https://doi.org/10.1152/jn.1992.68.5.1487

Sutter, M. L., & Schreiner, C. E. (1991). Physiology and topography of neurons with multipeaked tuning curves in cat primary auditory cortex. *Journal of Neurophysiology*, *65*(5), 1207–1226. https://doi.org/10.1152/jn.1991.65.5.1207

van Noorden, L. P. A. S. (1975). *Temporal Coherence in the Perception of Tone Sequences*. Institute for Perceptual Research. https://books.google.com/books?id=vh3_HAAACAAJ

Vliegen, J., & Oxenham, A. J. (1999). Sequential stream segregation in the absence of spectral cues. *The Journal of the Acoustical Society of America*, *105*(1), 339–346. https://doi.org/10.1121/1.424503

Wang, X. (2007). Neural coding strategies in auditory cortex. *Hearing Research*, *229*(1–2), 81–93. https://doi.org/10.1016/j.heares.2007.01.019

Wang, X., Lu, T., Snider, R. K., & Liang, L. (2005). Sustained firing in auditory cortex evoked by preferred stimuli. *Nature*, *435*(7040), 341–346. https://doi.org/10.1038/nature03565

Wang, X., Merzenich, M. M., Beitel, R., & Schreiner, C. E. (1995). Representation of a species-specific vocalization in the primary auditory cortex of the common marmoset: Temporal and spectral characteristics. *Journal of Neurophysiology*, *74*(6), 2685–2706. https://doi.org/10.1152/jn.1995.74.6.2685

Watkins, P. V., & Barbour, D. L. (2011). Rate-level responses in awake marmoset auditory cortex. *Hearing Research*, *275*(1–2), 30–42. https://doi.org/10.1016/j.heares.2010.11.011

Young, E. D., & Brownell, W. E. (1976). Responses to tones and noise of single cells in dorsal cochlear nucleus of unanesthetized cats. *Journal of Neurophysiology*, *39*(2), 282–300. https://doi.org/10.1152/jn.1976.39.2.282

Zhou, B., Green, D. M., & Middlebrooks, J. C. (1992). Characterization of external ear impulse responses using Golay codes. *The Journal of the Acoustical Society of America*, *92*(2 Pt 1), 1169–1171. https://doi.org/10.1121/1.404045

Zurita, P., Villa, A. E. P., de Ribaupierre, Y., de Ribaupierre, F., & Rouiller, E. M. (1994). Changes of single unit activity in the cat's auditory thalamus and cortex associated to different anesthetic conditions. *Neuroscience Research*, *19*(3), 303–316. https://doi.org/10.1016/0168-0102(94)90043-4